Synthesis and Characterization of Bone char/Aluminum Loaded Zeolite Y Composite for Removal of Fluoride from aqueous solution

Melat Mechal Kifetew

A Thesis Submitted to the Department of Chemical Engineering,

School of Mechanical, Chemical and Material Engineering

Presented in Partial Fulfillment of the Requirement for the Degree of Master's in Chemical Engineering (Specialization in Process Engineering)

Office of Graduate Studies

Adama Science and Technology University

September 2023 GC

Adama, Ethiopia

Synthesis and Characterization of Bone char/Aluminum Loaded Zeolite Y Composite for Removal of Fluoride from aqueous solution

Melat Mechal Kifetew

Advisor:

Dr. Mulugeta yilma

Co advisor:

Dr. Alemu Gizaw

A Thesis submitted to Department of Chemical Engineering

School of Mechanical, Chemical, and Material Engineering

Office of Graduate Studies

Adama Science and Technology University

September 2023 GC

Adama, Ethiopia

Declaration

I hereby declare that this Master Thesis entitled **"**Synthesis and Characterization of Bone char/Aluminum Loaded Zeolite Y Composite for Removal of Fluoride from aqueous solution**"** is my original work. That is, it has not been submitted for the award of any academic degree, diploma, or certificate in any other university. All sources of materials that are used for this thesis have been duly acknowledged through citation.

Melat Mechal Kifetew		06-11-2023
Name of the Student	Signature	Date

Recommendation of Advisors

We, the advisors of this thesis, hereby certify that we have read the revised version of the thesis entitled **"**Synthesis and Characterization of Bone char/Aluminum Loaded Zeolite Y Composite for Removal of Fluoride from aqueous solution**"** prepared under our guidance by Melat Mechal Kifetew submitted in partial fulfillment of the requirements for the degree of Mater's of Science in Chemical Engineering. Therefore, we recommend the submission of the revised version of the thesis to the department following the applicable procedures.

Mulugeta Yilma (PhD)	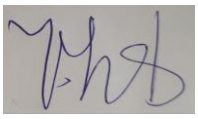	06-11-2023
Major Advisor	Signature	Date
Alemu Gizaw (PhD)		06-11-2023
Co-advisor	Signature	Date

Approval Page

We here by certify that the recommendation and suggestion given by the proposal review committee are appropriately incorporated into the final thesis proposal entitled **"**Synthesis and Characterization of Bone char/Aluminum Loaded Zeolite Y Composite for Removal of Fluoride from aqueous solution**"** by **Melat Mechal Kifetew.**

Mulugeta Yilma(PhD)	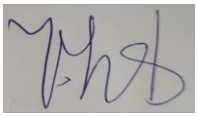	06-11-2023
Major Advisor	Signature	Date
Alemu Gizaw(PhD)		06-11-2023
Co-Advisor	Signature	Date

Approval of Board of Examiners

We, the undersigned, members of the Board of Examiners of the thesis by Melat Mechal Kifetew have read and evaluated the thesis entitled **"**Synthesis and Characterization of Bone char/Aluminum Loaded Zeolite Y Composite for Removal of Fluoride from aqueous solution**"** and examined the candidate during the open defense. This is, therefore, to certify that the thesis is accepted for partial fulfillment of the requirement of the degree of Master of Science in Chemical Engineering.

_____	_____	_____
Chairperson	Signature	Date
_____	_____	_____
Internal Examiner	Signature	Date
_____	_____	_____
External Examiner	Signature	Date

Finally, approval and acceptance of the thesis is contingent upon submission of its final copy to the Office of Postgraduate Studies (OPGS) through the Department Graduate Council (DGC) and School Graduate Committee (SGC).

_____	_____	_____
Department Head	Signature	Date
_____	_____	_____
School Dean	Signature	Date
_____	_____	_____
Office of Postgraduate Studies, Dean	Signature	Date

Acknowledgment

First, I would love to provide my immensely thanks to Almighty God for blessing me with achievements throughout my study, and for granting me with strength, power, and good health to attain my ambition. I would really like to express my genuine gratitude to my advisors Dr. Mulugeta Yilma and Dr. Alemu Gizaw for their continuous guidance, indispensable comments, encouragement, support and excellent supervision throughout my research work. Thank you for generously sharing your time, and for all your support to succeed this research. I would like to thank all staff of Chemical Engineering Department and specially, Mr. Hunegnaw Bayile Department head of Chemical Engineering. My thanks to technical stuff of Material science and engineering department, especially Mr. Demeke Tesfaye for their support. I am grateful to Adama Science and Technology University for facilitating such golden opportunity. Finally, my deep and sincere gratitude to my family, specially my mother Mrs. Frehiwot H/Mariam, I wouldn't be here without your unconditional love, continuous support, thank you for everything you have done for me. I am grateful to my childhood friends and my best Mrs. Eset Negash for their precious support, this thesis would not have been possible without the inspiration and support of several wonderful individuals. Finally, thank you all of class mate for being part of this journey and making this thesis possible.

Table of Contents

List of Tables

List of Figures

List of Acronyms

AC	Activated Carbon
ACF	Activated Carbon Fibers
ANOVA	Analysis of Variance
AZ	Aluminum Loaded Zeolite
BAZ	Bone char Aluminum Loaded Zeolite
BC	Bone char
BET	Brunauer-Emmett-Teller
DTA	Differential Thermal Analysis
DF	Degree of Freedom
EAR	East Africa Rift
EDTA	Trans1, 2-diaminecicIohexane-tetracetic acid
FT-IR	Fourier Transforms Infrared Spectroscopy
GAC	Granular Activated Carbon
HAP	Hydroxyapatite
ISE	Ion Selective Electrode
MER	Middle Ethiopian Rift
MDC	Modjo defluoridation Center
OECD	Organization for Economic Cooperation and Development
PZC	Point of Zero Charge
RSM	Response Surface Method
SEM	Scanning Electron Microscope
SNNPRS	Southern Nation and Nationalities Regional State
TDS	Total Dissolved Solids
TGA	Thermo-Gravimetric Analysis
TISAB	Total Ionic Strength Adjustment Buffer
VIF	Variance Inflation Factor
WHO	World Health Organization
XRD	X-ray Diffractometer
ZY	Zeolite Y

Abstract

Millions of people throughout the world suffer from health problems caused by high fluoride levels in water supplies. Fluoride has an intense stimulation and corrosion effect on the skin mucosa and dental fluorosis. Developing efficient and eco-friendly methods for water treatments are a very crucial activity due to the wide-scale concentration of fluoride ion. The adsorption process is the best among other technologies due to simple design, versatile, lowest cost for instrumentation. Hence, this work focus on synthesis and characterization of bone char and aluminum loaded zeolite Y for enhancing the removal efficiency of fluoride from water. Bone char (BC) and Aluminum loaded zeolite Y (AZ) were uniformly grinded, sieved and mixed in three different ratio (1:1, 1:3, 3:1) (BC to AZ) and pure bone char, zeolite Y and Aluminum loaded zeolite Y was compared. BC and AZ have high adsorption efficiency next to 3:1 Bone char and Aluminum loaded zeolite Y (BAZ) composite. The composite is confirmed successfully using XRD, FTIR, SEM and TGA. The BET specific surface area of BC, ZY and BAZ are determined to be 406.25 m^2/g, 523.120 m^2/g and 540 m^2/g respectively. Adsorption increase with the increase in the surface area of the adsorbent. The experiments have been designed by Central Composite Design (CCD) with three factors such as pH of the solution, contact time and adsorbent dosage. The result confirmed that 98.1% of fluoride ion was removed from water at optimum 60 min contact time, 0.5 g adsorbent dose, the pH level of 7.5. Furthermore, the adsorption parameters such as equilibrium isotherm, kinetics, and thermodynamic properties were conducted. The adsorption isotherm data were best fitted to the Langmuir with R^2 of 0.999 and a maximum adsorption capacity of 19.23 mg/g. In addition, the result of the kinetic model proved that pseudo-second-order provided a good description of the experimental data with a maximum R^2 of 0.999. The result of the thermodynamic parameters demonstrated that the adsorption process is spontaneous and endothermic. The removal efficiency of 68.73% of fluoride ion was found after 3 cycles following 90.4%, 85.8%, and 74.98% removal efficiency for the first, second and third desorption/adsorption cycles respectively. The recycle continue until the removal efficiency below 50%, which indicates wonderful reusability of the adsorbent. The result illustrates that BAZ is an excellent promising adsorbent for the removal of fluoride ions.

Key Words: Adsorption, Bone char, Zeolite, Composite, desorption, Fluoride

Chapter One

1. Introduction

1.1 Background of Study

Water has always been major issue due to its use, need, and scarcity. Millions of people die every year due to pollution of water by different contaminants that result in lack access to clean drinking water (Shahid & Choi, 2018). One of those pollutants is fluorine. Fluorine is an element that occurs naturally as the fluoride ion. It is the 24th most common element in the universe and the 13th most abundant in the earth's crust. Groundwater is naturally fluoridated in at least 25 nations around the world, including Bangladesh, China, India, South Africa, Tanzania, Kenya, and Tanzania (Podgorski & Berg, 2022). Moreover, the East African Rift (EAR) is the most known and documented hotspot for high fluoride contamination in groundwater linked to volcanic deposits. The Middle Ethiopian Rift (MER), one of the most researched regions of the African Rift, is where geogenic sources of fluoride associated to the storage of groundwater in volcanic sediments have identified frequently and evaluated (Colombani et al., 2018).

In Ethiopia, the predominant source of drinking water is wells and springs, as the country lacks a well-developed water network. However, groundwater in certain areas can contain high concentrations of fluoride, exceed 35 mg/L due to the dissolution of fluoride-containing bedrock (Asgari et al. 2019). Prolonged exposure to drinking water with fluoride levels exceeding the World Health Organization (WHO) guideline value of 1.5 mg/L can have detrimental health effects. These effects include potential damage to the liver, kidneys, and parathyroid glands, as well as the development of dental fluorosis, skeletal fluorosis, muscle fiber degeneration, and an increased risk of Alzheimer's disease (Nigri et al.,2016). There are several methods available to remediate water contaminated with fluorine ions. These techniques include chemical precipitation, ion exchange, membrane separations (ultrafiltration, reverse osmosis, and electrodialysis), and adsorption. Among those methods, adsorption is most common and advantageous approach due to its selectivity, straightforward methodology, regenerability and cost effectiveness. The cost of the adsorption process is determined by the cost of the sorbent per unit, and in recent years, research has focused on producing affordable adsorbents from inexpensive components (Lacson et al., 2021; Vocciante et al., 2014). Adsorbents appropriate for

defluoridation have been identified by numerous research; these include activated alumina, bone char, raw bauxite, activated carbon, and natural clays (Nigri et al., 2016). Bone char is a common adsorbent with cheap cost for de-fluoridating water. In comparison to other adsorbents such activated alumina, zeolites, and carbonaceous materials, it has demonstrated a number of advantages for the removal of fluoride. In a different scenario, Bone char can be considered a readily available and environmentally friendly adsorbent, as it is a green material with widespread availability. bone char was reported to be made of 80–90% HAP and 10% amorphous carbon(Biswas et al., 2021; Patel et al., 2015; Shahid et al., 2020).

Despite this, aluminum hydroxide is a fascinating and well-researched adsorbent for fluoride removal capacity. According to earlier research, aluminum hydroxide has an adsorption capacity of about 26.2 mg/g, which is sufficient to remove fluoride from water (Mulugeta et al., 2014). However, its removal capacity varies depending on their hydroxyl group densities, which also result in different Al contents after de-fluoridation. The fluoride removal capacities of different aluminum hydroxides can be ranked in ascending order as follows: boehmite, gibbsite, and bayerite. Among them, AlOOH has a maximum defluoridation capacity of 42.08 mg/g (Gai et al., 2022). However, despite its promising performance, the practical application of AlOOH is hindered by its high cost, particularly for continuous operation. To overcome these limitations and make use of the high fluoride removal efficiency of aluminum oxy-hydroxide, it is beneficial to utilize other porous materials with a high surface area as support. For instance, zeolites are excellent candidates due to their porous structure and large surface area.

From around 200 type of zeolite, Faujasite is one of natural occurring minerals and zeolite Y and X are synthetic form of it. Zeolite Y is preferred over zeolite X for fluoride removal due to the basic nature of Zeolite Y including large pore size, high surface area, and a high Si/Al ratio. Moreover, ZY is easily regenerable as result the reuse of zeolite Y reduces the need for frequent replacement, making it a cost-effective option for fluoride removal (Dessalegne et al., 2017; Gómez-Hortigüela et al., 2013; Julbe & Drobek, 2016). However, they have a surface that is negative charged permanently, which results in a limited anion adsorption capacity. This problem can be overcome by adding metallic or cationic surfactants to the surface of the zeolite in order to take the advantage of their high cation exchange property (Waghmare et al., 2015). Previous researcher studied the aluminum hydroxide supported on zeolite to remove fluoride ion and (Wirtu et al., 2021b). The regeneration and continuous operations of the adsorbent are limited

due to the soft nature of Aluminum hydroxide. So combining bone char and Aluminum load zeolite reduce the concentration aluminum remain in the treated water, considered for developing country, environmentally friendly and the synergistic effect of the two adsorbents resulting in enhanced overall fluoride removal efficiency. .

In this work, bone char and Aluminum loaded zeolite are synthesized whereas the host material bone is waste of cattle, which is easy to synthesize with accessible methods. On the other hand, sustainable starting material required for production of zeolite Y, therefore kaolinite is clay minerals, cost-effective, environmentally friendly and sustainable starting material for production of zeolite. Hence, the binary adsorbent prepared by a method which is not applied on any previous works for those materials.

1.2 Statement of Problem

The occurrence of huge concentration fluoride in ground water causes millions of people to die every year (Shahid & Choi, 2018). A recent study focused on a rural population residing in Ethiopia's Rift Valley, including 341 individuals between the ages of 10 and 70. The findings of this research are concerning, as they indicate that a significant number of Ethiopians, approximately 14 million people, are at a heightened risk of exposure to toxic levels of fluoride (Godebo, 2022). Finding sustainable solutions is still worth investigating since the people still have no access to clear water. Different physiochemical techniques have been employed to remove fluoride from the water. Adsorption proved to be the best technique among all due to its low cost, ease of operation, highest removal efficiency, fantastic reusability performance, and efficient method (Patel et al., 2015). To solve the issue of clean water, some local organizations generate bone char as an adsorbent.

In the Modjo De-fluoridation Center (MDC), for instance, 600 kg of bone per batch is placed into a concrete chamber furnace and heated to 450°C for 10 days. This process requires a lot of energy and takes time to produce bone char. Moreover, the generated bone has a weak capacity for adsorption despite its time and energy-intensive operation. Previous researcher studied the bone char modified using aluminum hydroxide to removal fluoride ion (Bundi, 2020). Wirtu et al. studied the aluminum hydroxide supported on zeolite to remove fluoride ion (Wirtu et al., 2021b). However, Aluminum hydroxide is limited for continuous production due to its nature thus the presence of aluminum as composite form with other material lead to exist Aluminum in high proportion resulting release of excessive amounts of aluminum ions into the treated water, which

have negative impact on environment and human health as well. Hence, the overall mass of aluminum hydroxide should be decreased by combining with other material.

Bone char is known for its high affinity for fluoride ions, due to Hydroxyapatite structure, raw bone availability, Environmental friendly and relatively easy to regenerate, making it a practical option for defluoridation applications while aluminum-loaded zeolite also has unique pore structure and high surface area provide numerous active sites for fluoride adsorption. Therefore, rather than using these individual adsorbents, by combining these materials, the composite takes advantage of their synergistic adsorption capabilities, resulting in a broader spectrum of fluoride removal. To the best of my knowledge, there is no previous work on the composite of bone char and aluminum loaded on zeolite adsorbent to enhance the removal efficiency of fluoride ion from water.

1.3 Objective

1.3.1 General Objective

The main objective of this work is to enhance the de-fluoridation of water using bone char / aluminum loaded zeolite Y Composite adsorbent.

1.3.2 Specific Objective

- ✓ Synthesize and characterization of bone char
- ✓ Synthesize and characterization Zeolite Y from locally available raw Kaolin clay by alkali fusion method.
- ✓ Synthesize and characterization of bone char/Aluminum loaded Zeolite Y
- ✓ Investigating and evaluating Bone Char (BC) and aluminum-loaded zeolite Y composite (BAZ) by mixing with different ratio (1:1, 1:3, 3:1) (BC to BAZ) and comparing the adsorption efficiency of fluoride with Bone char, Zeolite Y, Aluminum loaded Zeolite Y.
- ✓ Investigating and evaluating batch adsorption experiment to study the effect of operating parameters for fluoride removal by the adsorbent.
- ✓ Investigating the adsorption kinetics, equilibrium isotherm, and thermodynamics effect using batch adsorption experimental data
- ✓ Evaluating coexisting of ions within fluoride ion in water and the regeneration potential of the adsorbent.

1.4 Significance of Study

Water bodies are highly exposed to the presence of harmful pollutants, including toxic inorganic pollutants like fluoride, originating from natural and human activities. These pollutants have detrimental effects on aquatic ecosystems and pose risks to human health. Consequently, the utilization of a bone char/aluminum-loaded zeolite mixture as an adsorbent in this study holds significant importance in addressing such environmental issues, reducing water scarcity problems, and providing a valuable resource for future researchers. Moreover, this research bears relevance to the population residing in the Ethiopian Rift Valley, where fluorosis (both dental and skeletal) and related illnesses are prevalent. The findings of this study are expected to provide essential foundational knowledge on the synergetic effect of the bone char/aluminum-coated zeolite Y mixture, thereby serving as a valuable resource for further advancements in this field.

1.5 Scope of the Study

This study focuses on the removal of fluoride from water using bone char/ aluminum coated zeolite Y composite adsorbent. It started by synthesizing bone char, zeolite Y and Aluminum coated zeolite Y followed by mixing bone char and aluminum coated Zeolite Y by varying their ratio with appropriate amount. Instrumentation including SEM, XRD, FTIR, TGA and BET are used to characterize bone char, Zeolite Y, Aluminum loaded zeolite Y and the composite of bone char/ Aluminum loaded zeolite Y. The experimental optimization of the adsorbent was carried out using a response surface methodology (RSM) design. Several parameters were investigated, including the effect of solution pH, adsorbent dosage, contact time, and mixing ratio. Additionally, adsorption isotherm, kinetics, adsorption thermodynamics and reusability of the adsorbent were studied. Not only the effect of co-existing ion within fluoride ion but also the performance of bone char/ aluminum load zeolite Y composite for real water studied in this work.

Chapter Two

2. Literature Review

2.1 Groundwater

For the world's population, groundwater serves as a significant source of fresh water for home, commercial, and industrial needs. More than a third of the world's population receives their drinking water from groundwater, and of the 700 million people who do not now have access to enough water, the majority will need to do so in the future. Additionally, groundwater provides about 40% of the irrigation water needed and around 25% of all industrial supply (International & Hydrogeologists, 2022). Groundwater contamination is the introduction of unwanted substances into groundwater as result of human activity. It can also be created by nature as result of the deterioration of underground rock. One of the key elements of sustainable development for a country is ensuring a reliable and sustainable supply of drinking water. However, groundwater quality is seriously threatened by urbanization, agricultural practices, industrial activity, and climate change(Li et al., 2021). Organic and Inorganic contaminants found in groundwater include anions and oxyanions, such as F^{-}, SO_4^{2-}, and Cl^{-}, and major cations, such as Ca^{2+} and Mg^{2+}. Groundwater can exhibit elevated levels of Total Dissolved Solids (TDS), which encompasses the collective concentration of both inorganic and organic ligands present in the water. These contaminants are usually of natural origin, but human activities also can elevate levels in groundwater (Adimalla & Wu, 2019). Fluoride is a natural constituent of water, which originates from natural and anthropogenic sources such as industrial production, among which the concentration of fluoride from industrial wastewater is relatively high, and the pollution is the most serious(Wan et al., 2021).

2.1.1 Causes of Fluoride in Groundwater

Fluoride is frequently present as a natural component in water sources and wastewater. It may originate from either natural geological sources or industries that use fluoride-containing compounds as raw materials. The dissolution of fluoride in groundwater is dependent on chemical and physical processes that take place in the sub-surface environment. Among several fluoride bearing (Mulugeta et al., 2015) minerals, fluorite (CaF_2) is the predominant mineral that controls the dissolved fluoride concentration in the groundwater. Thus, fluoride-rich ground waters are often associated with rocks with low calcium content or high-pH conditions where sodium

bicarbonate dominates the groundwater composition (Mulugeta et al., 2015). Anthropogenic and geogenic activities are two major causes for increased fluoride concentration in groundwater The sources of fluorine can be anthropogenic, such as the usage of pesticides and industrial waste, as well as geogenic, like the existence of fluorine-bearing minerals in rocks and sediments (Aroua et al., 2023).

2.2 Source of Fluoride in Wastewater

Water is both the defining feature of our planet and a necessary for all elements of life (Laksmi & Hanin, 2022). Just 1% of the remaining freshwater is potable, and 97% and a half of all water is found in the oceans. There is currently a water issue on the planet quality brought on by continued population growth, industrialization, methods utilized in food production, rising standards of living, and ineffective water usage practices (Nyieku et al., 2022). Among a wide range of interpretations, the term "wastewater" there are many definitions in use. The phrase "wastewater" is used to refer to a variety of things and has several definitions. Broadly speaking, wastewater is any mixture of at least one of the following: black water-containing household effluent (excreta, urine, and fecal sludge). Water from commercial establishments, hospitals, and other institutions, as well as grey water (kitchen and bathing wastewater), industrial effluent, agricultural, horticultural, and other urban runoff, storm water, and aquaculture wastewater, either as dissolved or as suspended matter, are also included (Abir et al., 2023).

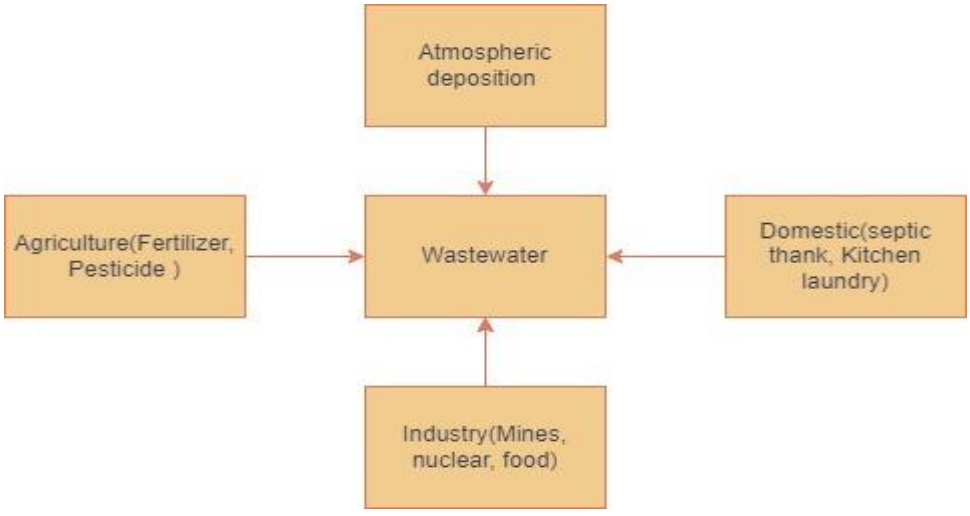

Figure 2. 1: Four main sources of wastewater (Dey et al., 2021).

2.2.1 Industrial Wastewater

The most polluting one is industrial waste discharged into the rivers. The biggest issue with industrial wastewater is the rising concentrations of synthetic substances that are released into the environment including some of them are chemical solvents, industrial by-products, dyes, heavy metals, radioactive waste, organic and inorganic pollutant (Awuchi, 2020).

Wastewater produced from various industries usually contains a lot of fluoride (10–10,000 mg L^{-1}), heavy metals and other anions. These anions and heavy metals may influence the de-fluoridation performance of adsorbents (Ajiboye et al. 2021).To solve this issue, some researchers investigated the effect of co-existing anions on the adsorption capacities of adsorbents by simulating wastewater. For example, Mehta et al. found that Cl^-, NO^{3-}, SO_4^{2-} and PO_4^{3-} had a slight impact on the de-fluoridation performance of the marble apatite adsorbent, but HCO^{3-} greatly reduced the de-fluoridation efficiency. wan et al showed that the Fe–Mg–La tri metal hydroxide de-fluoridation adsorbent had excellent anti-interference ability to Cl^-, NO^{3-}, SO_4^{2-}, CH_3COO^- and HCO^{3-}. Industrialization and urbanization are the main factors and sources for the production of a large amount of fluoride (Wan et al., 2021).

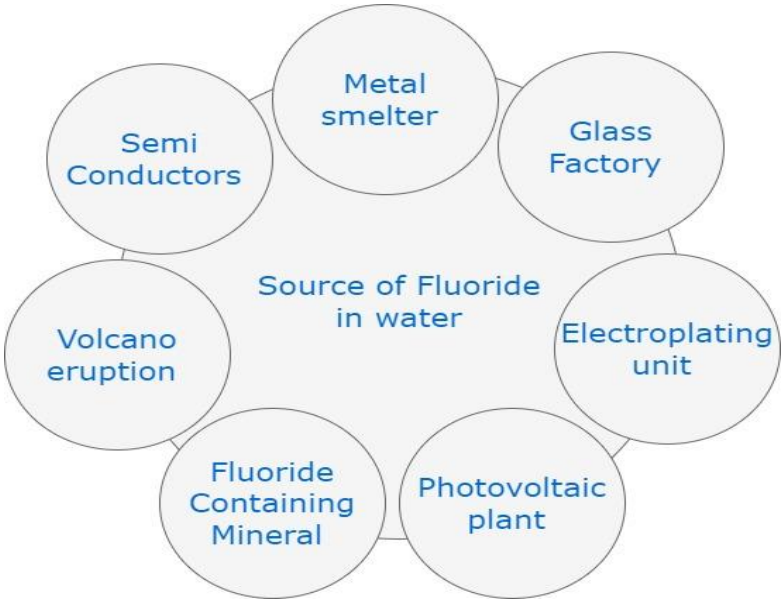

Figure 2. 2: Sources of fluoride in ground and surface water (Bhan & Singh, 2022).

2.3 Fluoride Pollution in the Glob

Fluoride (F^-) contamination in water has been recognized as one of the serious problems worldwide Fluoride. Fluorine-bearing minerals are usually associated with acidic igneous rocks, mineralized veins and sedimentary formations. Fluoride found in ground water all over the

world, area with high fluoride in groundwater includes Syria, Jordan, Egypt, Libya, Algeria and Morocco. It also includes the Rift Valley areas in Africa from Sudan through Kenya to Tanzania and Malawi. Another geographical area extends from Turkey through Iraq, Iran and Afghanistan to India, Northern Thailand and China (Ali et al., 2016).

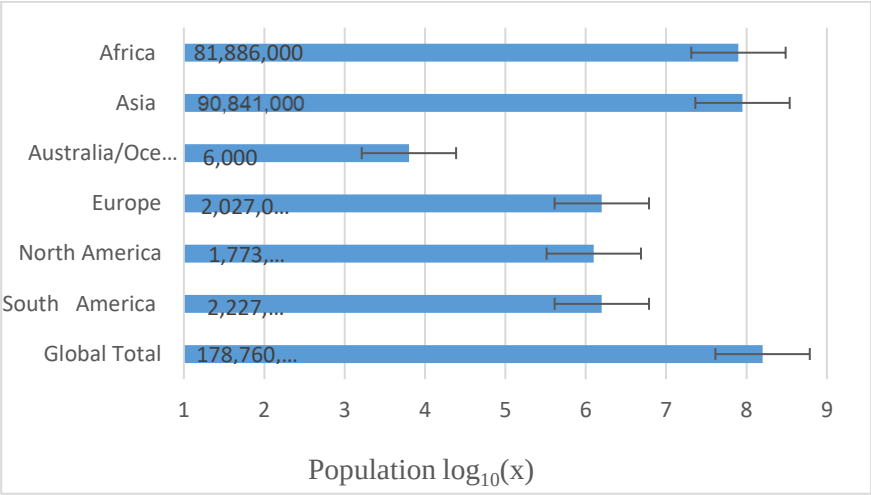

Figure 2.3: Population potentially exposed to fluoride >1.5 mg/L in groundwater (Podgorski & Berg, 2022).

In Ethiopia, associated with rift valley and semiarid climate are two major factors responsible for the high concentration of fluoride in both surface and subsurface water system have reported the high fluoride concentration of 264 mg/L in hot springs (Colombani et al., 2018). According to (Mehrotra et al., 2018), in Ethiopia, the regions that are facing excessive fluoride in ground water are Afar, Oromia and Southern Nations and Nationalities Regional States (SNNPRS).

Table 2.1: Fluoride content of water in various areas of Ethiopian rift valley (Mehrotra et al., 2018)

Sample site	**Fluoride (mg/l)**
Gewane (town)	0.7-2.5
Abadir (farm)	4.0
Koka (town)	26
Alem tena (village)	9
Abernosa (village)	36
Jido (village)	33.6+

2.3.1 Health Effect of Fluoride

Environmental contaminants like fluoride have significant health implications, particularly in low-income countries, where their impact is pronounced, resulting in dangerously high fluoride concentrations (Pillai et al., 2021). The rift valley region experiences an unusually high exposure to natural fluoride from the groundwater wells for which they depend on their drinking and cooking water. Around 14 million of those living in Ethiopia thought to be at high risk of dangerous levels of fluoride exposure. A wide range of fluoride concentrations in the drinking water is found, spanning from 0.3 mg/L to 15.5 mg/L. To put this into context, the typical low level of fluoride in most high-income countries (including where it is added to prevent tooth decay) is 0.7 mg/L and the World Health Organization recommends that drinking water should not contain a fluoride concentration higher than 1.5 mg/L. This means that shockingly, some people were ingesting ten times the recommended amount of fluoride. This was represented in urine samples from the participants, which showed an unusually high concentration (up to 39.5 mg/L) of fluoride, suggesting a significant amount of fluoride is also retained in the bone (Godebo, 2022). Therefore, considering the harmful effects of fluoride on human and environment an effectual and robust technique is the need of the hour to curb the problem associated with excessive fluoride in water.

Table2. 2: Effects of fluoride concentration (Pillai et al., 2021).

Fluoride	Concentration and effect
<0.5	Prevention of teeth cavities
0.5–1.5	Helps in bones and teeth development
1.5–4	Dental problems in children
>4	Dental and Skelton fluorosis
>10	Cancer

2.4 Method of Fluoride Removal

Fluoride removal by adsorption is a complex process, which involves many physical and chemical interactions between fluoride and the adsorbent. It is significant to comprehend the fluoride removal mechanisms, which is helpful to research and improve the de-fluoridation performances of adsorbents.

As shown in Fig. 2.5 the fluoride removal by adsorption usually involves four mechanisms, i.e. ligand exchange, ion exchange, electrostatic interaction and Lewis acid–base interaction (Gai & Deng, 2021).

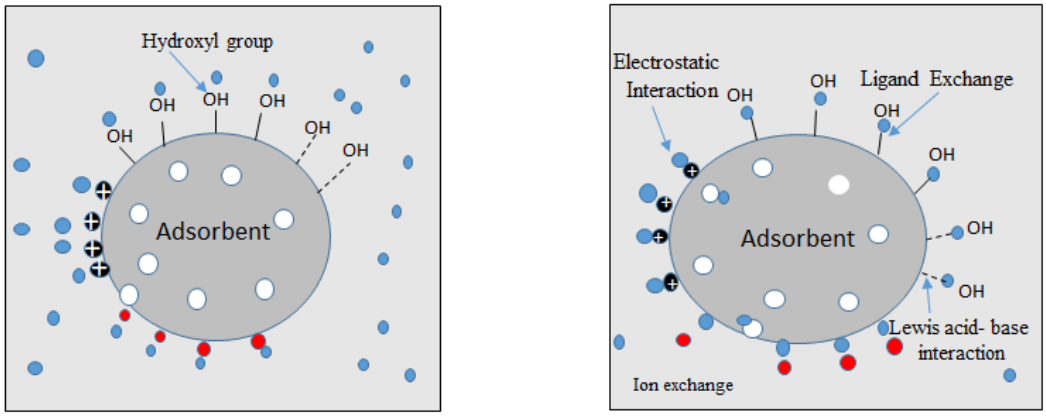

Before de-fluoridation

After de-fluoridation

Pore ○ F⁻ ● Positive charge anion SO^{-2}, CO^{-2}, NO^{-}, $C_2O_4^{-2}$

Figure 2. 4: Removal mechanisms of fluoride by adsorbents in aqueous solution(Gai & Deng, 2021).

2.4.1 Ligand Exchange

The introduction of metal oxide or hydroxide adsorbents into an aqueous solution results in the formation of a layer of hydroxyl groups on the adsorbent surfaces through a hydration reaction. If the metal has a stronger affinity for fluoride than the hydroxyl group, a ligand exchange reaction between fluoride and the hydroxyl group occurs (Gai et al. 2015).

$F^- + \equiv MOH \leftrightarrow \equiv MF + OH^-$ ..... Eq(2.1)

After the reaction, fluoride adsorbs on the adsorbent surface, and OH^- is released into aqueous solution. The ligand exchange mechanism has been successfully used to explain the fluoride removal by α-Al_2O_3 and Zn–Mg–Al tri metal oxide adsorbents. It can be concluded that surface hydroxyl groups are the active sites for fluoride removal, and increasing the surface hydroxyl groups could enhance the adsorption capacity (Gao et al., 2020).

2.4.2 Ion Exchange Processes

Ion exchange, fluoride can be removed from water supplies with a strongly fundamental anion-exchange resin containing quaternary ammonium functional groups, or an ion replacement process, in which the anions on the surface or inside of the adsorbent are replaced with fluoride

ions in aqueous solution (Gai & Deng, 2021). Some researchers found that several anions on the adsorbent surface could be replaced with fluoride ions, such as SO_4^{2-}, CO_3^{2-}, NO^{3-} and $C_2O_4^{2-}$. For example, the fluoride removal by tea waste supported Al_2O_3 and sulfate-doped Fe_3O_4/Al_2O_3 adsorbents is attributed to the ion exchange between SO_4^{2-} and F^- (Cai et al. 2015; Chai et al., 2013).

2.4.3 Electrostatic Interaction

An electrostatic interaction between F^- and the adsorbent occurs when the adsorbent is positively charged. The electrostatic interaction is closely related to the surface charge property of the adsorbent, which in turn depends on the point of zero charge (PZC) of the adsorbent and the pH value of solution. When the pH value is below the PZC of the adsorbent, the adsorbent is protonated and positively charged. In this case, there is an electrostatic attraction interaction between F^- and the adsorbent, promoting the fluoride adsorption on the adsorbent (B. Wang et al., 2021). The ion exchange is the main mechanism of F^- due to the high affinity of F^- to substitute the hydroxide group in the structure of the adsorbent. The mechanism is affected by the changes in the pH of the solution, in which it controls the isoelectric point of the bone char surface and hence affects its electrical attraction to entities in proximity to it. At pH levels below the point of zero charge, the surface of the adsorbent is positively charged and this will increase the affinity of the negatively charged F^- ions to adsorb onto the surface. The formation of fluoride precipitants on the surface of adsorbent takes part with high F^- concentrations (Alkurdi et al., 2019a).

2.4.4 Lewis Acid–Base Interaction

Lewis acid–base interaction, electron pair transfers, a Lewis acid is a species that accepts a pair of electrons from another species; in other words, it is an electron pair acceptor (Ferreira et al., 2010). Lewis acid-base interaction shares similarities with ligand exchange, with the distinction that the interaction between the metal and F- is relatively weak. For metal oxides and hydroxides, the metal ions are Lewis acids, and hydroxyl groups or F^- are Lewis bases (Gai et al., 2015). Surface hydroxyl group of the adsorbent can exchange with F^-, but the interaction between the metal and F^- is weak, and the formation of Al–F is attributed to the outer sphere complexation (Ferreira et al., 2010).

2.5 Technologies of De-fluoridation

Fluoride removal involves treating contaminated water to reduce the concentration of fluoride to acceptable limits. The de fluoridation techniques will be generally classified into two classes, specifically membrane techniques (Reverse osmosis, Dialysis, Electro dialysis and Nano filtration) and surface assimilation techniques (Ion exchange, Electro coagulation and Adsorption) (Bhatnagar et al., 2011). Among those techniques, adsorption is a well-studied and used de-fluoridation technology due to its simple design, convenient operation and low cost and has a straightforward operating system, and when coupled with inexpensive sorbents, its application in low-income communities may be feasible.

2.5.1 Adsorption

Adsorption is a surface phenomenon in which it is characterized by chemical species (adsorbate) from its vapor or liquid solution phase onto or near the surface of solid (adsorbent). The presence of excess surface occurs when the attractive energy of a substance with the solid surface that is adhesive work is higher than that of cohesive energy of the substance(K. Singh et al., 2013). Adsorption is the mass transfer operation of solute (adsorbate) exists in a fluid phase to the surface of solid phase (adsorbent) due to the existent of high molecular interaction between them. It is a process of the interface in which a film of adsorbates is created on the surface of the adsorbents of material. Thus, it is the result of surface energy (Bhan & Singh, 2022). The surface area or active site, the lack of selectivity, and the adsorption kinetics usually limit the efficiency of conventional adsorbents. Adsorption as a separation process is widely applied in our manufacturing economy and daily life. The adsorption process takes advantage of the ability of a particular solid to preferentially concentrate a particular substance in a solution (gas or liquid) on the surface. Therefore, the required purpose of purification or separation can be achieved by contacting the fluid with such a solid (Al-anber, 2011).

Physical and chemical adsorption are two different forms of adsorption. While chemical adsorption is brought on by chemical reactions between the adsorbate and the adsorbent that produce covalent or ionic bonds, physical adsorption increases the adsorbate concentration at the interface due to nonspecific van der Waals forces and is weakly specific and reversible (Gupta et al., 2016). The main characteristic of chemical adsorption is the large interaction potential, which leads to a high heat of adsorption close to the value of the chemical bond. This fact,

combined with other spectroscopy, electron spin resonance, and susceptibility measurements, confirms that chemical adsorption involves the transfer of electrons and the formation of true chemical bonds between the adsorbate and the solid surface (He et al., 2020).

Table 2. 3: The difference between chemical and Physical Adsorption (Abdalla et al., 2020; Gupta et al., 2016)

Parameters	**Chemical Adsorption**	**Physical Adsorption**
Force of Attraction	Strong attraction forces or chemical bond such as ionic bonds	Weak inter particle bond as van der waal armies
Temperature	Higher heat of adsorption	Low heat of adsorption
Electron transfer	electron transfer leading to bond formation between sorbate and surface	Not involve electron transfer, although polarization of sorbate may occur.
Adsorption layer	Monolayer only	Monolayer or multilayer
Kinetics Adsorption	Activated, may be slow and irreversible	Rapid, non- activated and fully reversible
Adsorption sites	Site specific, adsorbed molecule are fixed at specific sites	Not site specific, the adsorbed molecules are free to cover the entire surface

2.6 Adsorbents for De fluoridation of Water

2.6.1 Carbon-Based Materials

Carbon-based materials have demonstrated exceptional adsorption properties, making them highly advantageous for water treatment processes aimed at potabilization (Dhillon et al., 2016). Gupta et al. developed a micro Nano hierarchal web consisting of activated carbon fibers (ACF) and carbon nanofibers (CNF), impregnated with Al for the removal of fluoride from wastewater. It was observed that pre-treatment of the feed water was not required while using the Al-CNF for treating the wastewater with pH 5.0–8.0. Using a redox process, granular activated carbon (GAC) was coated with manganese oxides and the prepared sorbent (GAC-MnO_2) was used for fluoride removal from aqueous solution (Bhatnagar, 2015).Fluoride adsorption capacity of

impregnated activated charcoals was 3–5 times higher to that of plain activated charcoal (Ma et al., 2009).

2.6.2 Activated Carbon Based Adsorbents

Activated carbon (AC) is extensively utilized for the elimination of both organic and inorganic contaminants owing to its abundant surface area, cost-effectiveness, wide availability, and porous structure (Yagub et al., 2014; Zare et al., 2015). AC is a common adsorptive material, used for removing pollutants from water sources due to its enhanced porosity, significant surface area, and its adaptable surface chemistry. According to the application of the AC, it is produced in different forms, powdered activated carbon, granulated activated carbon and activated carbon fibers. The AC properties depend on the raw material source and the activation method. Modified activated carbon materials with the oxides and hydroxides of metals have been used to expand its available surface area and to strengthen its interactions with fluoride. The AC can be produced from different carbon rich materials including nutshell, lignin, pine cone mass, coir pith and so on. However, most of the ACs possess a negatively charged functional groups onto their surfaces, and hence, the AC demonstrates low adsorption removal of the anionic pollutants such as fluoride (Bacelo et al., 2020). Currently, one of the most widely applied carbon-based materials for fluoride removal is bone char (BC), which is considered as a conventional treatment with very good reported removal efficiencies (Nigri et al., 2017a).

2.6.3 Alumina-Based Adsorbent for De fluoridation

Aluminum, aluminum salts, alumina balls and other aluminum based adsorbents are widely used for defluoridation of drinking water, because of the high affinity between aluminum and fluoride ions which result in very high adsorption capacity by aluminum based adsorbents. Alumina is considered to be the most effective and widely used adsorbent for defluoridation of water (Mondal & George, 2015). Activated alumina is widely concerned in the direction of fluoride adsorption due to its large specific surface area, unique pore diameter structure, excellent adsorption performance, and adsorption efficiency. At present, both the World Health Organization and the US have identified activated alumina as one of the best available technologies (Affonso, Marques, et al., 2020). Recently, Alumina- and Al-based sorbents have been the materials of significant importance among the researchers for years in the field of defluoridation of water (Vithanage & Bhattacharya, 2015). Aluminum hydroxide, in addition to alumina, is a powerful defluoridation adsorbent with a substantially lower residual Al content

than alumina. Although aluminum hydroxide works well as a defluoridation adsorbent, its widespread use is constrained by its subpar defluoridation efficacy. The maximal defluoridation capacity of the adsorbent is 41.9 mg/g, and it can remove >95% fluoride in the first 2 min and achieve adsorption equilibrium in 2 h (W. Gai et al., 2021). (Gai et al., 2021; Gai et al., 2022) found that the defluoridation performance of different aluminum hydroxides follows the order of boehmite > bayerite > gibbsite. The maximum defluoridation capacities of boehmite, bayerite and gibbsite are 42.08, 2.97 and 2.74 mgm^{-2} respectively.

2.6.4 Zeolite

Zeolites represent a group of aluminum silicate minerals of a three-dimensional framework that consists of the Al, Si, and O_2 family of aluminum silicate minerals in mineralogy that has been studies since the 18^{th} century. Simply means minerals composed of aluminum, silicon, and oxygen, plus counter cations (Sommerville, 2017). Zeolites are highly significant in both science and industry due to their great surface area, nontoxicity, abundance, and hydrophilic quality (Magalhães et al.,2022).

Generally, chemical composition of a zeolite can be expressed as

$$M\,[(AlO_2)a(SiO_2)y].cH_2O \quad \text{Eq(2.2)}$$

where, M represents either an alkali metal, or an alkaline earth metal cation, c is the amount of water of crystallization per unit cell, a and y represent the total number of the $[SiO_4]^{4-}$ and $[AlO_4]^{5-}$ tetrahedral in a unit cell of the zeolite, respectively, thus, Al and M are present in equal proportions(Fletcher, 2019). The cations are mobile so can be replaced by ion exchange techniques, and the ratio y/a ranges from 1.0 to 5 (Fletcher, 2019; Sommerville, 2017).The porosity framework of zeolite makes it called a molecular sieve since it stores only a certain size of cations and stores water. Additionally, the open frameworks allow for a reversible exchange of guest ions and molecules (Sommerville, 2017). On describing, the framework's crystal chemistry starting from silicon it has a low valence; it follows that silicon atoms typically choose to bind with four of their neighbors, creating a tetrahedral geometry. Since silicon is +4 and each oxygen, anion has a -2 charge, if a SiO_4 entity could be isolated; it would have a charge of -4. However, because an oxygen atom connects two T atoms and shares electron density with both, a SiO_2 unit in a framework is neutral. Therefore, there will not be any charge in pure SiO_2 framework that is free of flaws. On the other side, aluminum has a +3 valence; the net charge is -1, when it is tetrahedral coordinated to four oxygen atoms in a framework. Each aluminum atom

has a negative charge that is balanced by a positive ion when they are joined to form an alumino silicate framework using tetrahedral made of silicon and aluminum (Khaleque et al. 2020). Zeolites can be manufactured from a variety of source materials, both natural and artificial. However, from an economic standpoint, not all raw materials can be used to create zeolite. They should be affordable, easily accessible, low-cost to produce, selective, high-yield, and less abundant in foreign chemicals (Johnson & Arshad, 2014).The searching for cost-effective, environmentally friendly and sustainable material needed for production of zeolite, this leads to the study on modification of kaolinite minerals. Kaolin is a white colored substance, which is also known as China Clay. Its fine particles size and color are the physical properties, which differentiate kaolin from other industrial clay base mineral (Lázaro, 2015). In kaolin, mineral such as feldspar decomposed to form a hydrous aluminum silicate or mineral kaolinite, which is the main component of kaolin. This is the process used to put the beneficiated clay to a more reactive phase metakaolin (semi-amorphous) as kaolin in its natural state is less reactive and forms hydrosodalite when reacted with sodium hydroxide (Patrylak et al., 2001). The sources of Al and Si is kaolinite for synthesis of several zeolites such as zeolite X and zeolite Y with faujasite structure (Moneim & Ahmed, 2015). Faujasite is a naturally occurring mineral, and Zeolite-X and Zeolite-Y are synthetic versions of it. They possesses one of the largest cavities and cavity openings of all known zeolites (Xu et al., 2009). The zeolite is referred to as zeolite X when the Si/Al ratio is between 1 and 1.5, and zeolite Y when it is more than 1.5. As a result, zeolite X contains more aluminum than zeolite Y (Díaz, 2017; Johnson & Arshad, 2014).

2.6.5 Aluminum Loaded Zeolite Adsorbent

Zeolites are crystalline alumino silicates are having a large surface area and are possessing permanent negative charge on their surface, due to which they have low adsorption capacity for anions. The adsorption capacity can be raised by changing the surface of the zeolite with the cationic surfactants or the metallic cation (Waghmare et al., 2015). The cations do not directly linked to the inorganic framework and are exchangeable with other cations, which make zeolites cation exchangers. However, taking the advantage of their high cation exchange property, the adsorption capacity of zeolites (for anions) can be increased by modifying their surface with multivalent metallic cations (Al^{3+}, La^{3+}, Fe^{+3},Na^{+1}) (Jagtap et al., 2012). Fluoride ions with a high electronegativity and a small ionic size (a hard Lewis base) should have a strong affinity towards Al(III) (a hard Lewis acid) stated in Pearson's hard and soft acids and bases (HSAB)

theory. Therefore, aluminum-containing materials have been investigated intensively for fluoride removal from water due to the properties such as small size, hard base nature, high electro negativity makes the fluoride compatible with metal ions (J. Chen et al., 2022). Additionally, (Tchomgui-Kamga et al., 2010) found that an Al_2O_3-based adsorbent obtained by dispersing Al_2O_3 in charcoals had a defluoridation capability of 5.67–13.64, depending on the temperature of carbonization. In addition to aluminum oxide, aluminum hydroxide and aluminum hydroxide-containing materials have also been investigated as de-fluoridation adsorbents. For instance, the adsorption capacities of fluoride by synthetic a Mg-Al-Zr triple-metal hydroxide composite (Wang et al., 2017) and an iron-aluminum nanocomposite (Mondal & Purkait, 2019) were reported to reach 17.73, 14.92, 22.9 and 25.09–28.07 mg/g, respectively. Therefore, aluminum hydroxide had a better performance for removal of fluoride from water than aluminum oxide, due to the presence of abundant hydroxyls on the former (He et al., 2019). Generally, aluminum (hydro)oxides, including hydroxides and oxyhydroxides of aluminum (represented here after as AlOOH) amended zeolites, are promising candidates due to their high capacity and specificity for fluoride removal (Du et al., 2017).

Table 2. 4: Adsorption capacity and other parameters of different adsorbents for removing

Adsorbents	pH	Temp. ^oC	Initial fluoride conc. (mg L^{-1})	Adsorption capacity (mg/ g)	Reference
Zn–Mg–Al oxide microsphere	7	25	10–100	84.24	(Gao et al., 2020)
Aluminum (hydr)oxide(AlOOH)	7.3-8.6	25-200	20 - 200	40 ± 2	(Mondal & George, 2015)
Ce–AlOOH	3.0	30	10–1000	62.8	(Tao et al., 2020)
MgO–biochar	8.0	25	-	83.05	(Wan et al., 2019)
Aluminum hydro(oxide)	5-9	-	15	80	(Zewge, 2016)

Zeolite modified With calcium and aluminum	4-8	-	10	8.03	(Waghmare et al., 2015)
Activated sepiolite	7	35	50–1500	170.0	(Lee et al., 2020)
Cerium loaded chitosan CTS-Ce	3	25	1000	975.4	(Affonso, Marques Jr, et al., 2020)
Natural hydroxyapatite	7	30	-	71.8	(Ren et al., 2019)
Porous MgO Nano plates	7	25	300	185.5	(Jin et al., 2016)
Aluminum modified food waste bio char	7.1	25	24-900	123.4	(Meilani et al., 2021)
Zn modified geo-polymer	5	25	10-80	60	(Sarkar et al., 2019)
Al_2O_3/carbon nanotube	6	25	50	28.7	(Araga et al., 2019)

2.7 Bone char Adsorbent

(OECD, 2018), it is expected that there will be an increase of 40 million metric tons in meat production within the next ten years, including 13% in poultry, 10% in pig meat and > 21% in sheep meat. Consequently, there will be a significant increase in meat and bone meal waste produced globally (Alkurdi et al. 2019). Bone char, is made from animal bones that are charred (burnt) and crushed has been used on large-scale application in the field for fluoride removal. It is a porous and cost effective adsorbent has been studied in water and wastewater treatments and has shown several advantages for fluoride removal in comparison to other adsorbents such as activated alumina, zeolites and carbonaceous materials (Dahi, 2016;Muro et al. 2017). Animal bones are composed about 70% of inorganic matter, mainly hydroxyapatite. The

chemical composition of hydroxyapatite is $Ca_{10}(PO_4)_6(OH)_2$ the remaining part of bones is composed of organic matter, mainly fibrous protein such as collagen and osteo calcin (Alkurdi et al., 2019; Delgadillo et al., 2017). Bone char (BC) showed very good adsorption capacity for fluoride, according to the pH_{PZC} of Bone char, the material have a positive charge under the conditions prevailing during the adsorption studies with both water types (Medellin et al. 2016). However, for this adsorbent, the main adsorption mechanism is related to the chemical structure of hydroxyapatite (HAP, main component of bone char), since OH^- and F^- in HAP are interchangeable. It is worth emphasizing that the organic component of bone char is predominantly responsible for adsorbing nonpolar organic substances, while the inorganic fraction contributes to its adsorption capacity (Rojas et al.2015).

2.7.1 Modification Bone char

Adsorption capacity of carbonaceous materials improved using suitable activation methods via increasing the surface area, pore volume or providing a diversity of pore sizes to the adsorbent; or altering functional groups on the surface increases the selectivity of the adsorbent toward specific contaminants. However, bone char examinations after different modification methods indicate that there are no significant increments in the surface area. Generally, adsorption capacity of bone chars improved using alteration of functional groups on the surface. The adsorption capacity decrease in the following order bone char > activated alumina > activated carbon (Delgadillo et al., 2017).

Table 2. 5: Adsorption capacity of bone char modified with different materials and their respective parameters

Bone char	**pH**	**Temp. (ºC)**	**Contact Time (h)**	**Initial fluoride conc. (mg/L)**	**Adsorption Capacity (mg/g)**	**Reference**
	7	30	2	10-100	15.01	(Rojas-Mayorga et al., 2015)

Aluminum chloride doped	7	30	2	10-100	29.23	(Rojas-Mayorga et al., 2015)
Aluminum sulfate doped	7	25	2	10-100	39.87	(Rojas-Mayorga et al.2015)
Aluminum sulfate doped	7	40	2	10-100	41.44	(Rojas-Mayorga et al., 2015)
Aluminum nitrate doped	7	30	2	10-100	40.60	(Rojas-Mayorga et al., 2015)
0.1M HCL washed	7.±0.2	25	50	10	6.2	(Nigri et al., 2017)
Al-impregnated	6±0.3	25	5	10	6.3	(Nigri et al., 2017)
1.0M HNO_3 and thermally treated	7.0	400		0.1-10	9.78	(Medellin-Castillo et al., 2016)
Cerium containing	7.0	30	24	50	13.6	(Zúñiga-Muro et al., 2017)
Thermally treated	7 - 7.5	400	3	10	4.87	(Nigri et al., 2016)

Aluminum Hydroxide loaded bone char	-	-	2	11.72	11.64	(Bundi, 2020)
Aluminum hydroxide loaded zeolite	5-8	25	3	10	12.12	(Dessalegn e et al., 2017)
Aluminum coated stilbite	3-10	25	6	10	11.52	(Wirtu et al. 2021)
Bone char	7.2	20	-	10	12.05	(Asgari et al. 2019)

2.7.2 Fluoride Adsorption by Bone char

Bone char, a carbonaceous material containing from 80-90% of hydroxyapatite and 10% carbon $Ca_{10}(PO_4)_6(OH)_2$ in its structure has been used to reduce the content of fluoride in water and wastewater. During ,the adsorption of fluoride, hydroxyapatite from the structure of bone char plays an important role in the process, which is attributed to the fact that OH^- and F^- in HAP are interchangeable (Patel et al., 2015).

$Ca_{10}(PO_4)_6(OH)_2(s) + 2F^-(aq) \rightarrow Ca_{10}(PO_4)_6F_2(s) + 2OH^-(aq)$……Eq(2.3)

The adsorption of fluoride by the bone char can occur through the formation of surface complexes at the sites phosphate ≡P- OH and hydroxyl ≡ Ca-OH, as reported by (Medellin et al., 2014). Also precipitation of CaF_2 cannot be neglected, since Ca^{2+} ions, released by residual calcite and/or hydroxyapatite, may react with the fluoride ions present in the solution, creating the super saturation for calcium fluoride, which culminates with its formation fluoride, which culminates with its formation (Medellin et al., 2014).

The main mechanism for fluoride removal by bone char is associated to electrostatic interactions between the charged surface of the adsorbent and the negative adsorbate ions in solution and not only due to ionic exchange between F^- and OH^- ions contained in the HAP structure. This is because at pH below pH-PZC= 8.4, the protonation reactions are favored by the formation of

positive complexes onto the mesoporous bone char structure (Brunson & Sabatini, 2009; Medellin et al.2014).

$\equiv P\text{-}OH + H^+ \rightarrow \equiv P - OH_2^+$ ..... Eq(2.4)

$\equiv Ca\text{-}OH + H^+ \rightarrow \equiv Ca - OH_2^+$ ..... Eq(2.5)

The replacement of hydroxide ions with fluoride ions results in a more acid resistant structure, fluoro apatite (Thole, 2013).

$Ca_5(PO_4)_3OH + F^- \longrightarrow Ca_5(PO_4)_3 F + OH^-$ ..... Eq(2.6)

Fluoroapatite being more resistant to acid attack compared to hydroxyapatite offers a protective layer to the tooth enamel against acids from foods. This prevents dental caries. Excessive fluoride intake however may enhance the reaction to go beyond replacement of hydroxide (Thole, 2013).

$Ca_5(PO_4)_3 F + 9F \longrightarrow Ca_5F_{10} + 3PO_4^{3}$ ..... Eq(2.7)

The ion exchange occurs between phosphate and fluoride ions. The resultant compound, calcium deca fluoride, is a very hard and brittle material not appropriately suited for the functions of the skeletal structure (Wambu et al., 2013).

2.8 Method to Improve Adsorption Capacity

2.8.1 Compound Synergy

Currently, composite materials for removing fluoride, such as graphene oxide and nanofibers supported on metal oxides, ternary metal oxides, hydroxides loaded on magnetic nanoparticles, and biomass modified by metal ions, etc. These materials showed an excellent adsorption performance with their and stability in the adsorption process due to their complex synergistic effect creates extensive attention (Wan et al., 2021).

2.8.2 Morphology Control

At present, many adsorbents had a positive charge in the adsorption process, but the specific surface area was minimal (Wang et al.2022). Different morphology and microstructure of adsorbents played an essential role in the adsorption process. For instance, adsorbent with large specific surface area, porous structure, hollow microspheres have high efficiency to remove the fluoride. The adsorption capacity of the adsorbent enhanced with providing more and higher density adsorption sites. Therefore, morphology control was an essential factor to improve the adsorption capacity (L. Huang et al., 2020a).

2.8.3 Strengthening of Functional Groups

In recent years, amino, sulfate, chlorine, and other anion functional groups were effectively active for ligand exchange with fluoride ions. Hence, it was a meaningful way to improve the performance of adsorbents by using them to modify and strengthen adsorbents. In addition, hydroxyapatite is less expensive and easy to obtain. However, its absorption efficiency in the adsorption process was very low, and its performance for removing fluoride was abysmal (Mahfoudhi & Boufi, 2017). To improve the removal efficiency of fluoride using hydroxyapatite, Chen et al. reported a combination of hydroxyapatite and sulfate-doped hydroxyapatite at high fluoride solution concentration. The maximum adsorption capacity of sulfate doped hydroxyapatite and hydroxyapatite reached 28.3 mg/g and 14.3 mg/g, respectively. The initial adsorption efficiency of sulfate-doped hydroxyapatite was three times that of hydroxyapatite. The mechanism study found that the synergistic effect between SO_4^{2-} and hydroxyl groups enhanced the exchange between SO_4^{2-} and fluoride (Chen et al., 2016).

2.8.4 Crystal Form

The experiment process, researchers identified the dominant crystal form through different proportions, which was also a method to improve the removing fluoride capacity of adsorbent significantly (L. Huang et al., 2020b). Because of certain active group and crystal structure, γ-AlOOH showed significant performance in removing fluoride in the water environment. The density functional theory (DFT) is used to reveal the adsorption mechanism, which confirms that the different kinds of fluoride (F^-, HF, HF^{2-}) had several effects on the adsorption process under different conditions (Wan et al., 2021).

2.9 Factors Affecting Adsorption

2.9.1 Effect of Initial Concentration and Adsorbent Dose

To determine the ideal circumstances for substance uptake during an adsorption process, it is critical to study the impact of modifying the solute starting concentration. The elimination effectiveness (removal percentage) of fluoride ions from adsorbent rises with increasing initial fluoride concentration up to a specific point. When there are no more empty sites left for adsorbate particles, no more adsorption will occur. According to the Fickian definition, which contends that the gradient of concentration is what drives molecular transport in solution, this can be explained (Hwang & Kärger, 2020).

(Smittakorn et al., 2010) examined the influence of increasing initial fluoride concentration on the removal efficiency a homemade bone char using synthetic water (1–6 mg/L) and surface water samples (3.5 mg/L). The finding revealed that both samples have almost the same removal capacity (0.130 and 0.157 mg/g, respectively) at 3.5 mg/L initial F^- concentration regardless to the availability of other ions in the field ground water, while, F^- uptake declined after increasing the initial concentration to 6 mg/L (for the synthetic samples). The percentage removal shows misleading; it does not show the amount of adsorption sites occupied by the adsorbate. The defluoridation capacity of aluminum-loaded zeolite increased with increase of the initial fluoride concentration, from 2 to 6 mg g^{-1} at initial concentrations of 5 to 15 mg L^{-1}, respectively. This may be due to the availability of a higher number of fluoride ions per unit mass of the adsorbents and/or the utilization of less accessible or energetically less-active sites because of increasing diffusivity of fluoride ions when initial concentration increases (Dessalegne et al., 2017). Gai et al. observed that 10 mg/L F^- decreased to 0.293 mg/L with an adsorbent dose of 5 g/L. Aluminum coated zeolite, which is below the WHO maximum contamination limit (1.5 mg/L). Aluminum coated zeolite showed expected maximum fluoride uptake capacity of 11.52 mg/g. This adsorption capacity is greater even from the commercial aluminum hydroxide (Gai et al., 2015). Different experimental conditions represented by the initial concentrations and adsorbent dose can significantly alter the results of F^- removal on adsorbent. For instance, (Nasr et al., 2011) used 15 g/L adsorbent for the removal of 2.5–10 mg/L fluoride, which represents a high dose compared to the literature. Thus, the presence of active sites on the adsorbent surface in solution reduce the effect of driving force due to the concentration gradient. (Sani et al., 2016) reported that in batch studies, raising Adsorbent dose from 4 to 10 g/L considerably increased fluoride removal efficiency from 63.2 to 86.7%, but after calculating the uptake of fluoride per unit weight bone char 1.58 and 0.87 mg/g, a different result was obtained. This result points to a decrease in the number of active sites that would be available to occupy additional F at higher solution concentrations.

2.9.2 Effect of pH Value

The pH of the drinking water principally depends upon geological characteristic of soil and weather conditions. Hence, it is necessary to study the effect of pH on uptake of fluoride ions. Some adsorbents work under a wide range of pH (3–12), some of them are best under acidic conditions while others adsorbents give optimum results under neutral pH (7). At low pH (acidic)

values, fluoride ion may form positive species that are readily adsorbed and as the pH is increased, association with hydroxyl ions results in formation of species that are negatively charged which may not be readily adsorbed (Mondal & George, 2015). The adsorption capacity of fluoride significantly affected by change of pH range in the solution. The point of zero charge (pH_{PZC}), which represent the pH value at which the surface charge is zero, for adsorbent samples from different origins is reported to range between 7.4 and 10. (Medellin-Castillo et al., 2014b; Nigri et al., 2017b). The results demonstrated that, although the isoelectric point was unaffected (pH_{PZC} = 8.4), increasing the ionic strength caused the adsorbents' surface charges to increase. The interaction between the negatively charged fluoride ions and the positively charged adsorbent surface (below pH_{PZC}) will result in an increase in fluoride removal capacity. Nevertheless, adsorbents will dissolve at very low pH levels (<3) and P will be released into the solution (Alkurdi et al., 2020a). Bone char surface washing with acid solutions can enhance the removal capacity due to the protonation of the functional groups of the HAP at pH values lower than PH_{PZC} (as they mainly are > 7). Accordingly, protonation reactions provide a positive charge on the surface of the adsorbent and increase the affinity of F^{-}. (Nigri et al., 2017b) reported that a maximum removal of 6.2 mg/g of F^{-} achieved after washing a commercial bone char with 0.1 M HCl owing to the increase in the positive surface charge. Surface protonation followed the equations below (Medellin-Castillo et al., 2014a).

$$\equiv P\text{-}OH + H^{+} \equiv \longrightarrow POH_2^{+} \quad \text{Eq(2.8)}$$

$$\equiv Ca - OH + H^{+} \equiv Ca^{-} \longrightarrow OH_2^{+} \quad \text{Eg(2.9)}$$

2.9.3 Equilibrium Contact Time

Adsorption equilibrium is the point at which the processes of adsorption and desorption are in balance. In other words, the amount of material desorbed from the adsorbent is equal to the amount of material adsorbed from the solution. Equilibria data is necessary for evaluating the adsorption process, characterizing an adsorbent, rating the adsorbate's removal capacity, and determining the appropriate rate of adsorption for use in industrial processes (Çeçen & Aktas, 2011). Another crucial element in determining the affinity of fluoride removal from water is the shaking time (contact time). The rate of adsorption also significantly increases at the first stage of the adsorption process and following, according to studies on the impact of contact time on the removal of fluoride ions that when adsorption rate decreases, equilibrium is reached. The adsorbent surface area, availability of surface active sites, adsorption binding constants of the

adsorbent, and the variation in the ionic size of the modified ions are all factors that affect the contact time between different adsorbents (Rahman et al., 2021).

2.9.4 Effect of Charring Temperature

Bone char can be synthetized through the calcination of bones under a low-oxygen environment. In particular, thermal processes with restricted presence of air at 500–600 ◦C are commonly used for the synthesis of bone char for water de-fluoridation(Moreno et al., 2010). In addition, (Kaseva, 2006), it has been suggested that heating cattle bones to temperatures above 600 °C may cause damage to the apatite structure of the bone, resulting in a reduction in adsorption effectiveness. Because the water treated with this adsorbent may taste and smell terrible, thermal treatments of bones at temperatures below 400 °C may result in a bone char that is not hygienically acceptable for water de fluoridation. Figueiredo et al straight forward's case study revealed that at 600 ^{o}C the organics were eliminated and a carbonate apatite was produced for animal bones (Figueiredo et al., 2010). In addition, (Kawasaki et al., 2009) used bones from cows, pigs, chickens, and fish in a pyrolysis process at 800 and 1000 °C to study the synthesis of bone char. Nevertheless, the organic material from the bone is removed through a heat treatment between 500 and 600^{o}C. Moreover, there are significant alterations in the bone's microstructure pores are created when the organic materials are burnt off, and the pore volume and diameter may be affected by this due to the close structural interlocking, the porosity (Kaseva, 2006). On the other hand, various authors reported calcinations temperature to range between 500-900^{o}C and time range of 1 to 8 hrs. The process of metakaolinization involves the loss of hydroxyl group and is followed by rearrangement of the octahedral layer to tetrahedral orientation in the calcined kaolin(Díaz, 2017; Johnson & Arshad, 2014; Patrylak et al., 2001).

Wardle and Brindley describe the metakaolinization reactions as follows:-

Kaolinite $500^{o}C$-$900^{o}C$ Metakaolinite Water

$$Si_2Al_2O_5(OH)_4 \rightarrow 2SiO_2.Al_2O_3 + 2H_2O \quad \text{Eq (2.10)}$$

2.9.5 Effect of Coexisting Ion

Groundwater polluted with fluoride contains several other ions that can contend with fluoride during the adsorption process. The nature of the adsorbent to adsorb fluoride selectively depends on charge, polarizability, size and difference in electronegativity. Anions are of the same charge

as fluoride ion; therefore, they produce an environment of competition in the result causing drop in adsorption capacity of the adsorbent (Mondal & George, 2015).

(Medellin-Castillo et al., 2007) examined the difficulty of removing fluoride from natural water due to the presence of chloride, nitrate, nitrite, sulfate, and phosphate. The presence of these anions had no impact on the uptake of F^-on the adsorbent, as evidenced by the fact that the concentration of the anions in solution did not change after the adsorption process. Nonetheless, adsorption studies revealed a decrease in the carbonate content, indicating a competition with F^- ions on the adsorbent surface. However, higher concentration fluoride adsorbed compared to the carbonate, shows the bone char surface would selectively remove F^- rather than carbonate. The same results were confirmed by (Medellin-Castillo et al., 2014a) while investigating the influence of these anions. The decrease of anion affinities toward adsorbent (at concentration < 0.3 mg/L) was in the following order $F^- > Cl^- > CO_3^{-2} > NO^{-2} \approx - NO^{-3} \approx - HCO^-_3 \approx - SO_4^{2-}$. Some researchers investigated the effect of co-existing anions on the adsorption capacities of adsorbents by simulating wastewater. For example, (Mehta et al., 2018) found that Cl^-, NO^{3-}, SO_4^{2-} and PO_4^{3-} had a slight impact on the de-fluoridation performance of the marble apatite adsorbent, but HCO_3^- greatly reduced the de-fluoridation efficiency.

2.10 Adsorption Regeneration

Regeneration is a very important aspect of adsorption from an economic and environmental point of view. The disposal of adsorbents is one of the problems associated with the adsorption methods. The regeneration can reduce the need for new adsorbents and additionally reduce the trouble of disposal of used adsorbents. There are several regenerating agents that can be used for adsorbent materials, depending on the type of adsorbent and the nature of the contaminants being removed. Some common regenerating agents are Basic solution, Acidic solutions, Organic solvent, Photocatalytic regeneration and soon (Kulkarni & Kaware, 2014). However, Sodium hydroxide (NaOH) is commonly used for the regeneration of adsorbent materials because it is an effective and relatively inexpensive regenerating agent.

Chapter Three

3. Methodology

3.1 Materials and Equipments

Chemicals and reagent were analytical grades and used without further purification. Sodium fluoride (NaF) (99.9% purity), Sodium Hydroxide (NaOH) (99.8% purity), Ethanol ($C2H_5OH$) (96% purity), Aluminum chloride ($AlCl_3$), Nitric Acid (HNO_3) (69% purity), Hydrochloric Acid (HCl) (35% purity), and Distilled water. The cattle bone residue was collected from Adama, the raw kaolin was collected from Di Yuan Ceramic factory which is found in the Eastern Zone, Ethiopia. The major equipment used were muffle furnace (model: SX-2.5-12), sieve (model: CEN-MKII-00-A), size reduction (ROHS), analytical balance (JA203H), beaker plastic bottles, Micro Processor pH-mV meter (SL-145), tray, vacuum pump, filter paper, magnetic stirrer (XMTD-231), jar test (SW6), crucible, conical and Erlenmeyer flasks, Measuring cylinders, aluminum foil and fluoride ion selective electrode (S-613F). Instrumental equipment such as x-ray diffractometer (model: XRD700s), scanning electronic microscope (SEM), TGA and Fourier transform infrared (FTIR) (model: JASCOFTIR-6600typeA).

3.3 Methods

3.3.1 Pre-treatment of Raw Bone

The raw bone was washed with fresh water and boil in deionized water at 90 ^oC for 24 hr to remove the excess of organic matter. The process followed by washing with hot distilled water, ground in to granular particle then sieved to a particle size of about 1–2 mm then the surface of these bone granules were treated with 0.5M HCl, washed using hot distilled water to remove the remains impurity (Rojas-Mayorga et al., 2015). Whatman filter paper was used as filter after the samples washing. Then dried in oven at a temperature of 105 ^oC overnight, continue until no change in weight observed, as shown in the figure 3.1. Finally, the sample was stored in plastic container.

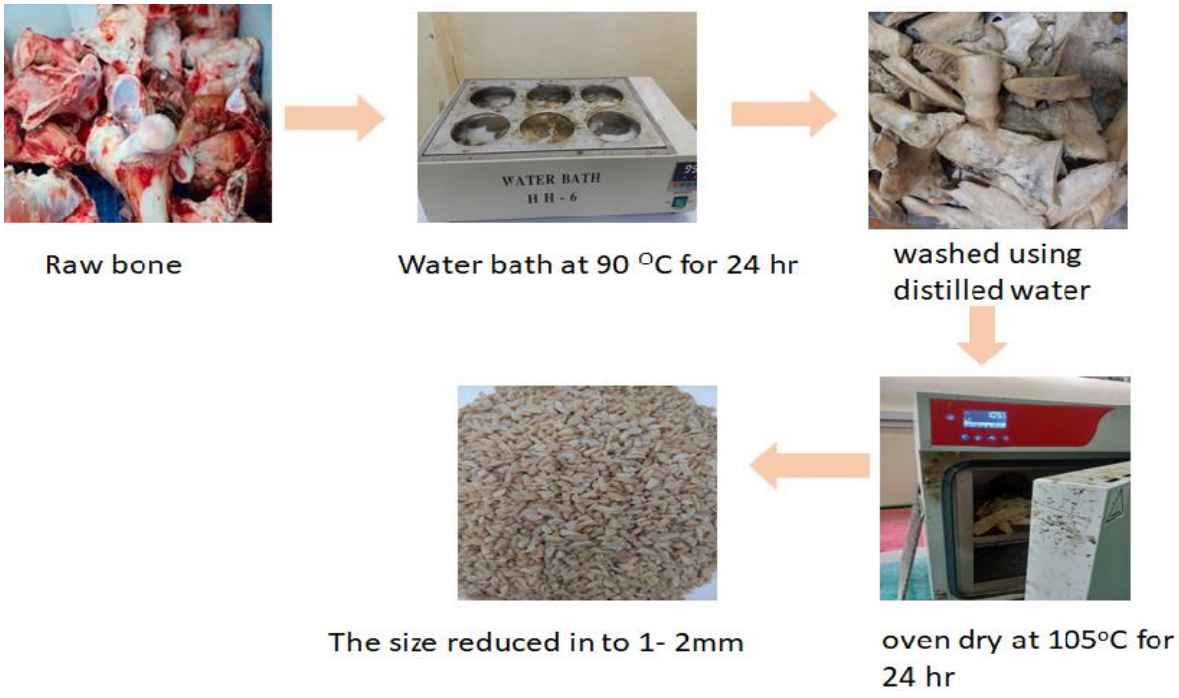

Figure 3. 1 Schematic representation of the pretreatment of raw bone

3.3.2 Synthesize Bone char

The treated raw bone was transferred to the furnace to carry out the calcination at the temperatures 450, 500, 550,600,650,700, 750 and 800 °C for the residence time 1,2, 3 and 4 hrs was prepared by modifying the earlier procedure (Alkurdi et al., 2019b). The optimization was done using one factor at a time and it was identified through the adsorption test. The calcination reaction was take place in muffle furnace at 600°C for 2hr and cooled until came to room temperature, the bone char was ground to pass through an 80-mesh sieve.

A portion of 60 g of BC and 500 mL of 0.1M HNO_3 solution add into beaker, which was placed on top of a stirring hot plate, the solution was heated at 80 °C and continuously mixed for 24 hr. Then the bone char was washed with deionized water several times to remove the excess acid present on the surface and oven dry at 80 °C for 24 hr, as shown in the figure 3.2. Finally stored in air tight low density plastic bag for later experiments.

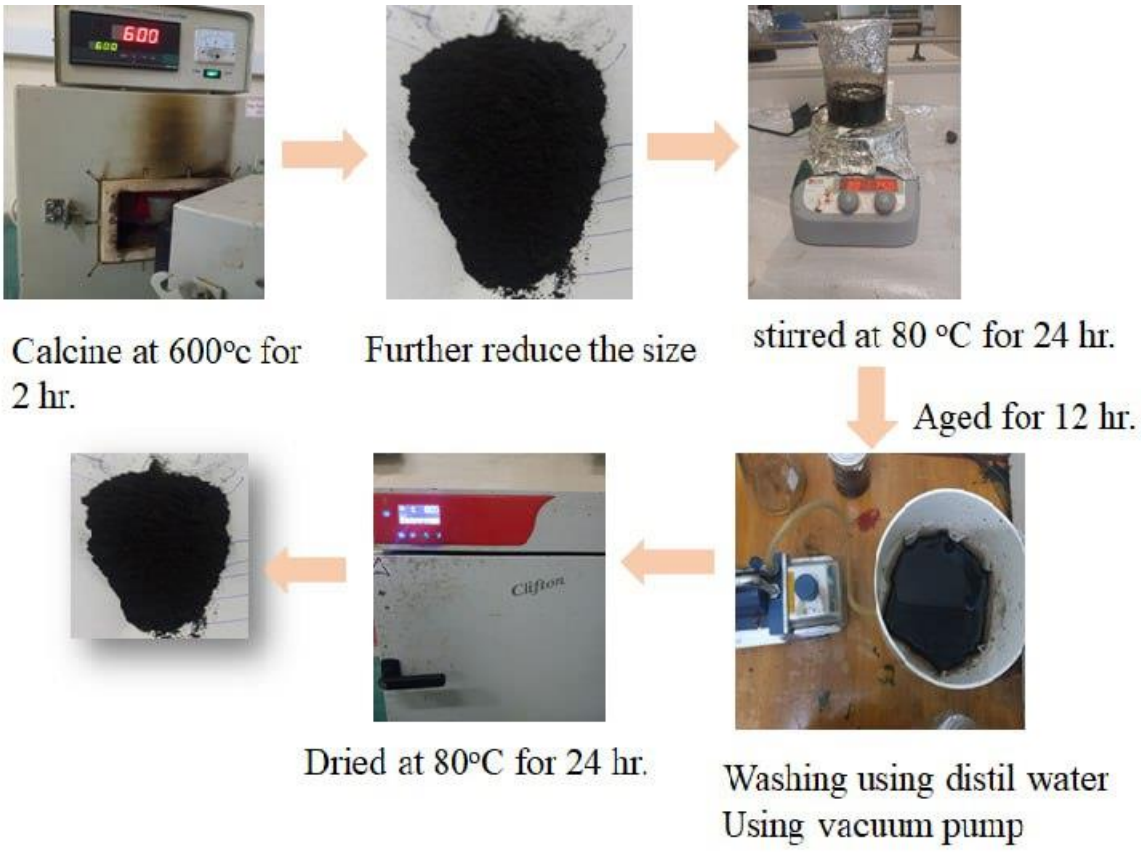

Figure 3. 2 Schematic representation of the preparation of bone char

3.3.3 Synthesize Zeolite Y

The kaolin was collected from Di Yuan Ceramic factory. Zeolite Y was synthesized from kaolin using alkali fusion method by earlier procedure (Ayele et al., 2016). At the beginning, the kaolin powder was crushed and sieved to have uniform size. The sample of 40g kaolin powder was activated by means of mechanical methods by crushing and mixing kaolin with 60g of NaOH for 30 min followed by calcining at 600 ^{o}C for 1 hr, the kaolin powder and NaOH was mixed in the ratio of 1.5 (Sodium to kaolin). The fused product (Metakaolin) was grounded using mortar and pestle then mixed with (400ml) distilled water at 50^{o}C for 2 hr in hot plate with stirring at 600 rpm for gel formation. The formed gel was aged at room temperature for 24 hr after that crystallization was takes place in water bath under static condition for 9 hr at 94.2 ^{o}C then aged until its came to room temperature, as shown in the figure (3.3). The solution was filtered out and washed several time until the pH reaches neutral. Finally, the product was dried in oven at 80 ^{o}C for 24 hr then stored in airtight low density plastic bag for later experiments.

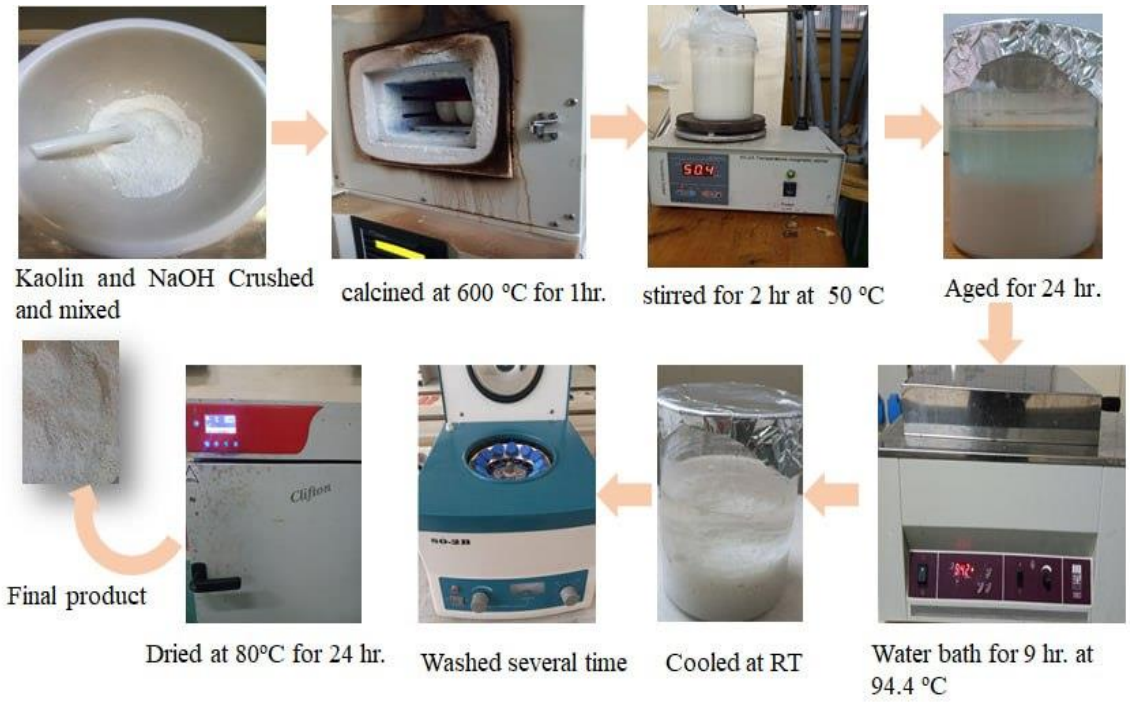

Figure 3. 3 Schematic representation of the preparation of Zeolite Y

3.3.4 Synthesize of Aluminum Loaded Zeolite Y

Aluminum loaded zeolite was prepared at room temperature and atmospheric pressure according to (Du et al., 2017).Wet impregnation method was used to synthesize aluminum loaded zeolite Y. As shown in the figure 3.4, 300 ml of 0.6M solution of aluminum chloride was added slowly in zeolite solution while stirring. After addition of aluminum chloride to the zeolites, the pH of the mixture was adjusted immediately to 5.3 with 5-M sodium hydroxide continually for 24 hr, this pH adjustment is to enhance the precipitation of AlOOH on zeolite Y surface. Then precipitate was dry in oven at 70 ^{o}C for 24 hr. Finally, the dried aluminum coated zeolite Y was washed with deionized water three times followed by ethanol to avoid contamination of sodium ions. Finally, the solid was dried at 60 ^{o}C for 24 hr, ground to pass through an 80-mesh sieve, and store in an airtight container for later experiments.

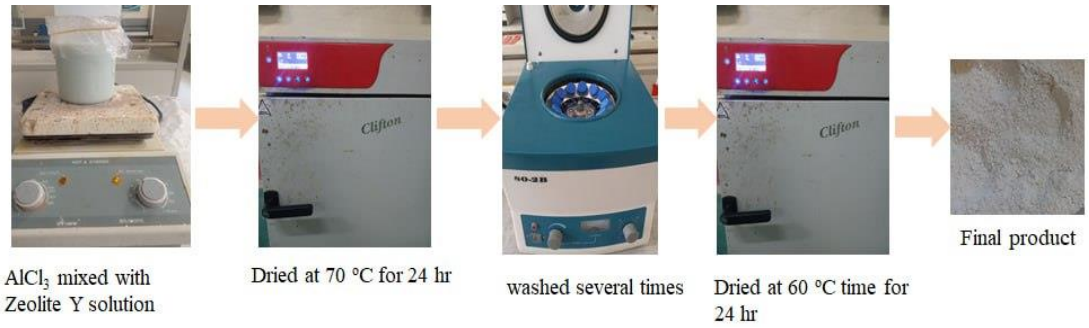

Figure 3. 4 Schematic representation of the preparation of Aluminum loaded zeolite Y

3.3.5 Synthesis of Bone char (BC)/Aluminum Loaded on Zeolite Y (AZ) Composite

Bone char/Aluminum loaded Zeolite Y Composite was synthesized by physical mixing. Typically, different weight ratio (1:1, 1:3, 3:1) of bone char to aluminum loaded zeolite Y samples Sonicated in 30 ml ethanol solution for 40 min then stirred further for 1 hr. Finally, the solution dried in oven at temperature of 60 ^{o}C for 24 hr, as shown in the figure 3.5. Then stored in plastic bag for further use.

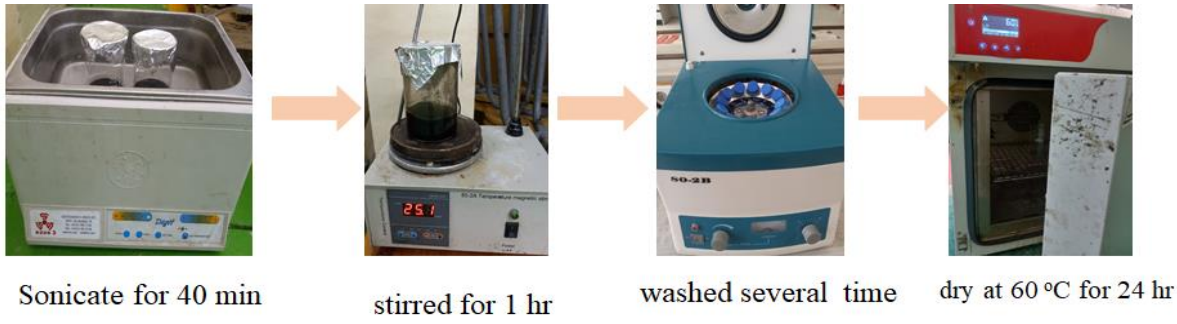

Figure 3. 5 The schematic representation of the preparation of bone char/aluminum loaded zeolite Y composite

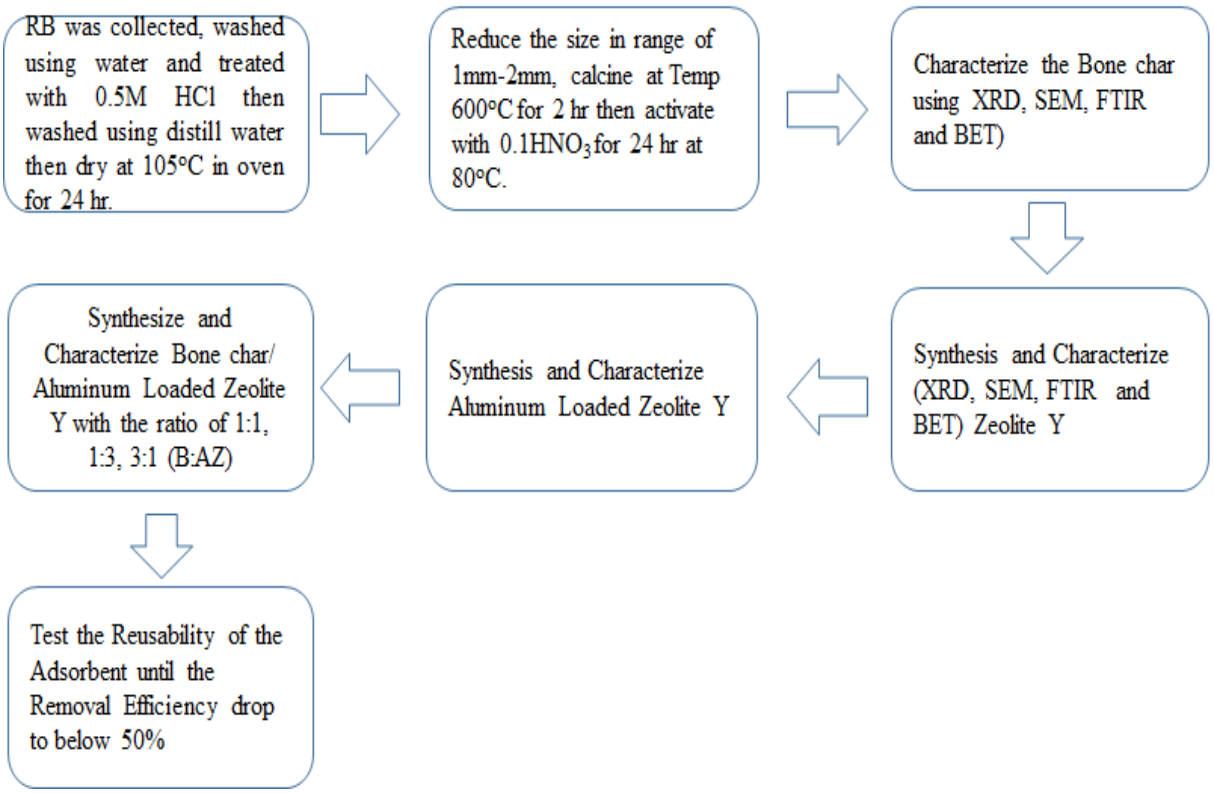

Figure 3. 6 Overall process of the experiment

3.4 Determination of Point of Zero Charge (PZC)

The point of zero charge of BAZ composite was determined using salt addition method. Typically, 40 mL of 0.1 M $NaNO_3$, 40ml of 0.1M NaOH and 0.1M HNO_3 were prepared in 10 different Erlenmeyer flasks and the initial pH of the solutions were adjusted to values from 3 to 12. Following that, 0.1 g of BC/AZ was added to each solution and shaken, at temperature of 30°C for 24 hr. Then, the solution was filtered using filter paper and final pH values were measured, as shown in the figure 3.7. The Pzc was obtained from the graph of ΔpH obtained by plotting the initial pH versus the solution pH at equilibrium (Wirtu et al., 2021a).

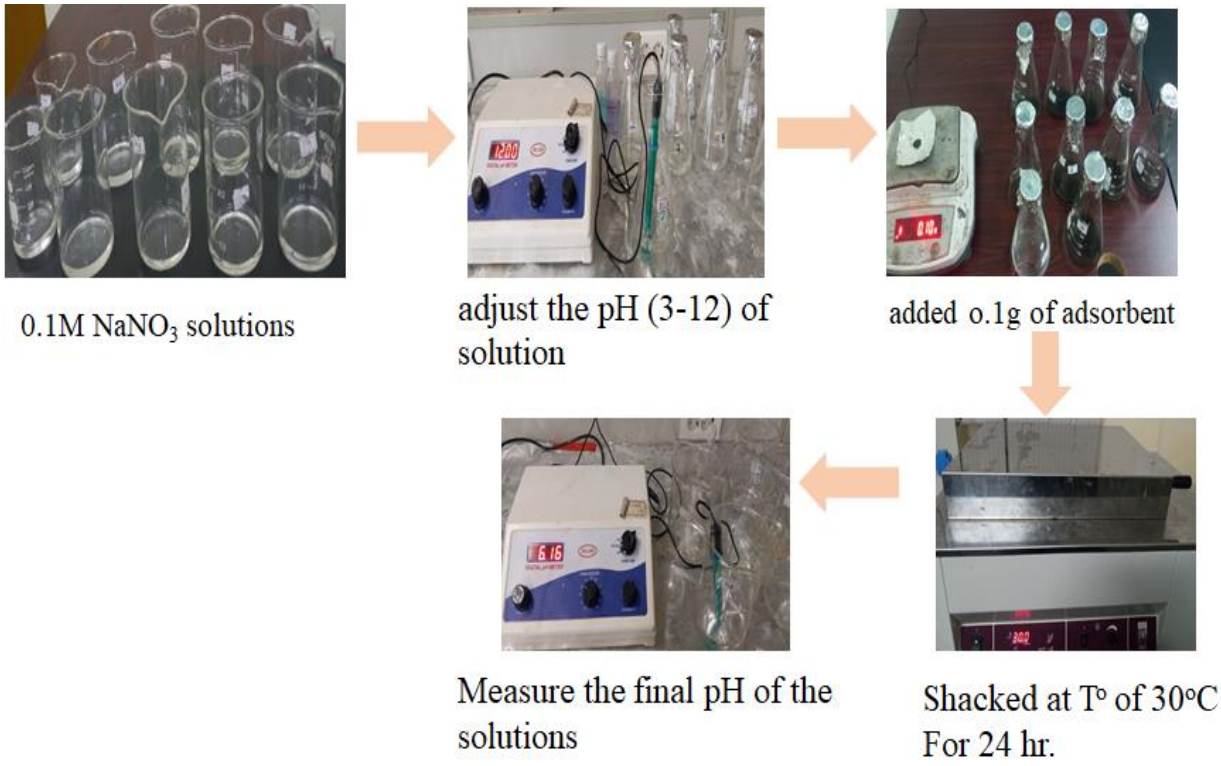

Figure 3. 7 Schematic representation of determination of PZC of the composite

3.5 Instrumentation Techniques

3.5.1 X-ray Diffraction (XRD) Instrument

X-ray scattering instrument is non-destructive analytical techniques, which provide information about the crystallographic structure. X-ray crystallography has two main purpose, namely fingerprint characterization of crystalline materials, and determination of their structure. When a beam of X-ray strikes the crystal, it gets scattered elastically into many specific directions, with its wavelength remaining unchanged.

A Crystalline phase of raw bone, bone char, Zeolite Y, Aluminum loaded zeolite Y and Bone char/Aluminum loaded zeolite composite were identified by powder XRD (XRD 7000S). The measurement condition for each test includes voltage = 40.0 (kV), current = 30.0 (mA), and scan range from 10.00 to 70.00 with 0.02 step size.

The average particles size are calculated by using Scherrer equation (Abraha, 2015).

$$D = \frac{K.\lambda}{\beta Cos\theta} \quad \text{.....Eq(3.1)}$$

Where, D is crystalline size, K = (0.9) is a Scherrer constant, λ is the wavelength of the x-ray, θ is Bragg angle of corresponding diffraction peak and β is full width at half maximum (FWHM)

$\lambda = 2dsin\theta$……..Eq(3.2)

Where: n = an integer tells "order" of reflection, λ = the wavelength of the incident X-rays,

d = inter planar spacing of the crystal and θ = the angle of incidence.

3.5.2 Fourier Transform Infrared Spectroscopy (FTIR) Instrument

FTIR has significant use for identifying chemicals that are either organic or inorganic. It can be used to quantify certain components within an unknown mixture. FTIR is the most useful tool for identifying types of chemical bonds (functional groups). Analysis functional group of raw bone, bone char, Zeolite Y and bone char/Aluminum loaded zeolite Y before and after treated. FTIR spectra of pure compounds are unique; they are like a molecular "fingerprint".

The attenuated total reflectance FTIR with model name FTIR-6600 type A and serial number A013861790 was used in the range of 4000 to 500 cm^{-1}. The sample for the FTIR analysis was prepared by weighting the amounts of sample, 1 gm, and Potassium Bromide (KBr) powder, 100 gm into an agate mortar. The FTIR pattern is plotted within the FTIR machine by generating the transmittance peaks (%) as the Y-axis versus wavenumber (cm^{-1}) as the X-axis.

3.5.3 Scanning Electron Microscope Analysis (SEM) Instrument

A scanning electron microscope (SEM) is a type of electron microscope that determine the images a sample by scanning it with a high-energy beam of electrons in a raster scan pattern. The electrons interact with the atoms that make up the sample producing signals that contain information about the sample's surface topography or morphological change. Analysis morphology of raw bone, bone char, Zeolite Y, Aluminum loaded zeolite Y and bone char/aluminum loaded zeolite Y before treatment.

3.5.4 Thermo-Gravimetric Analysis (TGA) Instrument

The thermogravimetric analysis and thermal stability of raw bone, Kaolinite and bone char/aluminum loaded zeolite Y samples were carried out using a thermogravimetric analyzer. The Nitrogen gas was used as carrier gas and the heating rate was set at 20^{o}C/min to determine the thermal stability of 10 mg of raw bone. The temperature was adjusted between 100 ℃ to 1000 ℃ and the decomposition of sample weight (%) against temperature (℃) was recorded.

This analysis resulted in two types of curves, the TGA curve and the derivative of the Thermogravimetric (DTG) curve.

3.5.5 Brunauer-Emmett-Teller (BET) Instrument

The textural properties of BC, Zeolite Y, Aluminum loaded zeolite Y (surface area, pore volume, and average pore diameter) were determined by the N2-BET method using a surface area and porosimetry analyzer (SA-9600 Series, Horiba Instruments, Inc.) at 200 ^{o}C degassing temperature for 2 hr in the presence of nitrogen gas.

3.6 Determination of Fluoride Concentration

3.6.1 Reagents and Stock Solutions

A stock solution of 1000 mg/L sodium fluoride solution was prepared by dissolving 2.21 g of anhydrous sodium fluoride (NaF previously dried for 2hrs at 105 ^{o}C and cooled in desiccators) in distilled water (Kadioglu et al., 2015). Standards at required concentration (2 mg/L, 4 mg/L, 6 mg/L, 8 mg/L, 10 mg/L and 12 mg/L) were prepared by appropriate serial dilution from the stock solution with distilled water.

3.6.2 Preparation of TISAB

TISAB was prepared by dissolving 56 g sodium chloride, 7 g hydrated trisodium citrate (Na3C6H5O7. 2H2O), 2 g ethylene di-amine tetra acetic acid (EDTA) (C10H16N2O8) in 500 mL de-ionized water. After shaking and stirring for 10 minutes the solution was mixed with 57 mL glacial acetic acid in a 1000mL volumetric flask. The pH was adjusted to 5.3 using 5 M sodium hydroxide and 1 M hydrochloric acid (Agarwal et al., 2003).

3.6.3 Calibration of Fluoride Ion Selective Electrode

Standard fluoride solutions were prepared from 1000 mg/L of sodium fluoride stock solution by diluting with double distilled water. 2 mL of TISAB was added to 2 mg/L, 6 mg/L, 8mg/L, 10mg/L, 12 mg/L and 14 mg/L standard fluoride solution. The ISE was placed in the beakers containing 10 mL of standard fluoride solutions and continuous shaking for 30 min at room temperature. The Px readings for each concentration were noted and calibration curve of Px (reading) versus the concentration of fluoride (mg/L) was plotted in figure 3.8. The coefficient of determination (R^2) value of the graph is 0.9806, which indicating that the equation highly effective in determining the unknown concentration.

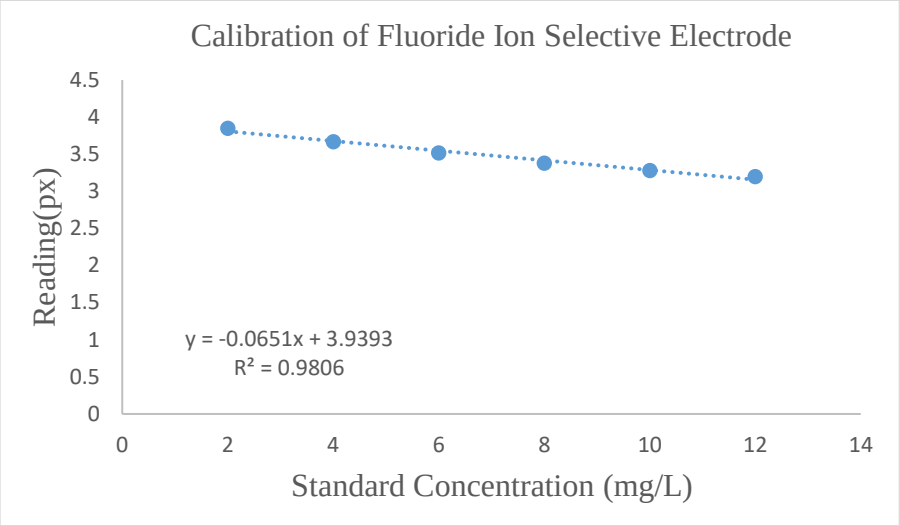

Figure 3. 8 Fluoride ion selective electrode calibration curve

3.7 De-fluoridation Studies

De fluoridation study was conducted in batch experiments for bone char/ aluminum loaded on zeolite Y with different controller parameter (adsorbent dosage, contact time and pH of the solution). The solution pH was adjusted using the addition of 0.1 M HNO_3 and NaOH. The experiment was conducted based on the design expert data to obtain the optimum condition of the parameters.

The amount of fluoride adsorbed per unit mass of adsorbent (capacity, qt), equilibrium adsorption capacity (qe) and fluoride removal efficiency (% R) relative to the initial concentration of the system was calculated as:

$$Q_e = \frac{(c_o - c_e)\times v}{M} \quad \text{.....Eq(3.3)}$$

Where, C_o and C_e are the initial and final equilibrium concentration of adsorbate (mg/L), V is volume of the solution (L) and M is the weight of dry adsorbent (g).

The amount of adsorbate adsorbed, Q_t (mg/g) at any time can be calculated using Equation below.

$$Q_t = \frac{(c_o - c_t)\times v}{M} \quad \text{.....Eq(3.4)}$$

Where, C_t is the concentration of adsorbate (mg/L) at any time.

The percentage removal of F^- ion from the solution was calculated by the following equation.

$$\%\text{Removal} = \frac{(c_o - c_t)}{c_o} \times 100 \quad \text{.....Eq(3.5)}$$

Where, C_0 (mg/L) is the initial F^- ion concentration and C_t (mg/L) is the final F^- ion concentration in the clarification.

3.8 Design Experiments

3.8.1 Response Surface Method

The effect of three factors (adsorbent dosage, contact time, and pH of solution were studied on the adsorption test for fluoride removal capacity. The studied response was fluoride removal efficiency. Levels of each factor is tabulated in the following table below; levels of factors were tested in preliminary experiment. The adsorbent dosage is start from 0.5- 4g with initial fluoride concentration of 10 mg/L were performed at contact time vary from 0 to 120 min under the pH range of solution 3-12. Totally, 20 experiments were performed.

Table3.1: Level for each factors

NO	Factors	Units	Level	
			Low	High
1	Adsorbent Dosage	g	0.5	4
2	pH range of the solution	-	3	12
3	Contact time	Min	0	120

Design Expert® version13 software was used to randomize design of the experiment and analysis of variance (ANOVA) was used for statistical significance of the experimental data. The experimental design involved three factors with two levels; adsorbent dosage, contact time and pH range was taken as independent variables and fluoride removal efficiency the output response.

3.9 Effect of Different Parameters on Fluoride Removal Efficiency

Different factors affect the defluoridation efficiency of an adsorbent including mixing ratio, adsorbent dose, pH level of the solution, initial fluoride concentration and contact time are main factors that should be deal during removal of fluoride.

3.9.1 Effect of Mixing Ratio bone char and aluminum loaded zeolite Y

Bone char and aluminum-loaded zeolite Y are both materials commonly used for fluoride removal. Bone char is known for its high affinity for fluoride ions, while aluminum-loaded zeolite Y can also adsorb fluoride effectively. The bone char and aluminum-coated zeolite was mixed with different ratio of (1:1, 1:3 and 3:1) (Bone char to Aluminum coated zeolite Y). The effect of mixing ratio and pure individual adsorbent were studied in batch experiment and screened out the best adsorbent, which have maximum adsorption capacity.

3.9.2 Adsorbent Dosage

The effect of adsorbent dose on the adsorption capacity and adsorption efficiency were carried out in batch adsorption experiment using 0.5 g, 1 g, 1.5 g, 2, 2.5, 3, 3.5 and 4g of the selected adsorbent ratio 0.5g/200ml of 10 mg/L fluoride ion solution at 1 h contact time and pH of the solution is 7.5.

3.9.3 Effect of Contact Time

The influence of the contact time of the adsorbent on the fluoride removal was investigated by varying the contact time from 20, 40, 60, 80, 100 and 120 min in order to investigate the effect of contact time. The batch adsorption experiments were conducted at optimum condition of adsorbent ratio 0.5g/200ml of 10 mg/L fluoride ion and pH of the solution is 7.5.

3.9.4 Effect of Initial Fluoride Concentration

The influence of raising fluoride initial concentration on the removal efficiency of the adsorbent was determined using synthetic water (5, 10, 15, 20, 25, and 30 mg/L). The batch adsorption experiments conducted at optimum contact time, pH of the solution and dosage.

3.9.5 Effect of pH of the Solution

Effect of pH was studied by varying the initial solution pH from 3 to 12, using 0.1 M HNO_3 or 0.1 M NaOH and keep the other parameters constant.

3.10 Adsorption Equilibrium Isotherms

Isotherms are the relationship between the equilibrium adsorbate concentrations in the liquid-phase and the equilibrium adsorption amount on the solid-phase at a known temperature. Researchers can use isotherms to model equilibrium adsorption data and explore adsorption information, including adsorption mechanisms, maximum adsorption capacity, and adsorbent properties (Wang & Guo, 2020a). Adsorption isotherm can be described as a curve that explains the phenomenon governing the retention (release) or mobility of a substance to a solid at constant

temperature and pH in an aqueous porous medium or aquatic environment (Berkessa et al., 2019).

3.10.1 Langmuir Isotherm

A monolayer of adsorption is assumed by the Langmuir isotherm on a uniform surface with a finite number of adsorption sites. No more sorption can occur at a location once it has filled (Nsami & Mbadcam, 2013). The linear form of an isotherm can be expressed as:

$$\frac{C_e}{q_e} = \frac{1}{Kq_{max}} + \frac{C_e}{q_{max}} \quad \text{.....Eq(3.6)}$$

Where, q_e (mg/g) is the quantity of adsorbate adsorbed on the adsorbent surface at equilibrium, q_{max} (mg/g) is the adsorbent's maximum adsorption capacity, and k (L/mg) is a Langmuir constant indicating the affinity of binding sites (Chahkandi et al., 2021).

3.10.2 Freundlich Adsorption Isotherm

The Freundlich isotherm, which applies to both monolayer (chemisorption) and multilayer adsorption, is based on the hypothesis that the adsorbate adsorbs onto the heterogeneous surface of an adsorbent (physisorption)(Ho et al., 2002). The Freundlich model's linearized form is written as:

$$\log q_e = \log K_f + \frac{1}{n} \log C_e \quad \text{.....Eq(3.7)}$$

Where, qe (mg/g) is the quantity of adsorbate adsorbed at equilibrium, K_f (mg/g) denotes the adsorption capacity, and $\frac{1}{n}$ denotes the Freundlich intensity factor, which indicates if an adsorption process is feasible (Chahkandi et al., 2021).

3.10.3 Temkin Isotherm Model

The Temkin isotherm assumes that the heat of adsorption is a function of the surface coverage with proportional linear relationships, taking into account interactions between adsorbent and adsorbate(Asmellash & Ayele, 2022). The Temkin isotherm has been used in the following equation.

$$q_e = B\, lnK_t + B\, lnC_e \quad \text{.....Eq(3.8)}$$

Where: B = $\frac{RT}{b}$; R is the gas constant (8.31 J/mol K), q_e is as defined before and T is the absolute temperature in K, K_T is the equilibrium binding constant (L/mg) related to the maximum binding energy, and B is related to adsorption heat.

3.11 Adsorption Kinetics Studies

Adsorption kinetics reflects the elaboration of the adsorption process as a function of time. Several models have been developed that describe the diffusion of solutes on the face of particle and within pores (similar as film distribution models, intra-particle diffusion models, out- of-diffusion models, and pore diffusion models) (Battas et al., 2019).

3.11.1 Pseudo–First-order Kinetic Model

In order to investigate the controlling mechanism of adsorption processes similar as mass transfer and chemical response, the pseudo-first-order and pseudo-second order equations were applied to model the kinetics of fluoride adsorption onto bone charcoal powder. This model is also known as Largergren model, proposed in 1898, which assumes a first order adsorption kinetics and can be represented by equation given below (Akbari et al., 2018)(Wang & Guo, 2020b).

$$\log(q_e - q_t) = \log(q_e) - \left(\frac{K_1}{2.303}\right)t \quad \text{.....Eq(3.9)}$$

Where: q_e = the amounts of fluoride ions adsorbed at equilibrium (mg/g), q_t = the amounts of fluoride ions adsorbed at adsorption capacity (mg/g), t = the adsorption at time, K_1 = the kinetic constant of pseudo-first-order adsorption (min^{-1}). The plot of log (qe – qt) versus t should give a linear relationship from which K_1 and q_e can be determined from the slop and intercept of the plot.

3.11.2 Pseudo–Second-Order Kinetic Model

The pseudo–second-order kinetic model is based on the assumption that the rate-limiting step is chemical sorption or chemisorption and predicts the behavior over the whole range of adsorption (Krstić, 2021).

The equation for the pseudo–second-order is given by

$$\frac{\mathrm{Dqt}}{\mathrm{dt}} = \mathrm{K_2(qe + qt)^2} \quad \text{.....Eq(3.10)}$$

After mathematical development, and taking into account the boundary conditions, the pseudo second order kinetic model is eventually expressed as follows

After mathematical development, and taking into account the boundary conditions, the pseudo–second-order kinetic model is finally expressed as follows:

$$\frac{t}{qt} = \frac{1}{K2qe^2} + \frac{t}{qe} \text{ With, h= } \mathrm{K_2}\, qe^2 \quad \text{.....Eq(3.11)}$$

Where: h is the initial sorption rate, qe is the amount of fluoride adsorbed at equilibrium $\left(\frac{\text{mg}}{\text{g}}\right)$ K_2 is the equilibrium rate constant of the pseudo– secorder model $\left(\frac{\text{g}}{\text{mg min}}\right)$. The plot of $\frac{t}{qt}$ as a function of time should give a linear relationship. From the slope $\frac{1}{qe}$ and the intercept 1/h or $1/(k_2 q_e^2)$, we can calculate the amount of adsorbate adsorbed at equilibrium and gives k_2, the second-order rate coefficient (Bullen et al., 2021).

3.11.3 Intra Particle Diffusion Model

Ions are transferred from the aqueous phase to the surface of the adsorbent as a result of the batch reactor's rapid churning. If the adsorbent is porous, the ions may then diffuse into the particles. The formula (Weber and Morris, 1963) mentioned in can be used to express the intra-particle diffusion (Phawachalotorn et al., 2023):

$q_t = k_p t^{0.5} + C$.....Eq(3.12)

Where, q_t is the amount of P(V) adsorbed (mg/g) at a given time t (min); k_p is the intra-particle diffusion rate constant; and C (mg/g) is the intercept of the intra-particle diffusion model. The plots of q_t versus $t^{0.5}$ yield straight lines passing through the origin and the slope gives the diffusion rate constant, k_p.

3.12 Adsorption Thermodynamics

For the process to be spontaneous, the thermodynamic requirement is that ΔG, must be added at a constant temperature and pressure, i.e. the Gibbs energy decreases. According to the equation,

$\Delta G = \Delta H - T\Delta S$ …….…….…….....Eq(3.13)

If ΔH has a sufficiently high negative value - ΔG can be negative because TΔS is positive. Therefore, the spontaneous adsorption process is a combination of these two factors is added ΔG. As adsorption proceeds, ΔH becomes increasingly negative, eventually ΔH becomes equal to TΔS, and ΔG becomes zero (Ibrahim & Bsharat, 2018).

3.13 Effect of Competitive Ions

To study the co-existing of ions three different ions such as Nitrate, chloride and Hydro carbonate were selected, which are commonly present in water, and competes with fluoride during the adsorption process (Alkurdi et al., 2019a). The sources of the ions include ($NaNO_3$), NaCl and Na_2CO_3 respectively. For each ions, 8 mg/L of each initial concentration for optimum 10 mg/L

of initial fluoride concentration conducted based on work (Alkurdi et al., 2019a). The adsorption of co-existing ions were involved at optimum operating parameters.

3.14 Regeneration of Adsorbent

After the adsorption process, BAZ placed in contact with a new fluoride solution, under the same conditions, to fully saturate the adsorbent (Du et al., 2015). The saturated BAZ was abundantly wash with deionized water to remove the excess of fluoride on the adsorbent surface. Afterwards, the saturated adsorbent dried in an oven at 60 °C for 24 h. Then 0.5g/200ml of saturated BAZ placed in contact with 0.5M NaOH solution (0.1 M) over 2 h, at constant stirring and temperature (200 rpm and 25 °C). After the regeneration process, the BAZ samples washed with deionized water until the stabilization of the pH (around 7), dry at 60 °C for 24 h and submit to new adsorption cycle using a 10 mg/L fluoride solution and solid/liquid ratio of 0.5 g/L. The recycle continue under the same condition until the adsorption efficiency is below 50%.

Chapter Four

4. Results and Discussion

4.1. Evaluation of Bone char on Removal of Fluoride

The removal efficiency of bone char is highly depending on calcination temperature and calcination time, the process of calcination has several purposes to bone char. Firstly, it activates the material by removing impurities and volatiles, resulting in increased surface area and pore volume. This activation enhances the adsorption capacity and efficiency of bone char calcination eliminates organic matter present in the bone char through high-temperature combustion. Generally, the calcination temperature and the duration of calcination affects the extent of activation and the degree of structural modifications. It is important to carefully optimize these parameters to achieve the desired properties and performance of the bone char (Alkurdi et al., 2020b; Patel et al., 2015)

4.1.1 Effect of Bone char Calcination

As shown in figure 4.1(a), it is observed that the bone char produced at a temperature of 600^{o}C for a calcination time of 2 hr had the highest adsorption capacity of fluoride ion. The temperature below 600 ^{o}C has lower adsorption capacity due to the presence of organic, impurities and volatile components. When the calcination temperature exceeds 600°C, the efficiency of fluoride ion removal by bone char decreases. The smallest removal efficiency of the bone char was obtained at a calcination temperature of 900^{o}C. This is probably because of the high temperature degradation of surface functional groups. Moreover, at high temperatures the hydroxyapatite structures are assumed to be damaged since high temperature tend to collapse the hydroxyapatite structure resulting in losing ions that play role in ion exchange (Patel et al., 2015).

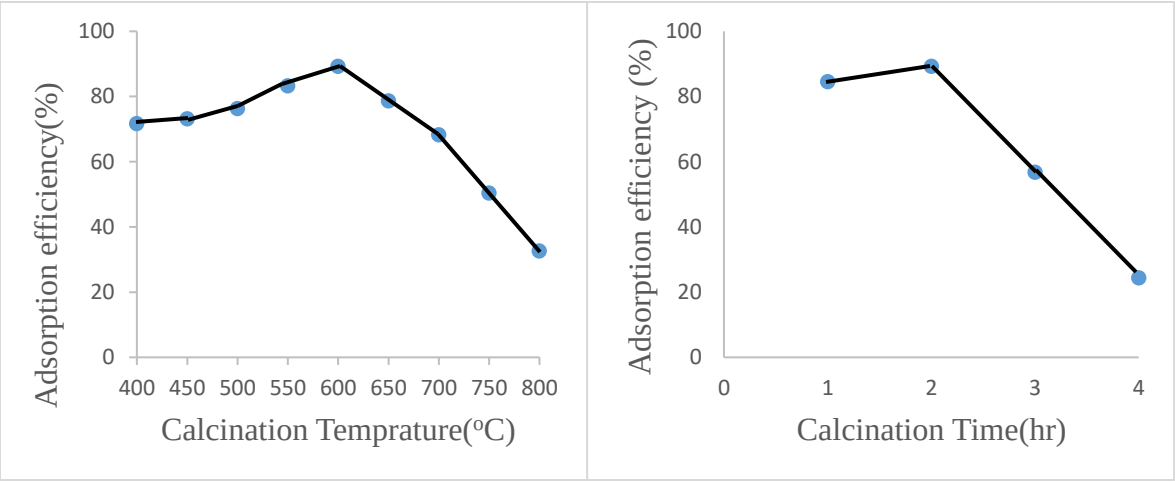

a) b)

Figure 4.1: Effect of Calcination temperature (a) and (b) calcination time on bone char removal efficiency

4.1.2 Effect of Calcination Time

The temperature with the highest adsorption efficiency was selected to examine the influence of time on the fluoride ion removal efficiency of bone char. As it is shown in Figure 4.1(b) the effect of calcination time on the adsorption capacity of bone char is not significant compared to the effect of temperature. The results in general show that, as the time of calcination for a given constant temperature activation increases the adsorption efficiency tends to decrease. This implies that production of a bone char at a given temperature for a prolonged time has a negative impact on the active surfaces of the bone char.

4.2 Characterization of Adsorbents

4.2.1 X- Ray Diffraction (XRD) Analysis

The XRD patterns of Raw Bone (RB), Bone char (BC), Zeolite Y, Aluminum coated zeolite Y, and composite of Bone char/Aluminum Loaded Zeolite Y samples were analyzed. Powder XRD (Shimadzu XRD-7000 X-ray diffractometer using Cu-Kα radiation) was used to determine sample crystallinity throughout this work. The XRD patterns confirmed that the diffraction peaks correspond to the crystal structure and phase purity of synthesized material. The diffraction peak of raw bone consists of a poorly crystalline phase compared to the bone char as shown in the figure 4.2 (a). This is probably due to the presence of organic substances resulting in less or relatively no visible peak splitting. A decrease in the peak width and a considerable increase in the peak height were observed with bone char. This indicates an

increase in the crystallinity. The peak positions for 2θ angles for raw bone 25.90, 31.02, 40.1, 46.58 and 49.6 and Figure 4.2 (b) locate at 2θ (degree) of 25.81, 31.71, 31.71, 39.61, 34.1, 39.9, 46.7, and 49.5 were assign to the planes (002), (211), (112), (130), (202), (310), (222), (213) respectively. It is a good match with XRD standard card number (82-1943) this show that bone char was synthesized effectively. Moreover, there was no impurity phases are formed (J. Huang et al., 2014).

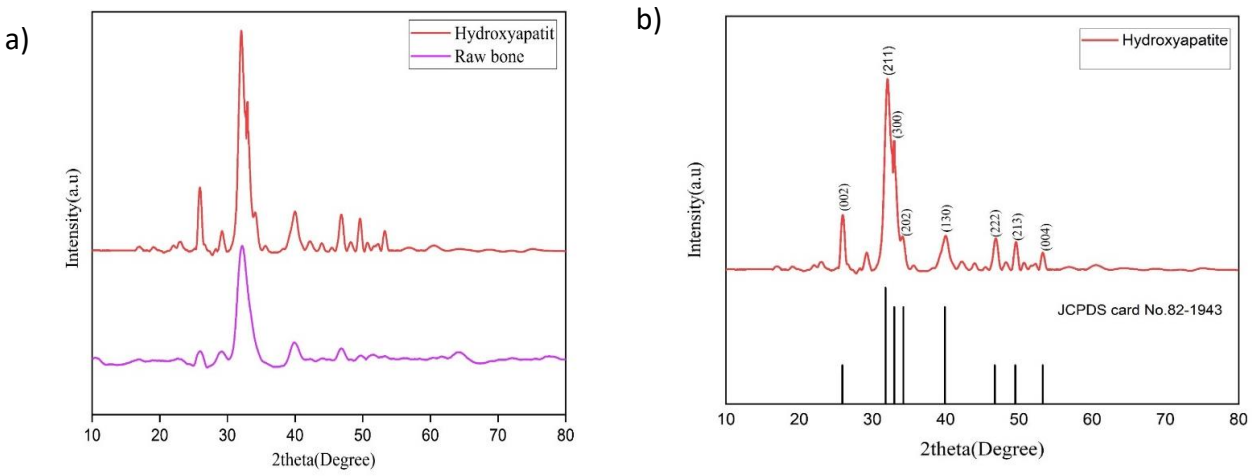

Figure 4. 2: XRD pattern of a) raw bone and bone char b, Hydroxyapatite with standard patterns from JCPDS card No of 82-1943

As shown in the figure 4.3(a), the Kaolin has many sharp peaks, which contains the kaolinite the main minerals and the quartz impurity. The x-ray diffraction analysis of the peaks shows a sharp peak with high intensity at 2θ = 12.34^{o}, the main peak used to identify kaolinite clay. Beside the kaolinite the 2θ angle at 38.67^{o} profiles, correspond to that of quartz impurity. These results are in agreement with (Ayele et al., 2015). Kaolinite and quartz are the dominant characteristics of natural kaolin (Treacy & Higgins, 2007). XRD pattern of Zeolite Y are shown in figure 4.3 (b) well known peaks were located at the diffractogram of synthesized Zeolite Y shows the presence of distinctive diffraction peaks at 2θ = 6.2°, 10.1°, 11.8°, 20.2°, 23.5°, 26.9°, 30.5°, 31.2°, and 32.2° corresponding to (111), (220), (311), (440), (533), (642), (822), (555) and (840) respectively (Rachman et al., 2018). The strongest peak for each zeolite Y was observed at 2θ=6.2, 23.5 and 31.2 then 2θ = 6.33˚, 26.8 and 31.2 for Zeolite Y which indicate high crystallinity.

Figure 4.3(c) shows the XRD pattern of aluminum loaded zeolite, aluminum inserted as extra-framework species (e.g., as aluminum cations). The aluminum incorporation can influence the nature and extent of the peak shift. The introduction of aluminum atoms into the zeolite framework alter the lattice parameters, resulting shift in the peak positions compared to the standard zeolite Y pattern. The diffraction peak locate at 2θ= 6.14°, 12.26°, 15.25°, 16.6°, 19.42°, 23.46°, 26.84°, 31.06° ,33.52° and new peak formed at 68.26°. Moreover, AZ led to decreased crystallinity in the zeolite structure, this result in peak broadening, where the diffraction peaks become wider and less intense. The presence of broader peaks compared to pure zeolite Y suggested the incorporation of aluminum. Generally, AZ introduce new diffraction peaks and alter the intensity of existing peaks. These changes indicated the formation of new phases or the disruption of the original zeolite structure due to the incorporation of aluminum species confirm that aluminum loaded zeolite Y synthesized successfully.

Bone char and aluminum loaded zeolite Y composite have different XRD pattern compared to their pure form. Figure 4.3(d) shows the XRD pattern of the three ratios (1:1, 1:3, 3:1) of BC to AZ adsorbents. The B to AZ ratio (1:1) XRD pattern shows the XRD pattern of the composite would exhibit features from both components because the composite is composed of equal amounts of bone char and aluminum-loaded zeolite Y. However, the relative contribution of features from bone char and aluminum-loaded zeolite Y in the XRD pattern can depend on nature of zeolite Y and bone char. The bone char is significantly denser or has a higher X-ray scattering power than zeolite Y. its diffraction peaks appear more prominent in the XRD pattern, potentially dominating the bone char features. Because bone char is primarily composed of hydroxyapatite ($Ca_{10}(PO_4)_6(OH)_2$), has a higher density because of the presence of calcium, phosphorus, and oxygen atoms densely packed in its crystal lattice.

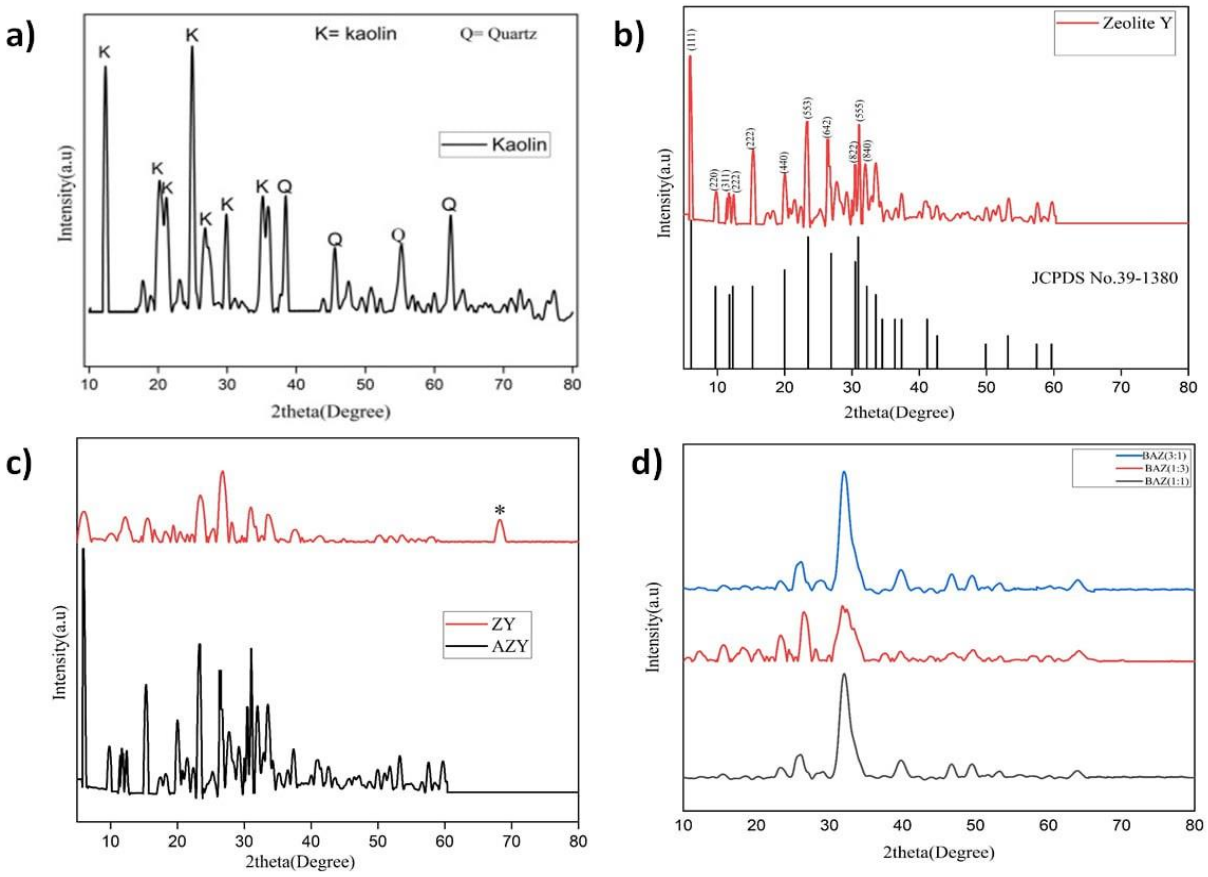

Figure 4.3: XRD pattern of a) kaolin, b) Zeolite Y(ZY), the standard patterns from JCPDS card No 39-1380 c) aluminum loaded zeolite Y (AZ), d) the composite of BAZ (1:1 BAZ, 1:3 BAZ, 3:1)

These elements contribute to a higher mass per unit volume, resulting in a higher density. On the other hand, zeolite Y is a porous material with a lower density compared to bone char. Zeolites are alumino silicate minerals consisting of a three-dimensional framework of interconnected channels and cavities.

The presence of these void spaces within the zeolite structure reduces its overall density. The composite of char/aluminum loaded zeolite Y with a 1:3 ratio, the basic observation were a predominance of the aluminum-loaded zeolite Y component over the bone char component since AZ (1:3) has higher proportion than BC. The presence of aluminum loaded onto zeolite Y influenced the XRD pattern of the composite, shifts in peak positions, broadening of peaks, or the appearance of new small peaks associated with the aluminum species and decrement in intensity is observed. The ratio (3:1) B to AZ, where bone char is in a higher proportion

compared to aluminum loaded zeolite Y. The XRD pattern is show the diffraction peaks associated with the crystal structure of bone char. These peaks are relatively stronger and more prominent compared to the zeolite Y peaks due to the higher concentration of bone char in the composite. The XRD pattern is exhibit diffraction peaks corresponding to the zeolite Y component. However, since zeolite Y is present in a lower concentration, its peaks relatively weaker compared to the bone char peaks. Moreover, shifts in peak positions, broadening of peaks, and the appearance of new peaks associated with the presence of aluminum in the zeolite Y phase is observed.

The crystallite size can be calculated by using Debye–Scherer strategy of equation (3.1), Where the crystal size is D, the X-ray wavelength is (1.5418 Å), the full-width half maximum of the diffraction peak is the β and the scattering angle is the θ (Rodriguez, Puzenat, & Thivel, 2016). As shown in Table 4.1 the crystalline size (D) of Bone char and Zeolite Y were calculated by using equation (2) and resulted in 5.001 nm and 42.5 nm respectively. The crystallite size of bone char is typically small because the carbonaceous material is amorphous, meaning it lacks a well-defined crystal structure. The lack of crystallinity in bone char contributes to its smaller crystallite size (Shahid et al., 2019).

On the other hand, zeolites are crystalline alumino silicate minerals. They have a well-defined crystal structure consisting of a three-dimensional framework of interconnected channels and cavities consisting silica, alumina, and other elements in the presence of water. Those Zeolite Y crystals formed through controlled crystallization which allows for the growth of larger, well-ordered crystals over extended periods. So larger crystallite of zeolite resulted. While Al loaded on Zeolite Y the crystallite size reduced to 22.5 nm. This were due to incorporation of Al in Zeolite Y disrupts the crystal lattice and introduces structural defects, which hinder the growth crystallite (Jamalluddin & Abdullah, 2014). Finally, crystallite size of BAZ composite with different ratio were calculated. It shows that as concentration of bone char reduced and amount Al loaded zeolite increased in the composite the larger crystallite size resulted.

Table4. 1: The average crystallite size, corresponding theta, FWHM for BC, Zeolite Y, AZ, 1:3BAZ, 1:1BAZ, 3:1BAZ

Sample name	Theta(degree)	FWHM Radians (β)	βcosθ	D-size (nm)
RB	32.23	0.028958	0.0289597	5.001
Zeolite Y	6.15258	0.0034	0.0034	42.5
Al + Zeolite Y	26.7792	0.00644	0.006435	22.5
3:1 BAZ	32.2347	0.0321	0.0321	4.5
1:1 BAZ	32.1221	0.0286	0.0286	5.064
1:3 BAZ	26.6675	0.0086	0.0086	16.84

4.2.2 Scanning Electron Microscope (SEM) Analysis

SEM was used to study surface morphology of Raw Bone, Bone char, Zeolite Y, Aluminum Loaded Zeolite Y and the composite of BAZ. As show in Figure 4.4 (a) needle like structure with less porosity and high agglomeration were observed for SEM image of raw bone (Baek et al., 2022) . When the bone is calcined, the bone char is less agglomerated with better dispersion and pore site observed (Figure 4.4b). This change were observed due to thermal decomposition and volatilization of organic components present in bone char, resulting in the collapse and shrinkage of the material. This can lead to a reduction in particle size. In addition, it may result in formation of new pore sites. The interconnected porosity makes it suitable for adsorption application. The morphology of Zeolite Y shows small sized cubic structure with interconnected pore sites which makes it suitable for adsorption (Figure 4.4 c). This zeolite's hierarchical porous structure makes it easier for molecules to diffuse into it more quickly, permitting more rapid adsorption kinetics (Taufiqurrahmi et al., 2011). For Al loaded ZeoliteY a small change in morphology were changed observed (Figure4.4 d). When Aluminum loaded it can substitute extra framework atoms, such as sodium (Na^+) or potassium (K^+) atoms which are originally present in the zeolite. Since Zeolite Y has a high surface area and a network of pores and channels. Aluminum hydro oxide species or smaller Al-containing molecules can be adsorbed onto the surface of the Zeolite Y or trapped within its pores. This adsorption process leads to the dispersion of aluminum species within the zeolite structure which partially block the pore site and form cluster (Dessalegne et al., 2017). The secondary composite of Bone char

with Al loaded Zeolite Y has the morphology of dispersed, less agglomerated, and porous structure (Figure4.4 e).

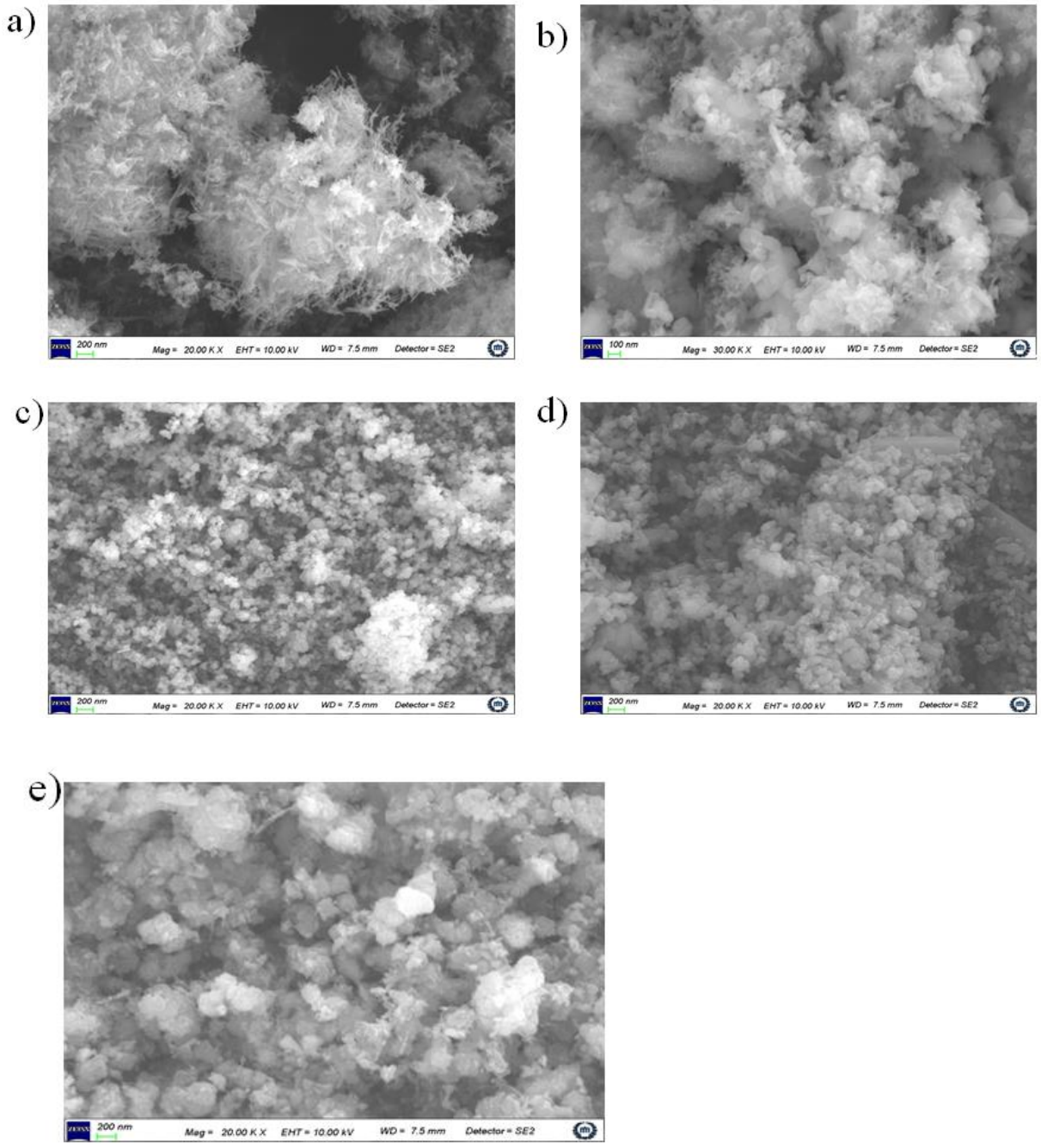

Figure 4.4:SEM image for a) Raw Bone, b) Bone char, c) Zeolite Y, d) Aluminum Loaded Zeolite Y , e) BAZ with 20KK Magnification

4.2.3 Fourier Transform Infrared Spectroscopy (FTIR) Analysis

The FTIR spectrum was used to identify the functional group of Raw Bone, Bone char, Zeolite Y, aluminum loaded zeolite Y and other impurity in the final product that was accomplished within 500 – 4000 cm^{-1}. Raw bone (RB) in Figure 4.5(a), the red line shows the FT-IR spectrum of the raw precursor where the broad band observed at 3445 cm^{-1} corresponding to the OH stretching vibration whereas 1650 cm^{-1} is been assigned to physically adsorbed water molecules (Guiar et al., 2005; Joschek et al., 2016). The absorption band at 2921 - 2854 cm^{-1} is assigned to the C-H stretching which were present in all samples with reduced intensities. The band of the phosphate group PO_4^{3-} was observed at 1023 – 921 cm^{-1}, the peaks of the carbonate group CO_3^{2-} are evident at 550, 1231 and 1442 cm^{-1}. The region 1950– 2200 cm^{-1} has a weak intensity band which is due to overtone (Ooi et al., 2007). Bone char (BC), purple line showed the band at 601 and 561 cm^{-1} corresponds to $PO^{3-}{}_4$. The C–O stretching vibrations at 872, 1453 and 1413 cm-1 has been assigned to CO_3^{2-} group, which appears under all the temperatures indicating that $CO_3^{2-}$is present until 600 ^oC. This band originates due to the carbonate substitution in the crystal lattice (Patel et al., 2015). Additionally, the bands of C=O and C=C (protein and collagen) were assigned to the peaks at 1636 cm^{-1} corresponding to the organic phase of bone material (Rojas-Mayorga, Bonilla-Petriciolet, Aguayo-Villarreal, Hernandez-Montoya, et al., 2013). The peak disappear when the temperature increase further causes the removal of bone components during calcination.

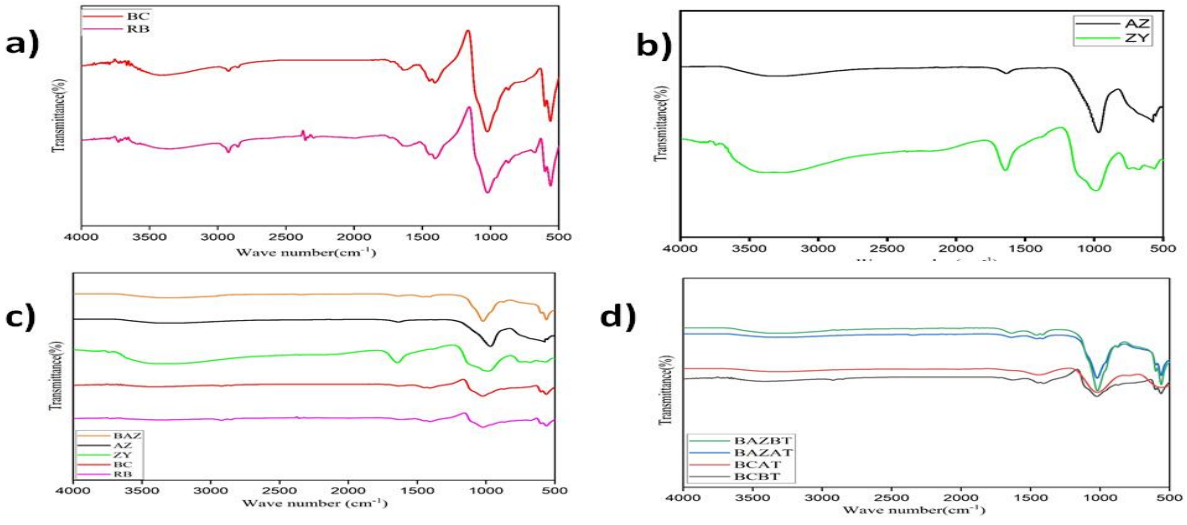

Figure 4. 5:a) Raw bone and bone char, b) zeolite Y and Aluminum loaded zeolite Y c) all samples , d) bone char /the aluminum loaded zeolite Y adsorbent, bon char before and after treatment

In the FTIR figure 4.5b, the green line (ZY) corresponds to zeolite Y spectra. Narrow band in the regions 1255-957 cm^{-1} attributed to the internal tetrahedron vibrations of Si-O-Si and Si-O-Al. This should be the strongest vibration band and assigned to a T–O (T= Si, Al) asymmetric stretching mode, which was shown at about 975.8 cm^{-1} in the FTIR spectrum of synthesized zeolite Y and a shoulder located at 1112 cm^{-1}. It was the characteristics of structural sensitive T-O external linkages. The weak peaks below 950 cm^{-1} wavenumber are possibly due to the vibration involving the ≡Al-OH nests created by the cation vacancies. The peaks found at 748 cm^{-1} shown in the FTIR spectral region (820-720 cm^{-1}) corresponds to the symmetric stretching vibration of SiO_4 groups while the bands around 450-650 cm^{-1} are related to either bending vibration of SiO_4 groups or in the vibration modes of the 4-membered rings of the silicate chains as reported by (Mgbemere et al., 2019). The water-bending vibration at 1,645.95 cm^{-1} indicates the presence of adsorbed water in zeolites. The broad band with a peak at 3456.78 cm^{-1} was due to the hydrogen bonding of water with OH groups, the b (Flanigen et al., 1971). The change in intensities and broadening of function group of –OH 3428-3436 cm^{-1} of AZ confirm that Aluminum loaded on zeolite. Moreover, decrement in transmittance at specific wavelengths (1636 cm^{-1}) and peak shift occurred from 1645 to 1636 cm^{-1} indicates loading of Aluminum on zeolite Y. Stretching bending vibration of Si-O, Al-O group and Si-O-M (M=Al) in spectrum were among the point indicating the adsorption insight of F^- up on AZ (Glaser et al., 2015). BAZ composite is FTIR spectra show bands associated with ZY, BC and AZ functional group after the inclusion of these materials confirm successful production of the composite. The adsorption of fluoride on to the adsorbent surface the peak intensities are modified and peak at 535 cm^{-1} could be related to related the Al-F interaction (Barathi et al., 2014). Figure 4.5d) the band at 873 cm^{-1} of the bone char after treatment has been assigned to CO_3^{2-} group. Bone char after treatment in the figure showed the band at 605 and 565 cm^{-1} corresponds to PO_4^{3-} bending vibrations.

4.2.4 Thermo- Gravimetric Analysis (TGA)

Thermal evaluation TGA/DTA is a crucial experimental technique that is frequently used to examine how synthesized materials thermally degraded (Patel et al., 2015). Figure 4.6 (a, b, c) displays the TGA and DTA traces of raw bone, Kaolin bone char/ Aluminum coated zeolite Y adsorbent were heated from 0 to 1000 °C at a rate of 10 °C/min. For all those samples there were no observable significant weight loss with respect to exothermic and endothermic reaction in the

spectrum for the sample calcined at 1000 ^{o}C. This indicates good thermal stability of the RB. As shown from the TGA/DTA of the RB Figure 4.6 (a) no additional weight loss occurred after 800 ^{o}C. The total weight loss up to 1000^{o}C were calculated and resulted 41.0.86 %. The raw bone (7.090mg) first weight loss of 2.002 mg occurred from room temperature to 400 $^{\circ}$C, which is related to the loss of moisture (i.e., 28.23%) and loosely bound absorbed water molecule. The second weight loss of 0.970 mg occurred between 400 to 580 $^{\circ}$C, which were a continuous weight loss (i.e., 13.681%) caused by the thermal degradation of organic substances such as proteins, collagen and fat tissues (Ooi et al., 2007). Finally, a weight loss of 0.062 mg (0.874%) was observed between 580 and 1000°C, further increasing the temperature caused the partial dehydroxylation process of hydroxyapatite and the decomposition of carbonates (Rojas-Mayorga, Bonilla-Petriciolet, Aguayo-Villarreal, Hernandez-Montoya, et al., 2013). In the dehydroxylation process, the hydroxyapatite loses OH^{-} during thermal treatment and this process is given by

$$Ca_{10}(PO_4)_6(OH)_2 \rightarrow Ca_{10}(PO_4)_6(OH)_{(2-2x)}O_x\square_x + xH2O \uparrow \ldots\ldots\ldots\ldots\ldots\ldots Eq(4.2)$$

Where, $\square$ is a vacancy, this dehydroxylation process may begin at 800–1000 ◦C depending on the operating conditions of the thermal treatment (Ooi et al., 2007).

The kaolin clay needed to prepare zeolite Y were calcined to activate and remove impurity as result thermal analysis is an important step to synthesize the desired product. According to TGA analysis from figure, 4.6(b) the kaolin's (9.13 mg) first weight loss of 0.098 mg occurred from 18 ^{o}c up to 114 ^{o}c attributable to the release of moisture and loosely bound absorbed water from the surface. Moreover, endothermic peak at 55 ^{o}c and 123^{o}C from DTA support the data. The second weight loss of 0.34 mg occurred between 123 ^{o}C and 185^{o}C and from DTA small endothermic peaks were shown at 277 ^{o}C and 453 ^{o}C that related to loss of dust and water in the pore site. After that it remain stable up to 480 ^{o}C and more significant weight drop by 0.41 mg occurred between 480 ^{o}C and 560 ^{o}C that supported by endothermic peak at 526 ^{o}C which indicates shift as result of the structures dissociation via de hydroxylation to meta kaolin which has an amorphous structure and very reactive (Caponi et al., 2017). As show in figure 4.6 (c), the composite (9.202mg) first weight loss of 1.439 occurred from room temperature to 580^{o}C. The second weight loss of 0.039mg occurred from 580 ^{o}C to 800 ^{o}C. Generally, there is no significant change in the composite, the use of ethanol, as a solvent to combine both adsorbents has no impact on composite adsorbent. The ethanol was removed during drying in oven at 60 ^{o}C for 24 hr.

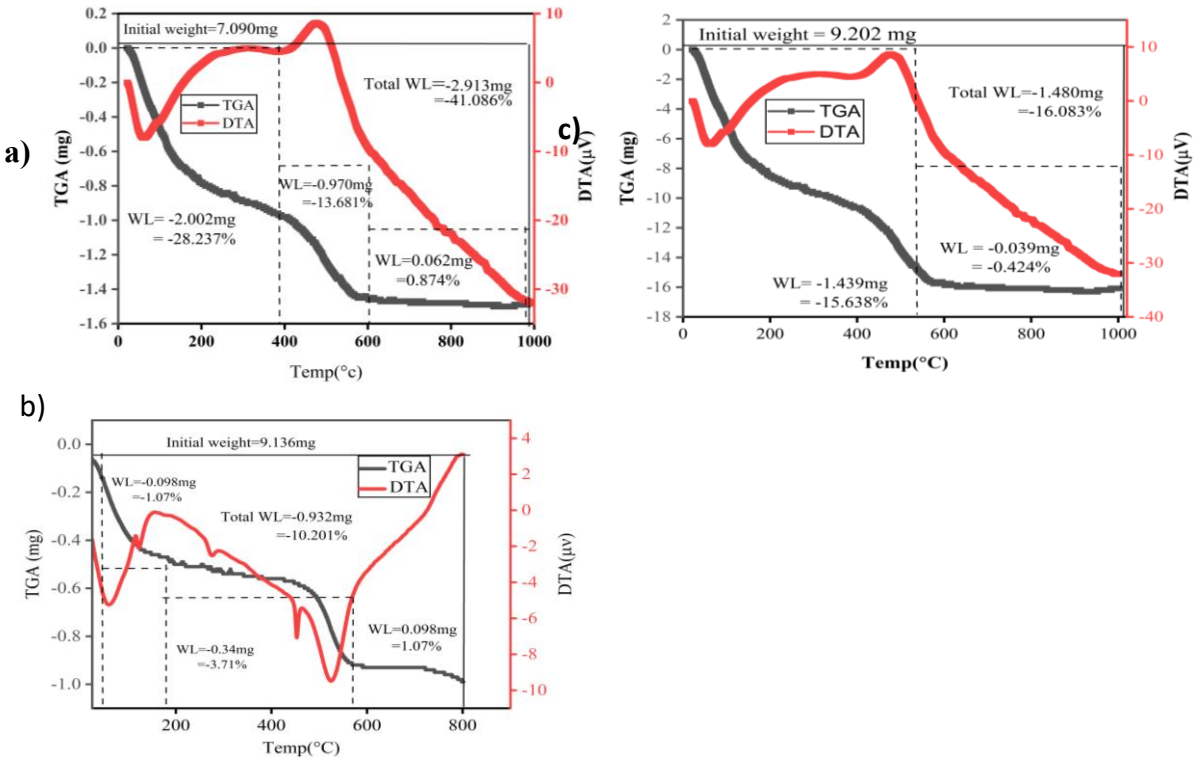

Figure 4. 6: The TGA- DTA graph of a) raw bone, b) Kaolin, c) (3:1) BAZ composite adsorbent

4.2.5 Brunauer-Emmett-Teller (BET) Analysis

The BET measure specific surface area of Bone char, Zeolite Y and bone char/Aluminum loaded zeolite Y. As shown in the table 4.2, it is evident that the surface area of ZY (zeolite Y) is significantly higher compared to bone char, measuring 523.120 m²/g and 406.249 m²/g, respectively. Zeolite Y known with high surface area and pore size, consequently, combining bone char with aluminum-loaded zeolite Y serves to increase the overall surface area of the adsorbent. This enhancement in surface area is aimed at improving the removal efficiency of the adsorbent.

Table 4. 2: BET data of BC, ZY and 3:1-BAZ

	BC	ZY	BAZ
Specific surface area($^{\alpha}S$)	406.249 m²/g	523.120 m²/g	540.249 m²/g
Total pore Volume ($\frac{P^o}{P}$)	1.124 cm^3/g	1.71 cm^3/g	2.4 cm^3/g
Mean pore diameter	1.383 A°	1.32 A°	1.83 A°

4.3 Design of Experiment Result Analysis

To investigate the effect of different parameter (pH of the solution, adsorbent dosage (3:1 BAZ) and contact time) on the removal efficiency of fluoride and the optimization ware carried out using surface response methodology in design expert 13 software.

Table4. 3: Information gives for build experimental analysis of adsorption efficiency of fluoride.

Study type	Response surface
Initial point	Central composite design
Center point	6
Design Model	quadratic polynomial
Run	20
Blocks	No

Table4. 4: Experimental result of fluoride removal from aqueous solution

Run	Adsorbent Dosage (g)	pH of the Solution	Contact Time (min)	Adsorption Efficiency (%)
1	2.25	7.5	60	92
2	4	3	0	40.9
3	4	3	120	50.5
4	2.25	7.5	60	92
5	2.25	7.5	60	92
6	2.25	7.5	0	58.8
7	0.5	12	0	46
8	0.5	7.5	60	98.1
9	2.25	12	60	73
10	4	7.5	60	85.6
11	4	12	0	40
12	2.25	7.5	60	92
13	2.25	3	60	62.1
14	2.25	7.5	60	90
15	2.25	7.5	120	85
16	2.25	7.5	60	95
17	0.5	3	0	48.01
18	0.5	3	120	75
19	0.5	12	120	80

20	4	12	120	58.3

4.3.1 Analysis of Variance (ANOVA)

Analysis of variance (ANOVA) generated by Design Expert software version 13 is used to study the model adequacy, model significance, model fitness and correlations between the predicted and observed values. The summary of the analysis of variance (ANOVA) is given in Table 4.5

Table4. 5: Analysis of variance influence of the factors studied on fluoride removal

Source	Sum of Squares	DF	Mean Square	F-value	P-value	
Model	7639.72	9	848.86	110.05	< 0.0001	significant
A- Adsorbent Dosage	515.67	1	515.67	66.85	< 0.0001	
B- pH of solution	43.22	1	43.22	5.60	0.0395	
C- Contact time	1324.57	1	1324.57	171.72	< 0.0001	
AB	1.91	1	1.91	0.2477	0.6294	
AC	136.87	1	136.87	17.74	0.0018	
BC	30.85	1	30.85	4.00	0.0734	
A^2	17.82	1	17.82	2.31	0.1594	
B^2	1301.41	1	1301.41	168.72	< 0.0001	
C^2	832.98	1	832.98	107.99	< 0.0001	
Residual	77.14	10	7.71			
Lack of Fit	64.30	5	12.86	5.01	0.0508	not significant
Pure Error	12.83	5	2.57			
Cor Total	7716.85	19				

From the ANOVA (Analysis of Variance) Table, 4.5 results the higher F-Value and the lower P-value (<0.0001) indicates significance for the regression model. As the result demonstrates the model, the F-value of 110.05 implies it is significant there is only a 0.01% chance that an F-value this large could happen due to noise. The p-value less than 0.05 implies that the model is statistically significant. They are extremely indispensable to understand the interaction among the independent variables. The result showed that A-Adsorbent Dosage, B -pH of the solution and C-Contact time are the major important variables in the adsorption process with P-value < 0.0001, < 0.0001, and 0.0395 respectively. From the second polynomial model, $B^2$and C^2 are significant models terms with P-values for both models < 0.0001. In the case of

interaction effects, AC (adsorbent dosage and contact time), and BC (pH of the solution and contact time) are significant model terms for fluoride removal. Where there p-values are 0.0018, 0.0734 respectively. The Lack of Fit of the F-value 5.01 implies the Lack of Fit is not significant relative to the pure error. There is about 5.08% chance that a Lack of Fit F-value large could occur due to noise. As shown from the ANOVA result, the interaction effects of adsorbent dosage and pH of the solution (AB) did not influence the adsorption process due to their highest P-value. Their P- values were 0.6294 that is greater than 0.1, which indicates the model terms are not significant. In the same way, quadratic term A^2 was insignificant factor within p value 0.1594, that did not affect the adsorption process.

Regression model equation

Table 4. 6: Regression coefficients in terms of coded factors

Factor	Coefficient Estimate	DF	Standard Error	95% CI Low	95% CI High	VIF
Intercept	91.02	1	0.9548	88.89	93.15	
A-Adsorbent Dosage	-7.18	1	0.8783	-9.14	-5.22	1.0000
B-pH of solution	2.08	1	0.8783	0.1221	4.04	1.0000
C-Contact time	11.51	1	0.8783	9.55	13.47	1.0000
AB	0.4888	1	0.9819	-1.70	2.68	1.0000
AC	-4.14	1	0.9819	-6.32	-1.95	1.0000
BC	1.96	1	0.9819	-0.2241	4.15	1.0000
A^2	2.55	1	1.67	-1.19	6.28	1.82
B^2	-21.75	1	1.67	-25.49	-18.02	1.82
C^2	-17.40	1	1.67	-21.14	-13.67	1.82

The coefficient estimate provides the estimated change in response per unit change in factor value while all other factors are held constant. In an orthogonal design, the intercept is the overall average response of all runs. The coefficients are modifications based on the factor settings that are made around that average. VIFs are 1 when the factors are orthogonal; VIFs more than 1 imply multi-collinearity; the higher the VIF, the more severe the factor correlation. VIFs less than 10 are generally acceptable.

The Coefficients in Terms of Coded Factors for fluoride removal from ANOVA result

Adsorption Efficiency = 91.02 -7.18A +2.08B+11.51C+ 0.4888 AB - 4.14AC + 1.96BC + 2.55 A^2 - 21.75 B^2-17.40 C^2

The Final Equation in Terms of Actual Factors

Adsorption Efficiency = 10.65898 -5.94626 Adsorbent Dosage +16.00011 PH Range + 0.806038 Contact time + 0.062063 Adsorbent Dosage * pH of the solution - 0.039393 Adsorbent Dosage * Contact time+0.007273 pH of the solution * Contact time + 0.831317 Adsorbent Dosage^2- 1.07428 pH of the solution ^{2}- 0.004834 Contact time^2

The equation in terms of actual factors can be used to make predictions about the response for different levels of each factor.

4.3.2 Model Adequacy

The regression model was set up to be significant with the correlation coefficient of determination of R- Squared, shaped R- Squared, and prognosticated R- Squared having a value, and0.9450 independently as shown from table4.7. The probity fitness of the model was measured by a measure of determination R^2, which measured how well the real experimental data points have been approached together with the retrogression model. As the result in a table,4.7 expressed the value of R^2 = 0.9900 indicates the better fit of experimental data to that of prognosticated bone The value of larger Retrogression measure(R^2) approach to 1 illustrates, the validity of model in which it implies an respectable agreement among the factual and predicted data. It implies 99.0 of the experimental variable studied attributed for the fluoride removal. The predicted R ^{2} of 0.945000 is in reasonable agreement with the shaped R^2 of 0.9810; i.e. the difference is lower than 0.2. Thus, this demonstrates that the measured data truly well fitted with a quadratic model of the predicted value. Adeq Precision measures the signal- to-noise rate. A rate lower than 4 is desirable, the rate of 24.686 indicates an respectable signal.

Table 4. 7: Model adequacy measures

Std. Dev.	2.78	R^2	0.9900
Mean	72.72	Adjusted R^2	0.9810
C.V. %	3.82	Predicted R^2	0.9450
		Adeq Precision	31.3141

The figure 4.7 indicates the relationship of Actual and predicted value, which can be introduced from the regression model equations of a Design Expert chart based on predicted and actual percent fluoride removal. The straight line shows the predicted values and the small rectangles

represent the actual experimental values. The straight line is very close to the actual values and has a correlation coefficient R^2 equal to 0.99, which confirms the accuracy of the model. The result confirmed that all the actual and predicted values are close to the line of perfect fit. Both showed the good agreement between them.

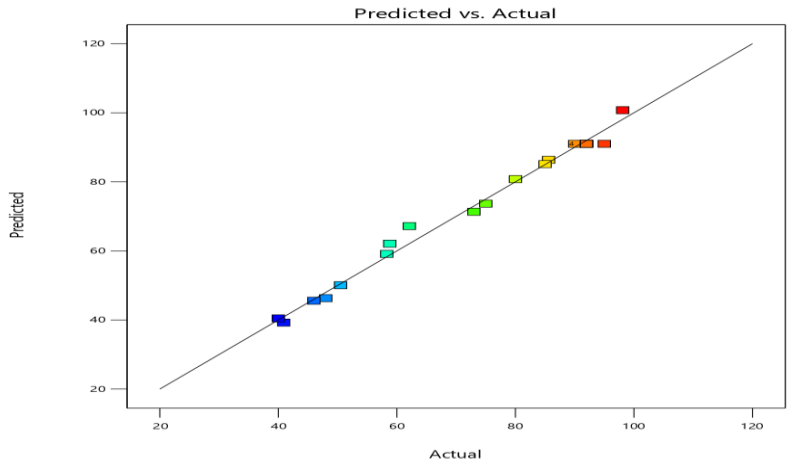

Figure 4. 7: Predicted Vs Actual value fluoride removal adsorption plot

4.3.3 Optimization of the Response

To find the optimum value of each independent variables, four statistical metrics such as the larger regression coefficient (R^2), smaller lack of fit F-value, lower p-value and higher sum squares have been used. The response optimization was used to identify the combination of independent variables particularly, Contact time, pH of the result, and adsorbent cure within the response of fluoride removal effectiveness. The objective of the process was to gain high fluoride removal efficiency. Thus, it has been set as outside while the process parameters similar as contact time, Adsorbent dosage, and pH of the solution have been set as "within the range". According to the result attained from optimizer Design- Expert interpretation 13 software the maximum optimum removal effectiveness of fluoride was achieved 98.1 by using 7.5 pH, 60 min contact time, and 0.5 g adsorbent dosage using constant 10 mg/ L initial fluoride concentration.

4.3.4 Response Surface Plots of Interaction Effects

The effect of the interactions between the three independent input and one output variables and their interactions on the dependent variables can be seen using three-dimensional (3D) response surface plots. As observed from figure 4.8- 4.10, it indicates the Plots of three-dimensional response surfaces of function of two variables with response and the remaining variables at the

central level of the other variables. At lower pH values that indicates as acidic medium, the hydration surface of bone char/ Aluminum loaded zeolite Y (BAZ) undergo a protonation reaction. The dissolved fluoride ion was embedded in the adsorbent surface to obtain positive charge. However, an increase in pH of solution leads to OH^- concentration in the solution increased and as result de protonation reaction takes place on the hydrated surface of the adsorbent to obtain a negative charge.

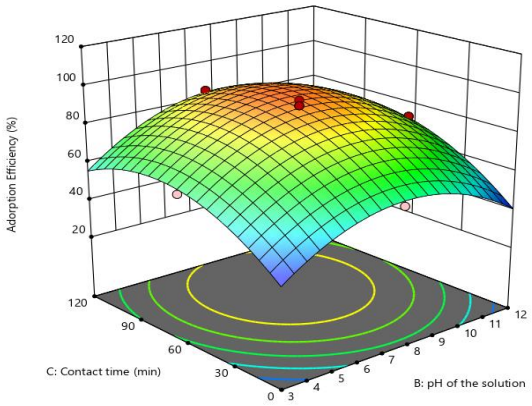

Figure 4.8: 3D interaction effect of pH and time on Adsorption efficiency of fluoride

Figure 4.8 show the pH of aqueous solution is one of the important factors that affect the adsorptive removal of species at the adsorbent solution interfaces. In addition, the pH of the solution could influence the surface charges and degree of ionization of the adsorbate.

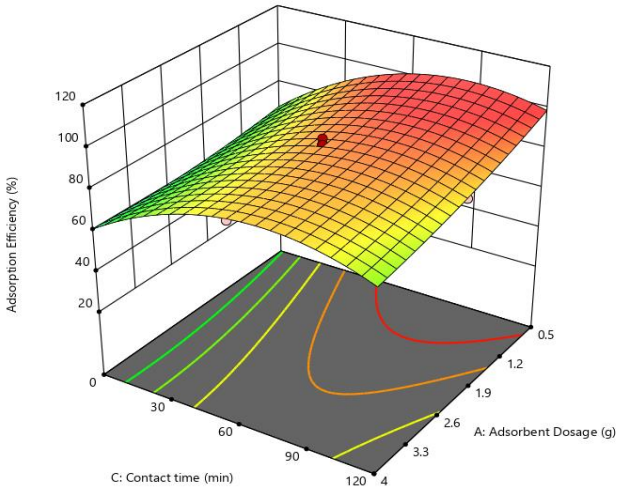

Figure 4. 9: 3D interaction effect of Adsorbent dose and contact time on fluoride removal

Figure 4.9 illustrates 3D interaction effect of Adsorbent dose and contact time on fluoride removal efficiency at constant pH and initial Fluoride concentration. As the adsorbent dose increases, there was an increment of fluoride removal efficiency until certain point beyond that point the adsorption efficiency decreases. The adsorbent has reached the maximum adsorption capacity within one hour. In the other words, the surface coverage of the adsorbent was already saturated Fluoride in one hour. Therefore, it can be concluded that the percentage of Fluoride removal was highly dependent on adsorbent dosage, pH of the solution and contact time.

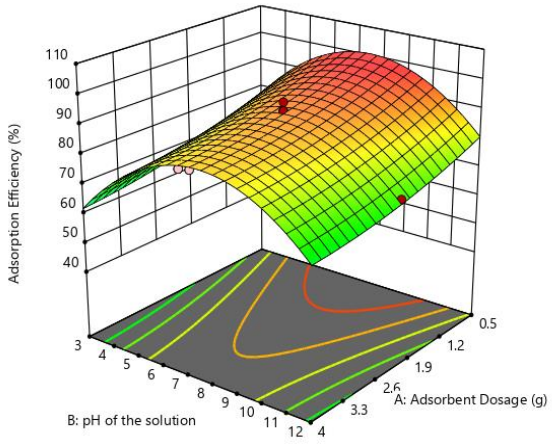

4.10: 3D interaction effect of Adsorbent dose and pH of the solution on fluoride removal

Figure 4.10 explained the 3D interaction effects of Adsorbent dose and pH on fluoride removal efficiency while both time and initial fluoride concentration remains constant. The sorption process was carried out on the molecules and surfaces of the BAZ adsorbents. Therefore, the adsorbent amount had a meaningful effect on the fluoride removal efficiency. The adsorbent dose has a direct and indirect effect on the process and costs like the other parameters. As it can be observed from the graph as adsorbent dose of BAZ increases, the fluoride removal efficiency decreases in the model. It is commonly understood that increasing the adsorbent dosage should lead to an increase in adsorption rather than a decrease. The higher the adsorbent dosage, the greater the number of available adsorption sites, resulting in increased adsorption capacity. However, there could be certain cases where an excessively high adsorbent dosage may result in a decrease in adsorption. This can occur if the adsorbent becomes overcrowded or if the excess adsorbent starts to interfere with the adsorption process. For example, if the excess adsorbent particles agglomerate or form blockages, they may hinder the access of adsorbate molecules to the active adsorption sites, leading to reduced adsorption efficiency. In this case,

Zeolites have a porous structure. The void spaces within the zeolite framework contribute to have many adsorptions site, the unique property of zeolite used to reduce the overall mass of the adsorbent dosage (Dessalegne et al., 2017; Wirtu et al., 2021b). Therefore, is essential to optimize the dosage for a specific system, in this study specific initial fluoride condition, volume of solution and other parameters are taken Constant, the optimum value of adsorbent dosage is 0.5g beyond this limit the adsorption capacity gradually decrease due to the unique characteristics of the adsorbent.

4.4 Determination of Point Zero Charge

The point zero charge of the composite was determined using salt addition method. The composite had a pH_{PZC} of 8.4, indicating that at a pH lower than 8.4, the composite's surface has a positive charge favoring the process of adsorption of fluoride, and thus be a surface on which it absorbs anions (anionic exchanger). On the other hand, the material surface have negative charges at a solution pH value greater than the PZC and thus be a surface, which absorbs cations (cationic exchanger).

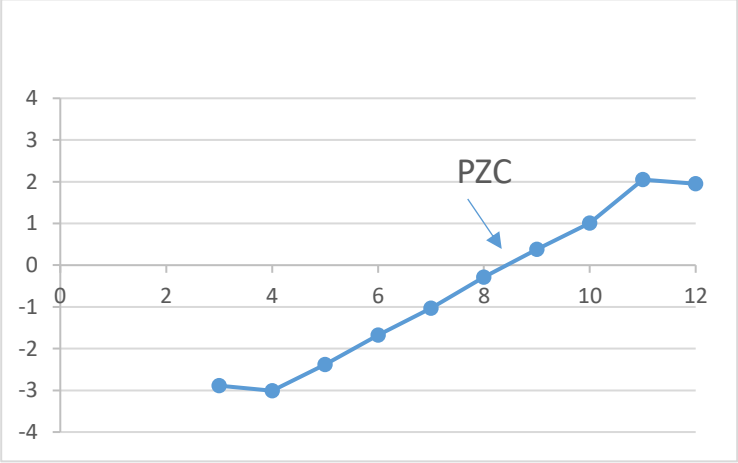

Figure 4. 11: Determination of point of zero charge on BAZ

4.5 Effect of Different Parameters on Fluoride Adsorption Efficiency

Three adsorption parameters were selected and tested their effect on the removal efficiency of the composite for fluoride removal mixing ratio. Adsorbent dose, contact time, initial fluoride concentration and pH of the solution were examined to evaluate the effect of each parameter.

4.5.1 Mixing Ratio of bone char and aluminum loaded zeolite Y

The effect of mixing ratio and pure individual adsorbent were studied. The two materials at an appropriate ratio, the materials take advantage of the synergistic effect, resulting in enhanced fluoride adsorption capacity. The Interaction between bone char and aluminum loaded zeolite Y create more efficient adsorption system. To select the appropriate mixing ratio series experiment is conducted at optimum condition 0.5 g/200ml adsorbent dosage, 7.5 pH of the solution, 60 min contact time and 10 mg/L initial fluoride concentration. The ratio of (3;1)(BC to AZ) was selected through the adsorption process, which has maximum adsorption capacity.

As show in the figure 4.12, zeolite Y has the lowest adsorption efficiency due to negative charge on the surface of zeolite cause repulsion between the charge on zeolite Y surface and F^- as result removal efficiency of fluoride decrease to 4.77 %. On the other hand, Bone char is known for its high affinity for fluoride ions, while aluminum-loaded zeolite also exhibits effective fluoride adsorption, their adsorption efficiency corresponding to 89.32 and 82.48 % respectively. BAZ (3:1) has highest removal efficiency because the mixture of bone char and aluminum-loaded zeolite provide a greater number of active adsorption sites for fluoride ions. The bone char particles and aluminum-loaded zeolite particles have different pore structures and surface properties, which can increase the availability of binding sites for fluoride ions. This higher number of binding sites contribute to improved adsorption efficiency. Moreover, the combination of bone char and aluminum-loaded zeolite enhance the physical properties of the composite. The presence of aluminum-loaded zeolite, which typically has a higher mechanical strength, provide structural support to the bone char particles. This prevents the compaction or breakdown of bone char during the adsorption process, ensuring efficient contact between the adsorbent and the water.

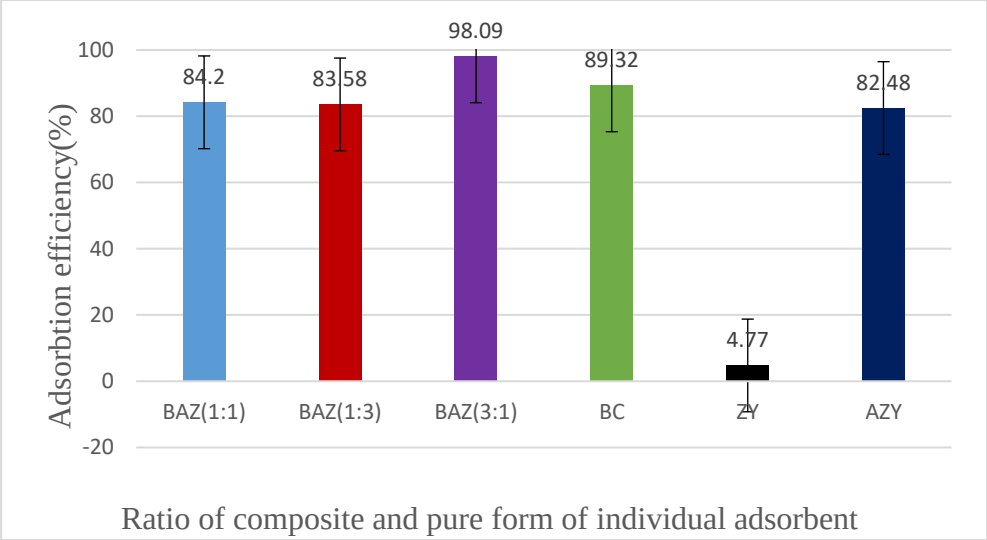

Figure 4.12: Effect of mixing ratio of the composite and pure individual adsorbents on fluoride removal efficiency

4.5.2 Adsorbent Dosage

Figure 4.13 shows percentage removal of fluoride ion from water on composite adsorbent at pH= 7.5, 60 min contact time and 10 mg/L initial fluoride concentration at varied adsorbent dose. The dose of the adsorbent increases from 0.5 g - 4 g increased by 0.5. Defluoridation increases as adsorbent dose increases due to the availability of more active sites to absorb fluoride ion. However, further increase in the adsorbent dosage lead to decrease in removal efficiency of the adsorbent due to overcrowding of adsorbent particles; create aggregation and hindering the movement of the target pollutant molecules (Dessalegne et al., 2017; Wirtu et al., 2021b).

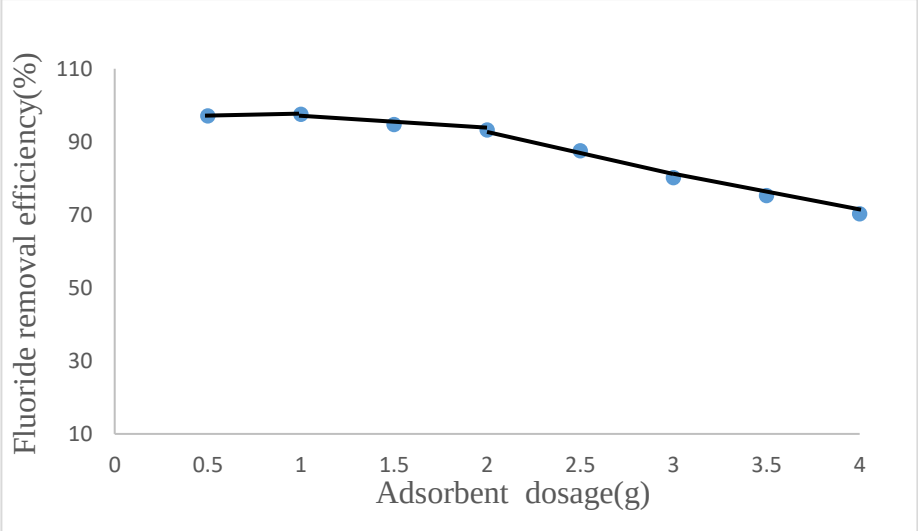

Figure 4.13: Effect of adsorbent dose on fluoride removal efficiency of BAZ composite

4.5.4 Effect of Initial Concentration of Fluoride

For a fixed mass of adsorbent (0.5 g), at constant contact time (60 min) and pH=7.5 the removal efficiency of the adsorbent decreased as concentration of fluoride increases shown in figure 4.14. Significant change was not observed for fluoride concentration less than 10 mg/L this is due to the availability of active adsorbent site up to some range of fluoride ion concentration. However, there is a sharp decrease in fluoride removal efficiency for a solution having fluoride concentration more than 10 mg/L, this is due to the utilization of all the energetically active site of the adsorbent. The removal efficiency was highest at lower and desired concentration of fluoride and decreased as concentration gets over the optimum range indicating the specific adsorption sites were available for F^- adsorption.

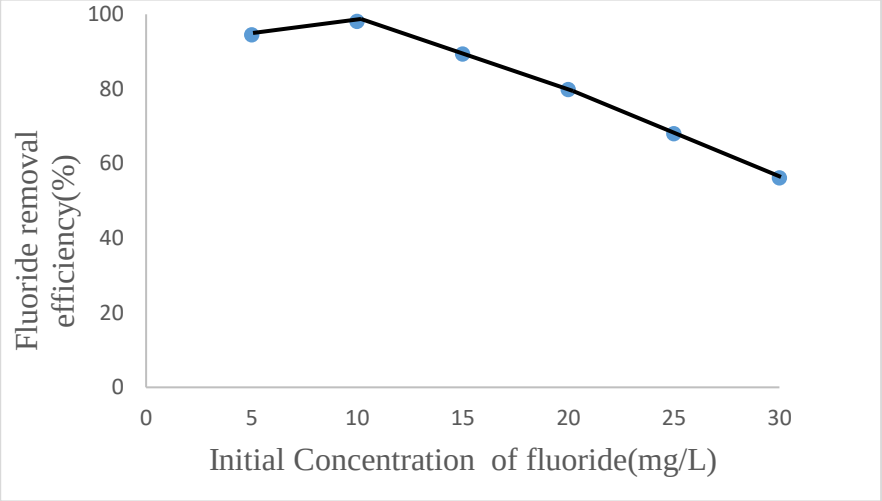

Figure 4. 14: Effect of initial fluoride concentration on fluoride removal efficiency of BAZ composite

4.5.5 Effect of Contact Time

The effect of the length of contact time between fluoride water and the composite on percentage removal of fluoride could be observed in figure 4.15, beyond the 60 minutes, the adsorption efficiency of the composite gradually diminishes. This decline can be attributed to the saturation of adsorption sites, the release of previously adsorbed molecules, and the existence of competing interactions that hinder the adsorption process. Generally, after equilibrium no more fluoride ion would be adsorbed rather desorption incident occurred on prolonged contact time (Shahid et al., 2020).

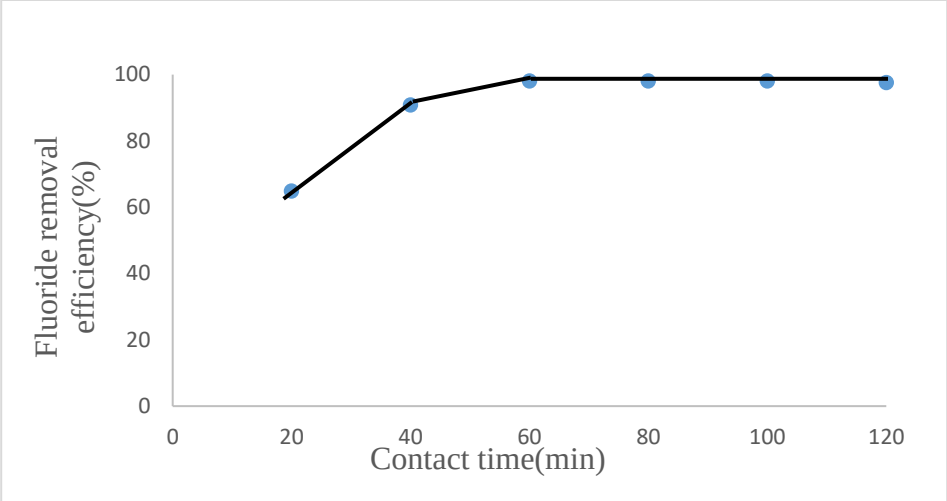

Figure 4. 15: Effect of contact time on fluoride removal efficiency of BAZ composite

4.5.6 Effect of pH of the Solution

The effect of pH on removal of fluoride was shown in figure 4.16. The solution containing 10 mg/L fluoride concentration and 0.5 g of the composite material were adjusted to various pH range (3- 12) mixed for 1 h and the residual fluoride concentration was analyzed. The adsorption data was not performed at pH < 3 since bone char is slightly dissolved and dissolution occurred (Alkurdi et al., 2020a; Shahid et al., 2019).

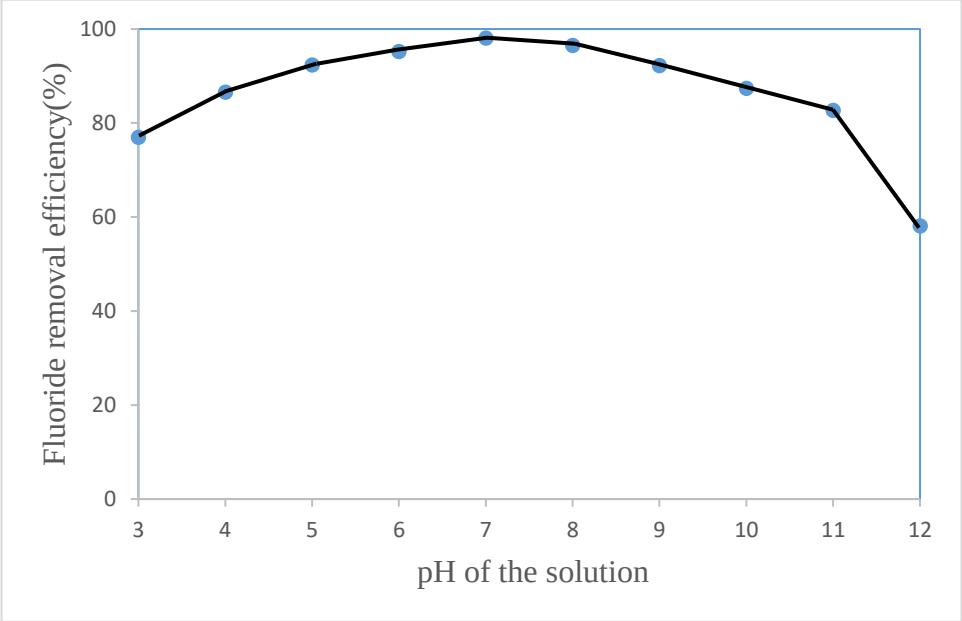

Figure 4. 16: Effect of pH of the solution on fluoride removal efficiency of BAZ composite

As figure 4.16 show, the adsorption capacity of the composite is affected by the solution pH. The. The adsorption efficiency diminished while increasing the pH from 7 to 12 because change in pH alters the surface charge of the adsorbent and electrostatic interactions between the F^- anions in solution. In the acidic medium, the surface of the adsorbent is highly protonated, and hence more F^- ions can be attracted, at higher pH the surface of the adsorbent becomes negatively charged (deprotonated) and fluoride leads to comparatively low adsorption. The effect of pH on the adsorption efficiency can be clearly illustrated by dealing surface charge of composite (PZC). When the solution pH is below the PZC of 8.4, the F^-anions were attracted to the positively charged surface of the composite, caused by the protonation of the hydroxyapatite hydroxyl groups, thus favoring F^-accumulation onto the surface. The surface charge of composite became more positively charged while decreasing the pH below its PZC. Hence, more F^-anions were attracted to the surface resulting in an increase in the adsorption capacity of the composite. At pH above the PZC, adsorption of F^- was slightly decrease because the bone char surface was negatively charged, due to deprotonation of the hydroxyapatite hydroxyl groups, causing a mutual repulsion between F^-anions and the composite surface. Adsorption at pH value above the PZC was not due to an electrostatic attraction but to a chemical interaction with sufficient energy that overcome the surface-fluoride repulsion forces.

4.6 Equilibrium Isotherm

Adsorption system can be designed with the aid of adsorption isotherms typically referred to as equilibrium isotherms, which constitute the amount of solute adsorbed per unit weight of sorbent. These isotherms use equilibrium concentration of sorbent at a fixed temperature. To remove the fluoride ions from the water, a particular design is optimized in order to generate proper correlations for experimental data, which is referred to as adsorption isotherm (Batool et al., 2018).

4.6.1 Adsorption Isotherm

The interaction of adsorbate with adsorbent can be identified by studying isotherm, which is a critical to optimizing and designing the desired adsorption system (Zhang et al., 2015). The equilibrium concentration of fluoride ion at constant optimized parameters of 60 min contact time, 0.5g/200 mL of bone char/Aluminum loaded zeolite Y and, 7.5 pH of the solution and 10mg/L initial fluoride concentration were carried out at a room temperature. The adsorption of isotherm data for F^- ion was analyzed by applying three commonly used isotherms,

Langmuir, Freundlich and Temkin Isotherms. Their correlation coefficients and constant parameters of sorption of F^- by bone char/Aluminum loaded zeolite Y were obtained from the slop and intercept of the graph for each equation of the isotherms.

4.6.1.1 Langmuir Isotherm

The adsorption isotherm determines the difference between the amounts of sorption and the solute concentration at equilibrium. The adsorption isotherm of fluoride ion using bone char/Aluminum loaded zeolite Y composite was investigated. The concentration of fluoride ions in their respective equilibrium phase at room temperature was studied to obtain maximum adsorption capacity of Bone char/Aluminum Loaded Zeolite Y composite fluoride removal. As shown in table 4.9 the result obtained from Langmuir model indicates that the value of separation factor ($R_{L)}$ for all initial fluoride concentrations were greater than 0 and less than 1, which implies that the Langmuir isotherm is favorable. The maximum adsorption capacity (q_{max}) can be determined from the intercept of Langmuir plots of $1/C_e$ vs $1/q_e$. The maximum adsorption capacity (q_{max}) and energy of adsorption (K_L) from Langmuir isotherm model were to be determined 19.23 mg/g and 1.23 L/mg respectively. The values of correlation factor (R^2) gained for Langmuir isotherm equals to 0.999.

Table 4. 8: Model adequacy measures

Isotherm	**parameters**	**Value**
Langmuir	q_{max} (mg/g)	19.23
	K_L (L/mg)	1.219961
	R^2	0.999
Freundlich	n	2.19
	1/n	0.456
	k_f (mg/g)$(1/mg)^{1/n}$	4.053
	R^2	0.958
Temkin	B (J/mole)	1.878
	K_T	15.98916
	R^2	0.985

Table 4. 9: The values of RL at various initial fluoride concentrations

C_o (mg/L)	R_L
5	0.141
10	0.076
15	0.052
20	0.039
25	0.032
30	0.027

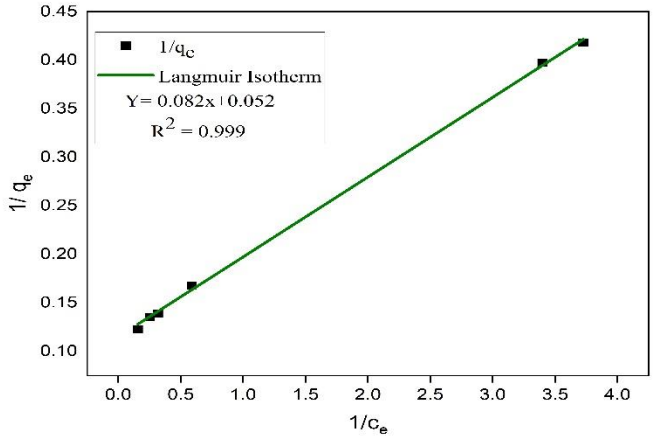

Figure 4.17: Langmuir isotherm for fluoride adsorption by BAZ

4.6.1.2. Freundlich Isotherm

Freundlich isotherm is an empirical equation that can be employed to describe the heterogeneous systems. The magnitude of the exponent 1/ n indicates the favorability of the adsorption. 1/ n is a heterogeneous factor, which is related to adsorption intensity or face diversity. The value of 1/ n < 1 which equals to0.456 indicates normal adsorption (Alkurdi et al., 2019b). In order to reach a favorable adsorption process, the value of n should be in the range of 1 to 10. Table 4.8 depicts the value of n was 2.19, which verified favorable adsorption. From the Freundlich isotherm model the values of constant parameters similar as K_f and n were determined by direct retrogression plot of log (qe) and log(Ce). From the Freundlich isotherm model anatomized showed the equilibrium isotherm data fit to the experimental data, which implies that adsorbed fluoride forms a monolayer face content on the bone char/ Aluminum

loaded Zeolite Y (BAZ) and the chemisorption adsorption medium takes place. The values of correlation factor (R^2) gained for Freundlich isotherm equals to0.958.

As (Keshtkar et al., 2016) studied, the Langmuir and Freundlich adsorption isotherms relative parameters were calculated from their separate pitch and intercept of the direct plots high correlation portions of Langmuir (R^2>0.999) and Freundlich (R^2>0.958) indicated that both the Langmuir and Freundlich models were nicely fit the experimental data in this study. The result attained from adsorption equilibrium isotherm verified that the fitting the equilibrium data to both Langmuir and Freundlich isotherm models suggest that the presence of heterogeneous and homogenous adsorption shells on the adsorbent involved during the adsorption of fluoride ions. By comparing the values of correlation factor(R^2), the Langmuir models more suitable fits to with the equilibrium sorption which gives a larger R^2 equals to 0.999 and maximum adsorption capacity of 8.689 mg/ g for fluoride ion adsorption.

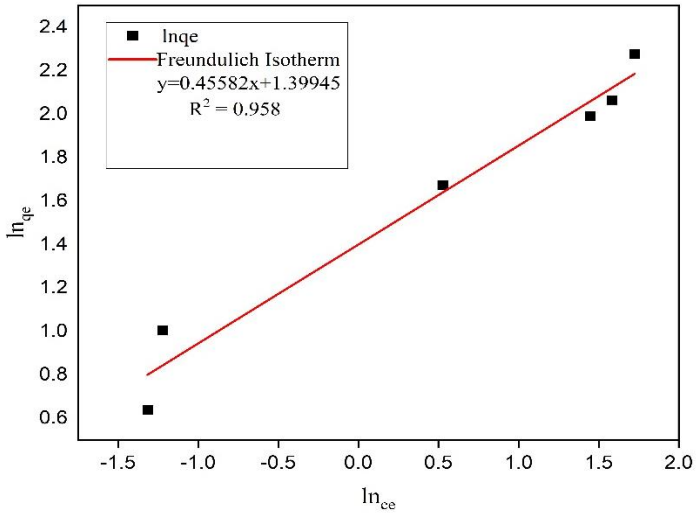

Figure 4. 18:Freundlich isotherm models for fluoride adsorption by BAZ

4.6.1.3. Temkin Isotherm

The correlation coefficient (R^2) obtained from this model was 0.9756. The result showed that the experimental data fitted to the model. However, when comparing with Langmuir and Freundlich the result found by Temkin model was the smallest correlation coefficient. According to previous study by (Wang & Guo, 2020b) for Temkin isotherm the following is predicted: a positive B (heat) value would indicate that fluoride ion binds to Bone

char/Aluminum loaded zeolite Y, B_T expresses heat of adsorption for a particular adsorption experiment.

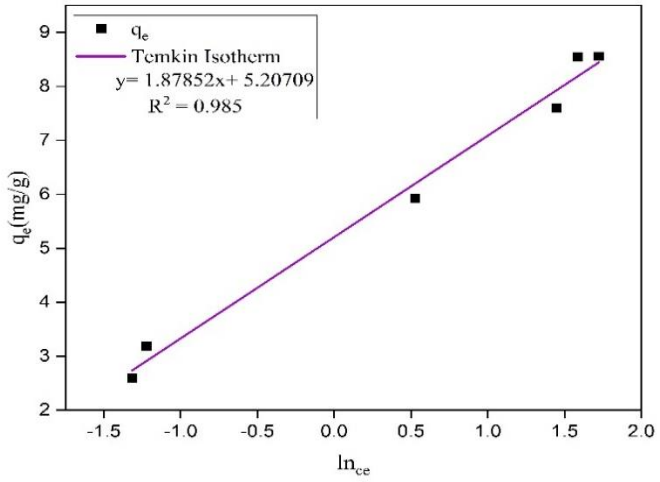

Figure 4. 19: Temkin isotherm models for fluoride adsorption by BAZ

4.7 Adsorption Kinetics

Kinetic Experiments were investigated to examine the rate of fluoride adsorption on bone char/ Aluminum loaded Zeolite Y adsorbent and the time needed to reach equilibrium. The purpose of studying equilibrium kinetic is to identify the adsorbent retention time and give information about the specified time to reach the maximum capacity of adsorption and the controlling medium in the process that includes mass transfer or chemical responses (Tohfegar et al., 2019). In this study Pseudo-first-order, Pseudo-second order and Intraparticle diffusion kinetic models were investigated to obtain the best kinetic models for fluoride removal. The kinetics study time dependence of fluoride was investigated from 0 to 120 min at constant room temperature, 10 mg/L initial fluoride concentration, pH =7.5, adsorbent dose = 0.5 g/200 ml. Comparing the correlation coefficients of three kinetic models, it revealed that the pseudo-second-order model best fit the adsorption kinetic of fluoride onto bone char Aluminum loaded Zeolite Y and the adsorption processes were chemisorption. As shown in the figure 4.20 the Pseudo-second-order rate model show the best agreement with the experimental results, which implies that the whole process was controlled by chemical adsorption is the rate limiting way of the process. Pseudo-second-order kinetic model predicts that adsorption gets involves valance forces through sharing of electrons among fluoride ions and the BAZ. In addition, the experimental adsorption capacity agreed with that of calculated adsorption capacity, which proved the model adopted is reasonable. The value of kinetic parameters were summarized in table 4.10.

Table 4. 10: Kinetics model parameters for Pseudo-first-order, Pseudo-second-order, and Intraparticle Diffusion

Kinetics	**parameters**	**Value**
Pseudo-First Order	q_e (mg/g)	0.784
	K_1 (min^{-1})	-0.00027
	R^2	0.94
Pseudo-Second Order	$q_{e\ calc}$(mg/g)	1.045
	K_2 (g/mg.min)	0.0045
	R^2	0.999
Intraparticle Diffusion	K_p (mg/g.$min^{1/2}$)	0.007
	R^2	0.988

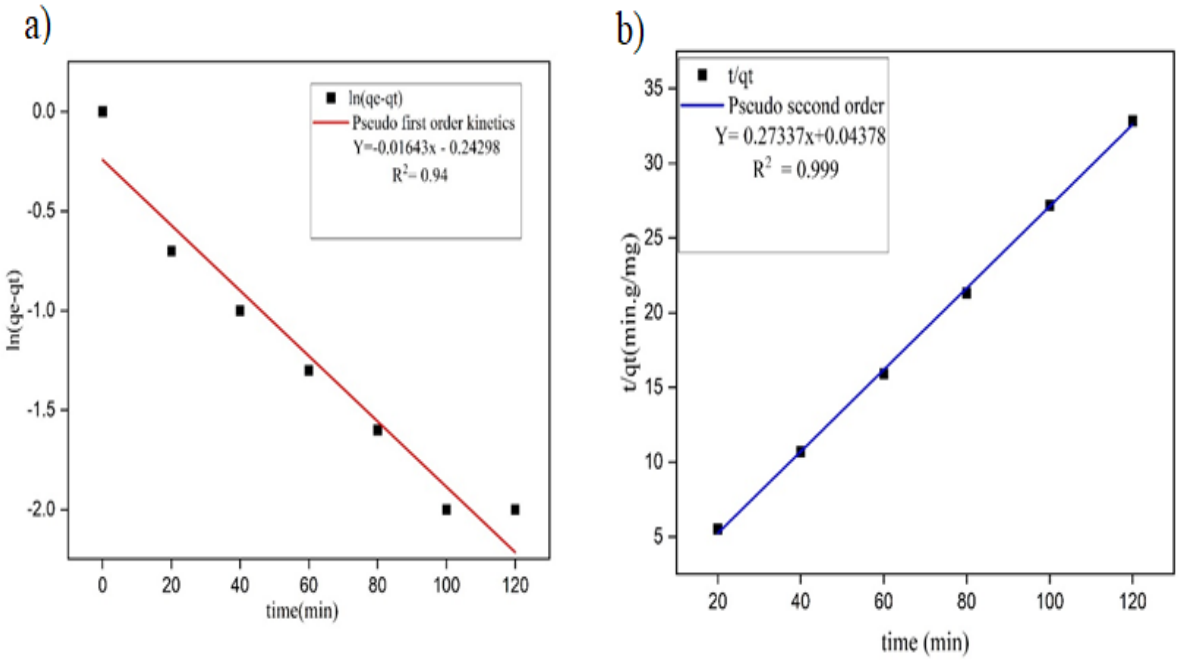

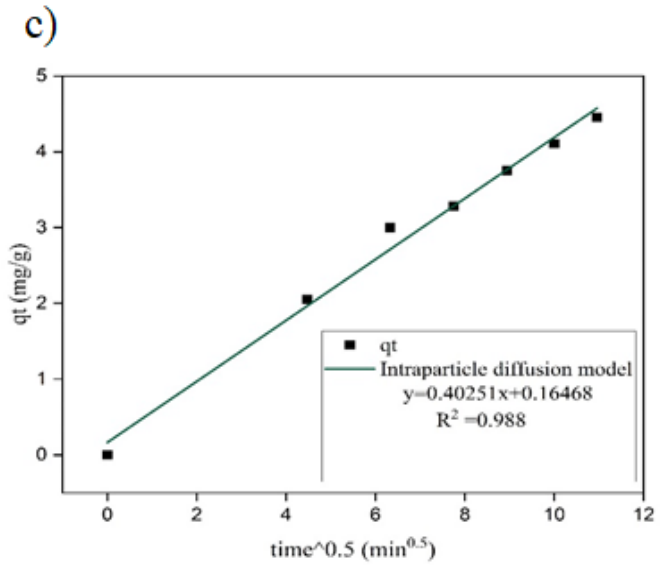

Figure 4. 20:a) Pseudo first order, b) second order kinetics and c) Intra particle for sorption of fluoride ions

The intraparticle diffusion model can be describe the rate of adsorption process depends on the speed at which adsorbate diffuses towards adsorbent. The result analyzed from the adsorption equilibrium data of intraparticle diffusion model the graph $t^{0.5}$ versus q_t was linear which demonstrates that the intra-particle diffusion was involved inside the adsorption process. In the other case, the model expresses that intraparticle diffusion is not the only rate-determining step due to the graph $t^{0.5}$ versus q_t did not pass through the origin as observed from figure 4.20c. This shows that intraparticle diffusion became not the only rate-limiting step within the adsorption of fluoride. Consequently, other mass transfer processes like film diffusion and bulk diffusion could be there in determining the mass transfer mechanism of fluoride ions from the bulk solution to the BAZ composite adsorbent surface. The diffusion process may affect the fluoride ion adsorption process on BAZ composite as result of the porous structure of the adsorbent and the attractive effect of fluoride ions.

4.8 Thermodynamics Study

The thermodynamics parameters determined for fluoride adsorption on BAZ at three temperature of 298 K, 303 K and 313 K independently. As it summarized in table 4.11, the particular values ΔG^o found to be -6.39,-6.509 and-6.753 which confirms that the spontaneous and feasibility of adsorption process as result of negative values of Gibbs free energy change at

all temperatures. As temperature increases, the magnitude of ΔG^o also more negative for fluoride adsorption, which implies that further naturalness of the adsorption takes place at advanced temperature. Advanced temperature makes the adsorption easier due to advanced driving force of adsorption. Similar results were found (Singh et al., 2015), the positive value of change in enthalpy ΔH^o (0.817 KJ/mol) confirms the endothermic nature of sorption process and indicates the adsorption of fluoride come more favorable at advanced temperature. In the other case the positive values of ΔS^o (24.18 J/ KJ/mol) demonstrates that the process is entropy driven and the randomness between solid- solution interface increases throughout adsorption process.

The report studied by (Ogata et al., 2015) found similar result, increase in randomness of fluoride ion on Bone char/ Aluminum loaded zeolite Y was as result of number of desorbed water molecules is larger than that of adsorbed fluoride ion and the adsorption of fluoride controlled by positive entropy change. In addition, the presence of complaint state in the adsorption process is due to the combination of fluoride with particle sites spots to form stable structures (Zhang et al., 2015).

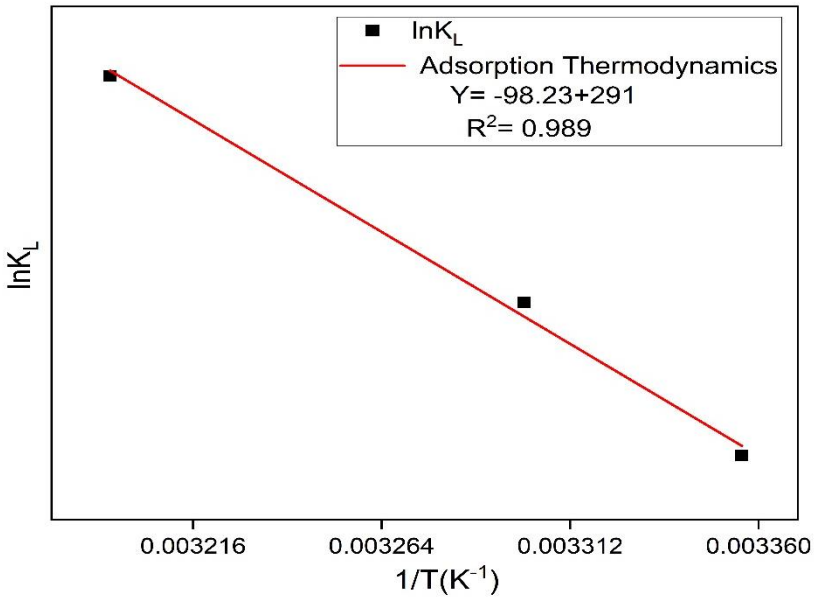

Figure 4. 21: Adsorption thermodynamics of fluoride on BAZ composite

Table 4. 11: Thermodynamic parameters of fluoride adsorption on BAZ

Adsorbent	qe (mg/g)	T^o (K)	K_L	ΔG^o (KJ mol^{-1})	ΔH^o (KJ mol^{-1})	ΔS^o (J mol^{-1} K^{-1})	R^2
Bone char/Aluminum loaded zeolite Y	3.89	298	13.192	-6.39 1	0.81672	24.1843	0.989
	3.88	303	12.883	-6.509			
	3.86	313	11.439	-6.753			

4.9 The Effect of Co-existing Ions

Typically, the common inorganic pollutants, which include PO_4^{3-}, Cl^-, NO_3^-, HCO^-_3 and CO_3^- constantly, exist with F^- in natural water sources that can act as contending ions and intrude with the sorption process of F^-, reduce the efficiency. Therefore, it is necessary to estimate the effect of the contending anions. Adding the coexisting anion would cause decrement in fluoride sorption capacity, which would affect from the competitive effect of anions for available active site of the adsorbent. Thus, the goods of these competitive anions delved in this study. As Figure 4.22 shown demonstrates the effect of three co-existing ion similar as Nitrate, Chlorides and Hydro carbonates of 8 mg/L of each on fluoride removal at optimum parameters were investigated . The results indicated that the anions have substantial effect on fluoride removal. The effect of Nitrate insignificant as compared to Hydrocarbon and chlorides. The presence of chloride ion within fluoride reduces the probabilities of fluoride removal efficiency from 98.1 to 71.54.

In addition, Hydro carbonate were another competitive ion, which reduce the fluoride removal performance to 79.15. Thus, chloride was the topmost contender for fluoride followed by Hydro carbonates and Nitrate. (Alkurdi et al., 2019a) confirmed that chloride ions were the most influential ions, which compete with fluoride. These is as result of high concentration of chloride leads to lack of available surface area on BAZ adsorbent sites. For enhancing adsorption efficiency some fundamental characterization of ions should be considered for the selective adsorptions includes the solubility, ionic radius, hydration energy and bulk coefficient (J. He et al., 2020). The competing anions reduce the removal efficiency of fluoride in the order

of chloride > Hydro carbonate > Nitrate. The effect of chloride ion obtained from greater tendency of chloride to undergo ion exchange reaction.

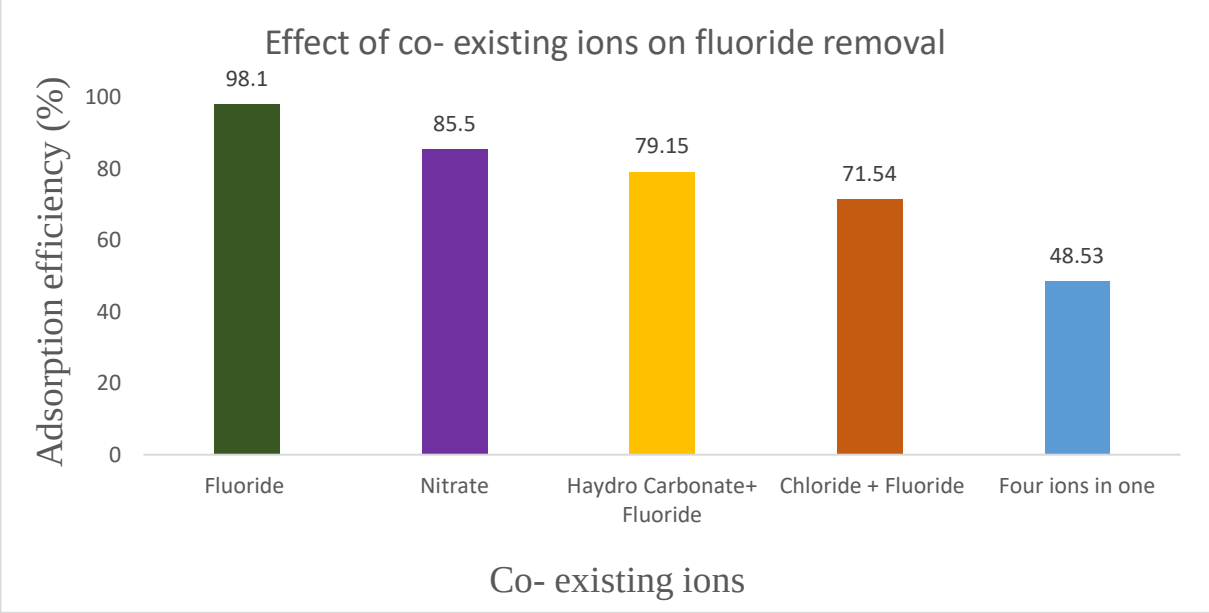

Figure 4. 22: Effects of Co-existing ions in fluoride removal by BAZ

4.10 Regeneration Study

To assess the durability of this adsorbent, regeneration studies were carried out for the adsorption of fluoride over five consecutive adsorption five desorption cycles. A solution of 0.1M of NaOH was chosen as the eluent in the desorption process. High reusability of adsorbent is very indispensable for any adsorbent, which significantly increase the economic value of the adsorption process. To study regeneration study 0.5 g of adsorbent dose, 7.5 of pH of the solution, 10 mg/L of initial fluoride concentration at 1 hr. contact time with removal efficiency of 98.1% contacted to regenerate BAZ. As shown in bar graph figure 4.23, the removal efficiency of the first cycle was 90.44% while the second cycle resulted 85.8%. At the third, fourth, and five cycle the removal efficiency of fluoride ion was 74.98, 68.73% and 47% respectively. This value ensures that the prepared adsorbent could be reused different times without any loss of adsorption ability. Therefore, BAZ is a promising adsorbent for removal of fluoride ion from contaminant water.

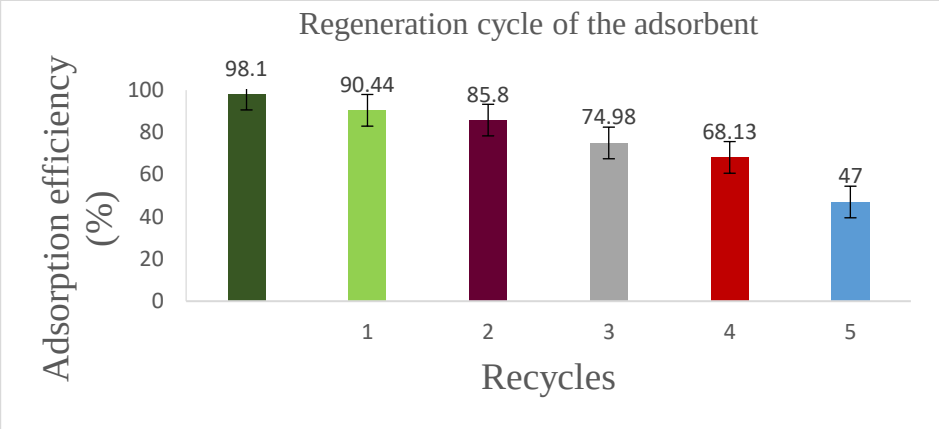

Figure 4. 23: Reusability performance of BAZ

4.11 Removal of Fluoride from Real Water

In order to apply the laboratory experimental result into the practical real world application, the investigation carried out by taking the real water, which have 10.0 mg /L amount of total fluoride from north of meki. The laboratory report indicates the real water contain high concentration of HCO_3^{-1}, SO_4^{-} and Cl^{-}, which have the value 930 mg/L, 10 mg/L, 140 mg/L respectively. The adsorption process is conducted at optimum parameter includes pH = 7.5, contact time =60 min, BAZ dose = 0.5 g/200 ml. The removal efficiency of the adsorbent drops to 75%, the result shows significant decrement in removal efficiency of the adsorbent due to the presence of large amount of Hydro carbonate, chloride, and sulfate. Real water has complex and diverse compositions, including high concentrations of interfering substances, complex organic compounds, or heavy metals. These substances can compete with fluoride ions for adsorption sites on the adsorbent or form complexes that reduce the availability of active sites. This competition and interference can lead to a decrease in the removal efficiency. Moreover, real water contains suspended solids, colloidal matter, or organic compounds that can adhere to the surface of the adsorbent and form a fouling layer. This fouling layer can block or reduce the accessibility of the active sites, inhibiting effective fluoride removal.

4.12 Comparison Study of Fluoride by Different Adsorbents

The synthesized Bone char/ Aluminum loaded zeolite Y composite adsorbent was compared with different adsorbents reported in related works for fluoride removal from water. As Table 4.12 indicated, the optimum pH, isotherm model, kinetics models, and q_{max} were compared for fluoride removal.

Table 4. 12: Adsorption capacities and other parameters for removal of fluoride by different adsorbent

Adsorbent	**Optimum pH**	**Initial fluoride conc(mg/L**	**Isotherm**	**kinetics**	**q_{max} (mg/g)**	**Reference**
Commercial bone char	5	1-20	Langmuir and Freundlich	Pseudo-first order	7.74	(Medellin-Castillo et al., 2014b)
Zeolite(Ethiopia)	6.7		Langmuir	Pseudo-second order	0.47	(Gómez-Hortigüela et al., 2014)
Cow bone char	7.4±0.4	10	Langmuir	Pseudo-first order	6.2±0.5	(Nigri et al., 2017a)
Bone char	7	10-100	Langmuir	Pseudo-second order	7.32	(Rojas-Mayorga, et al., 2013)
Aluminum hydroxide loaded zeolite	5.5-6.5		Freundlich	Pseudo-second order	18.12	(J. Chen et al., 2022)
Zeolite modified With calcium and aluminum	4-8	10	Langmuir	Pseudo-second order	8.03	(Waghmare et al., 2015)
BAZ	7.5	10	Langmuir	Pseudo-second order	19.23	This study

5. Conclusions and Recommendations

5.1 Conclusion

The bone char/Aluminum loaded zeolite Y composite was prepared by physical mixing with different proportion. The bone char was prepared simply by calcining raw bone at 600 ^{o}C for 2 hr and activated with 0.1 HNO_3. On the other hand, Zeolite Y synthesized from kaoline clay by alkali fusion method and then Aluminum loaded zeolite Y synthesized by wet impregnation method. The composite of bone char and aluminum loaded zeolite Y prepared by varying ratio (1:1,1:3,3:1) and labeled as 1:1BAZ, 1:3 BAZ, 3:1 BAZ. Those composites, pure bone char and zeolite Y efficiency on removal of fluoride were compared. Among all Adsorbents, the 3:1 BAZ (bone char to aluminum loaded zeolite Y) composite exhibits significant efficacy in the removal of fluoride from water. This can be credited to the exceptional properties of aluminum loaded zeolite Y. Furthermore, the incorporation of aluminum-loaded zeolite Y as a constituent of the composite enhances the overall efficiency of the adsorbent while also reducing the required quantity of adsorbent dosage. The XRD, FTIR, SEM and BET confirm that the bone char, Zeolite Y, aluminum loaded zeolite Y and bone char/ aluminum loaded zeolite Y composite synthesized effectively. The FTIR result analysis confirmed that fluoride ion was successfully adsorbed by BAZ composite. The specific surface area of BC, ZY and BAZ are 406.249 m^2/g, 523.120 m^2/g and 540.120 m^2/g respectively.

The Response Surface Method (RSM) adopted to explore the model equation for fluoride removal efficiency. The central composite design was selected to study the effect of variation in pH of the solution, contact time, and adsorbent dose. The validation of the model using ANOVA analysis verified that the quadratic model selected is accurate, and statistically significant with a p-value less than 0.05. The optimum removal efficiency of 98.1% was obtained at pH= 7.5, t = 60 min, and dose = 0.5 g. The result shows the interaction effect of those parameters had a significant effect on the adsorption process.

The Langmuir isotherm model was in better agreement with the experimental data with maximum adsorption capacity and correlation coefficient (R^2) of 19.231 mg/g, and 0.999 respectively. This suggests that the adsorption process followed monolayer adsorption onto the surface of a finite number of identical adsorption sites. Fluoride adsorption kinetics was explained properly through the pseudo-second-order kinetics model (R^2 = 0.999), which indicated that the chemical

adsorption became the controlling mechanism of the adsorption process. In addition, the thermodynamics parameters recommended that the fluoride removal is spontaneous and endothermic in nature.

The effects of competing ion on fluoride adsorption by bone char/Aluminum loaded zeolite Y composite was found to follow this order NO_3^- < HCO^-_3 < Cl^-. Adsorption regeneration study of BAZ composite was investigated using 0.1M of NaOH as an eluent, which is the most prominent desorption agent. The adsorption- desorption of five cycles carried out successfully. According to this study, the result found indicates that the adsorbent is determined to be the best promising and effective for removal of fluoride ion from water.

5.2 Recommendation

For the future work, the following recommendations suggested based on the result obtained from this study.

- It is recommended that study the effects of adsorption parameters such as particle size and agitation speed.
- The sample is characterized by XRD, FTIR, TGA, and BET. The sample need further characterization such as SEM-EDX and XRF
- Designing and scale up of adsorption column and analysis of the economic viability of large scale production could be the main area of future study
- The regeneration of the adsorbent was investigated by using NaOH as eluent agent. The determination of the most preferable regenerating solution is a very essential. Therefore, further studies on effectiveness of other regenerating solutions such as H_2SO_4, HCl, $NaNO_3$, NH_4Cl, HNO_3 and $CaCl_2$ should be investigated.

Reference

Abdalla, M. M., Lung, C. Y. K., Neelakantan, P., & Matinlinna, J. P. (2020). A novel, doped calcium silicate bioceramic synthesized by sol–gel method: Investigation of setting time and biological properties. *Journal of Biomedical Materials Research - Part B Applied Biomaterials*, *108*(1), 56–66.

Abdullahi, T., Harun, Z., & Othman, M. H. D. (2017). A review on sustainable synthesis of zeolite from kaolinite resources via hydrothermal process. *Advanced Powder Technology*, *28*(8), 1827–1840.

Abir, T. M., Datta, M., & Saha, S. R. (2023). Assessing the Factors Influencing Effective Municipal Solid Waste Management System in Barishal Metropolitan Areas. *Journal of Geoscience and Environment Protection*, *11*(1), 49–66.

Abraha, K. (2015). Various sizes of the synthesized Fe_3O_4 nanoparticles assisted by mechanical vibrations. 22(April), 175–180.

Adimalla, N., & Wu, J. (2019). Groundwater quality and associated health risks in a semi-arid region of south India: Implication to sustainable groundwater management. *Human and Ecological Risk Assessment*, *25*(1–2), 191–216.

Affonso, L. N., Marques, J. L., Lima, V. V. C., Gonçalves, J. O., Barbosa, S. C., Primel, E. G., Burgo, T. A. L., Dotto, G. L., Pinto, L. A. A., & Cadaval, T. R. S. (2020). Removal of fluoride from fertilizer industry effluent using carbon nanotubes stabilized in chitosan sponge. *Journal of Hazardous Materials*, *388*(December 2019).

Affonso, L. N., Marques Jr, J. L., Lima, V. V. C., Gonçalves, J. O., Barbosa, S. C., Primel, E. G., Burgo, T. A. L., Dotto, G. L., Pinto, L. A. A., & Cadaval Jr, T. R. S. (2020). Removal of fluoride from fertilizer industry effluent using carbon nanotubes stabilized in chitosan sponge. *Journal of Hazardous Materials*, *388*, 122042.

Agarwal, M., Rai, K., Shrivastav, R., & Dass, S. (2003). Deflouridation of water using amended clay. *Journal of Cleaner Production*, *11*(4), 439–444.

Ajiboye, T. O., Oyewo, O. A., & Onwudiwe, D. C. (2021). Simultaneous removal of organics and heavy metals from industrial wastewater: A review. *Chemosphere*, *262*, 128379.

Akbari, H., Jorfi, S., Mahvi, A. H., Yousefi, M., & Balarak, D. (2018). Adsorption of fluoride on chitosan in aqueous solutions: determination of adsorption kinetics. *Fluoride*, *51*(4), 319–327.

Al-anber, M. A. (2011). Thermodynamics Approach in the Adsorption of Heavy Metals.

Alemu, S., Mulugeta, E., Zewge, F., & Chandravanshi, B. S. (2014). Water defluoridation by aluminium oxide–manganese oxide composite material. *Environmental Technology*, *35*(15), 1893–1903.

Ali, S., Thakur, S. K., Sarkar, A., & Shekhar, S. (2016). Worldwide contamination of water by fluoride. *Environmental Chemistry Letters*, *14*(3), 291–315.

Alkurdi, S. S. A., Al-Juboori, R. A., Bundschuh, J., Bowtell, L., & McKnight, S. (2020a). Effect of pyrolysis conditions on bone char characterization and its ability for arsenic and fluoride removal. *Environmental Pollution*, *262*, 114221.

Alkurdi, S. S. A., Al-Juboori, R. A., Bundschuh, J., Bowtell, L., & McKnight, S. (2020b). Effect of pyrolysis conditions on bone char characterization and its ability for arsenic and fluoride removal. *Environmental Pollution*, *262*(September 2018), 114221.

Alkurdi, S. S. A., Al-Juboori, R. A., Bundschuh, J., & Hamawand, I. (2019a). Bone char as a green sorbent for removing health threatening fluoride from drinking water. *Environment International*, *127*(December 2018), 704–719.

Alkurdi, S. S. A., Al-Juboori, R. A., Bundschuh, J., & Hamawand, I. (2019b). Bone char as a green sorbent for removing health threatening fluoride from drinking water. *Environment International*, *127*, 704–719.

Araga, R., Kali, S., & Sharma, C. S. (2019). Coconut-shell-derived carbon/carbon nanotube composite for fluoride adsorption from aqueous solution. *Clean–Soil, Air, Water*, *47*(5), 1800286.

Aroua, M., Boulahdid, M., Radakovitch, O., Benhalima, M., Guendouzi, Y., Fowler, S. W., & Ambrosi, J.-P. (2023). Sediment pollution: An assessment of anthropogenic and geogenic trace element contributions along the central Algerian coast. *Marine Pollution Bulletin*, *186*, 114398.

Asgari, G., Dayari, A., Ghasemi, M., Seid-mohammadi, A., Gupta, V. K., & Agarwal, S. (2019). Efficient fluoride removal by preparation, characterization of pyrolysis bone: Mixed level design experiment and Taguchi L8 orthogonal array optimization. *Journal of Molecular Liquids*, *275*, 251–264.

Asgari, G., Dayari, A., Ghasemi, M., Seid-Mohammadi, A., Gupta, V. K., & Agarwal, S. (2019). Efficient fluoride removal by preparation, characterization of pyrolysis bone: Mixed level design experiment and Taguchi L8 orthogonal array optimization. *Journal of Molecular Liquids*, *275*, 251–264.

Asmellash, T., & Ayele, M. T. (2022). Phosphate removal using natural and Al/Cu modified Ethiopian zeolites. *Cogent Engineering*, *9*(1).

Awuchi, C. G. (2020). Related papers Indust rial and Communit y Wast e Management : Global Perspect ive Chinaza G Awuchi Food Addit ives and Food Preservat ives for Domest ic and Indust rial Food Applicat ions.

Ayele, L., Pérez-Pariente, J., Chebude, Y., & Díaz, I. (2015). Synthesis of zeolite A from Ethiopian kaolin. *Microporous and Mesoporous Materials*, *215*, 29–36.

Ayele, L., Pérez-Pariente, J., Chebude, Y., & Díaz, I. (2016). Conventional versus alkali fusion synthesis of zeolite A from low grade kaolin. *Applied Clay Science*, *132–133*, 485–490.

Bacelo, H., Pintor, A. M. A., Santos, S. C. R., Boaventura, R. A. R., & Botelho, C. M. S. (2020). Performance and prospects of different adsorbents for phosphorus uptake and recovery from water. In *Chemical Engineering Journal* (Vol. 381).

Baek, J. W., Kim, K. S., Park, H., Park, N. G., & Kim, B.-S. (2022). Enhanced Biocompatibility and Osteogenic Activity of Marine-Plankton-Derived Whitlockite Bone Granules through Bone Morphogenetic Protein 2 Incorporation. *Bioengineering*, *9*(8), 399.

Barathi, M., Kumar, A. S. K., Kumar, C. U., & Rajesh, N. (2014). Graphene oxide–aluminium oxyhydroxide interaction and its application for the effective adsorption of fluoride. *Rsc*

Advances, *4*(96), 53711–53721.

Batool, F., Akbar, J., Iqbal, S., Noreen, S., Nasir, S., & Bukhari, A. (2018). Study of Isothermal , Kinetic , and Thermodynamic Parameters for Adsorption of Cadmium : An Overview of Linear and Nonlinear Approach and Error Analysis. 2018.

Battas, A., El Gaidoumi, A., Ksakas, A., & Kherbeche, A. (2019). Adsorption study for the removal of nitrate from water using local clay. *Scientific World Journal*, *2019*.

Bhan, C., & Singh, J. (2022). Defluoridation of fluoride contaminated water by adsorption process : A Defluoridation of fluoride contaminated water by adsorption process : A review. December 2022.

Bhatnagar. (2015). *(PDF)* Removal of fluoride from aqueous solution using graphite: A kinetic and thermodynamic study.

Bhatnagar, A., Kumar, E., & Sillanpää, M. (2011). Fluoride removal from water by adsorption-A review. *Chemical Engineering Journal*, *171*(3), 811–840.

Biswas, P. P., Liang, B., Turner-Walker, G., Rathod, J., Lee, Y.-C., Wang, C.-C., & Chang, C.-K. (2021). Systematic changes of bone hydroxyapatite along a charring temperature gradient: An integrative study with dissolution behavior. *Science of the Total Environment*, *766*, 142601.

Brunson, L. R., & Sabatini, D. A. (2009). An evaluation of fish bone char as an appropriate arsenic and fluoride removal technology for emerging regions. *Environmental Engineering Science*, *26*(12), 1777–1784.

Bullen, J. C., Saleesongsom, S., Gallagher, K., & Weiss, D. J. (2021). A Revised Pseudo-Second-Order Kinetic Model for Adsorption, Sensitive to Changes in Adsorbate and Adsorbent Concentrations. *Langmuir*, *37*(10), 3189–3201.

Bundi, R. (2020). Enhancement of Defluoridation Efficiency of Bone Char using Surface Modification and Sequential application with Bamboo Char.

Cai, H., Chen, G., Peng, C., Xu, L., Zhu, X., Zhang, Z., Dong, Y., Shang, G., Ke, F., & Gao, H. (2015). Enhanced removal of fluoride by tea waste supported hydrous aluminium oxide nanoparticles: anionic polyacrylamide mediated aluminium assembly and adsorption mechanism. *Rsc Advances*, *5*(37), 29266–29275.

Caponi, N., Collazzo, G. C., Jahn, S. L., Dotto, G. L., Mazutti, M. A., & Foletto, E. L. (2017). Use of Brazilian kaolin as a potential low-cost adsorbent for the removal of malachite green from colored effluents. *Materials Research*, *20*, 14–22.

Çeçen, F., & Aktas, Ö. (2011). Activated carbon for water and wastewater treatment: integration of adsorption and biological treatment. John Wiley & Sons.

Chahkandi, B., Gheibi, M., & Takhtravan, A. (2021). Behavior evaluation of freundlich and langmuir isotherms in cadmium preconcentration using solid phase extraction method for linear and nonlinear numerical computational patterns.

Chai, L., Wang, Y., Zhao, N., Yang, W., & You, X. (2013). Sulfate-doped Fe3O4/Al2O3 nanoparticles as a novel adsorbent for fluoride removal from drinking water. *Water Research*, *47*(12), 4040–4049.

Chen, J., Yang, R., Zhang, Z., & Wu, D. (2022). Removal of fluoride from water using aluminum hydroxide-loaded zeolite synthesized from coal fly ash. *Journal of Hazardous Materials*, *421*, 126817.

Chen, L., Zhang, K.-S., He, J.-Y., Xu, W.-H., Huang, X.-J., & Liu, J.-H. (2016). Enhanced fluoride removal from water by sulfate-doped hydroxyapatite hierarchical hollow microspheres. *Chemical Engineering Journal*, *285*, 616–624.

Colombani, N., Di Giuseppe, D., Kebede, S., & Mastrocicco, M. (2018). Assessment of the anthropogenic fluoride export in Addis Ababa urban environment (Ethiopia). *Journal of Geochemical Exploration*, *190*(April), 390–399.

Dahi, E. (2016). Africa's u-turn in defluoridation policy: from the nalgonda technique to bone char. *Fluoride*, *49*(4).

Delgadillo-Velasco, L., Hernández-Montoya, V., Cervantes, F. J., Montes-Morán, M. A., & Lira-Berlanga, D. (2017). Bone char with antibacterial properties for fluoride removal: Preparation, characterization and water treatment. *Journal of Environmental Management*, *201*, 277–285.

Dessalegne, M., Zewge, F., & Diaz, I. (2017). Aluminum hydroxide supported on zeolites for fluoride removal from drinking water. *Journal of Chemical Technology and Biotechnology*, *92*(3), 605–613.

Dey, S., Haripavan, N., Basha, S. R., & Babu, G. V. (2021). Current Research in Chemical Biology Removal of ammonia and nitrates from contaminated water by using solid waste bio-adsorbents. *Current Research in Chemical Biology*, *1*, 100005.

Dhillon, A., Nair, M., & Kumar, D. (2016). Analytical methods for determination and sensing of fluoride in biotic and abiotic sources: a review. *Analytical Methods*, *8*(27), 5338–5352.

Díaz, I. (2017). Environmental uses of zeolites in Ethiopia. *Catalysis Today*, *285*, 29–38. https://doi.org/10.1016/j.cattod.2017.01.045

Du, J., Asce, S. M., Sabatini, D. A., Asce, M., & Butler, E. C. (2015). Preparation , Characterization , and Regeneration of Aluminum (Hydr) Oxide – Amended Molecular Sieves for Fluoride Removal from Drinking Water. 1–8.

Du, J., Sabatini, D. A., & Butler, E. C. (2017). Evaluation of aluminum hydroxide-amended zeolites in fluoride removal: Column filtration and regeneration. *Journal of Environmental Engineering*, *143*(4), 4016092.

Ferreira, D., Marais, J. P. J., Coleman, C. M., & Slade, D. (2010). Proanthocyanidins: Chemistry and biology. *Comprehensive Natural Products II: Chemistry and Biology*, *6*, 605–661.

Figueiredo, M., Fernando, A., Martins, G., Freitas, J., Judas, F., & Figueiredo, H. (2010). Effect of the calcination temperature on the composition and microstructure of hydroxyapatite derived from human and animal bone. *Ceramics International*, *36*(8), 2383–2393.

FLANIGEN, E. M., KHATAMI, H., & SZYMANSKI, H. A. (1971). Infrared structural studies of zeolite frameworks. ACS Publications.

Fletcher, R. E. (2019). The Location and Effect of Aluminium in Zeolites. UCL (University

College London).

Gai, W.-Z., & Deng, Z.-Y. (2021). A comprehensive review of adsorbents for fluoride removal from water: Performance, water quality assessment and mechanism. *Environmental Science: Water Research & Technology*, *7*(8), 1362–1386.

Gai, W.-Z., Deng, Z.-Y., & Shi, Y. (2015). Fluoride removal from water using high-activity aluminum hydroxide prepared by the ultrasonic method. *Rsc Advances*, *5*(102), 84223–84231.

Gai, W.-Z., Zhang, S.-H., Yang, Y., Sun, K., Jia, H., & Deng, Z.-Y. (2022). Defluoridation performance comparison of aluminum hydroxides with different crystalline phases. *Water Supply*, *22*(4), 3673–3684.

Gai, W. Z., & Deng, Z. Y. (2021). A comprehensive review of adsorbents for fluoride removal from water: Performance, water quality assessment and mechanism. *Environmental Science: Water Research and Technology*, *7*(8), 1362–1386.

Gai, W. Z., Deng, Z. Y., & Shi, Y. (2015). Fluoride removal from water using high-activity aluminum hydroxide prepared by the ultrasonic method. *RSC Advances*, *5*(102), 84223–84231.

Gai, W. Z., Zhang, S. H., Yang, Y., Sun, K., Jia, H., & Deng, Z. Y. (2022). Defluoridation performance comparison of aluminum hydroxides with different crystalline phases. *Water Supply*, *22*(4), 3673–3684.

Gai, W., Zhang, S., Yang, Y., Zhang, X., & Deng, Z. (2021). Separation of Excess Fluoride from Water Using Amorphous and Crystalline AlOOH Adsorbents.

Gao, M., Wang, W., Yang, H., & Ye, B.-C. (2020). Efficient removal of fluoride from aqueous solutions using 3D flower-like hierarchical zinc-magnesium-aluminum ternary oxide microspheres. *Chemical Engineering Journal*, *380*, 122459.

Glaser, T., Müller, C., Sendner, M., Krekeler, C., Semonin, O. E., Hull, T. D., Yaffe, O., Owen, J. S., Kowalsky, W., & Pucci, A. (2015). Infrared spectroscopic study of vibrational modes in methylammonium lead halide perovskites. *The Journal of Physical Chemistry Letters*, *6*(15), 2913–2918.

Godebo, T. R. (2022). Using Innovative Technology to Investigate Bone Disorders Induced by Environmental Contaminants. *Scientia*.

Gómez-Hortigüela, L., Pérez-Pariente, J., Chebude, Y., & Diaz, I. (2014). Controlled growth of hydroxyapatite on the surface of natural stilbite from Ethiopia: application in mitigation of fluorosis. *RSC Advances*, *4*(16), 7998–8003.

Gómez-Hortigüela, L., Pérez-Pariente, J., García, R., Chebude, Y., & Díaz, I. (2013). Natural zeolites from Ethiopia for elimination of fluoride from drinking water. *Separation and Purification Technology*, *120*, 224–229.

Guiar, E. D. E., Ria, C. L. D. L., Epartment, N., Aneiro, E. O. F. D. E., Epartment, H. N., Of, E., Hemistry, N., & Nstitute, H. (2005).

Gupta, V. K., Carrott, P. J. M., Singh, R., Chaudhary, M., & Kushwaha, S. (2016). Cellulose: a review as natural, modified and activated carbon adsorbent. *Bioresource Technology*,

216, 1066–1076.

He, J., Yang, Y., Wu, Z., Xie, C., Zhang, K., Kong, L., & Liu, J. (2020). Review of fluoride removal from water environment by adsorption. *Journal of Environmental Chemical Engineering*, *8*(6), 104516.

He, Y., Zhang, L., An, X., Wan, G., Zhu, W., & Luo, Y. (2019). Enhanced fluoride removal from water by rare earth (La and Ce) modified alumina: Adsorption isotherms, kinetics, thermodynamics and mechanism. *Science of the Total Environment*, *688*, 184–198.

Ho, Y. S., Porter, J. F., & Mckay, G. (2002). Divalent metal ions onto peat : Copper , Nickel and lead single component systems. 1–33.

Huang, J., Chen, M., Kuo, W., Sun, Y., & Lin, F. (2014). The characterization and evaluation of cisplatin-loaded magnetite – hydroxyapatite nanoparticles (mHAp / CDDP) as dual treatment of hyperthermia and chemotherapy for lung cancer therapy. *Ceramics International*, 1–12.

Huang, L., Yang, Z., He, Y., Chai, L., Yang, W., Deng, H., Wang, H., Chen, Y., & Crittenden, J. (2020a). Adsorption mechanism for removing different species of fluoride by designing of core-shell boehmite.

Huang, L., Yang, Z., He, Y., Chai, L., Yang, W., Deng, H., Wang, H., Chen, Y., & Crittenden, J. (2020b). Adsorption mechanism for removing different species of fluoride by designing of core-shell boehmite. *Journal of Hazardous Materials*, *394*(December 2019), 122555.

Hwang, S., & Kärger, J. (2020). Diffusion in nanopores: correlating experimental findings with "first-principles" predictions. *Adsorption*, *26*(7), 1001–1013.

International, & Hydrogeologists, A. of. (2022). Groundwater – more about the hidden resource - IAH - The International Association of Hydrogeologists.

Jagtap, S., Yenkie, M. K., Labhsetwar, N., & Rayalu, S. (2012). Fluoride in drinking water and defluoridation of water. *Chemical Reviews*, *112*(4), 2454–2466.

Jamalluddin, N. A., & Abdullah, A. Z. (2014). Low frequency sonocatalytic degradation of Azo dye in water using Fe-doped zeolite Y catalyst. *Ultrasonics Sonochemistry*, *21*(2), 743–753.

Jin, Z., Jia, Y., Zhang, K.-S., Kong, L.-T., Sun, B., Shen, W., Meng, F.-L., & Liu, J.-H. (2016). Effective removal of fluoride by porous MgO nanoplates and its adsorption mechanism. *Journal of Alloys and Compounds*, *675*, 292–300.

Johnson, E. B. G., & Arshad, S. E. (2014). Hydrothermally synthesized zeolites based on kaolinite: A review. *Applied Clay Science*, *97*, 215–221.

Joschek, S., Nies, B., Krotz, R., & Göpferich, A. (2016). Chemical and physicochemical characterization of porous hydroxyapatite ceramics made of natural bone. *Biomaterials*, *21*(16), 1645–1658.

Julbe, A., & Drobek, M. (2016). Zeolite Y type. Springer.

Kadioglu, Y., Gulaboglu, M., Ozturk, M., & Dogan, N. (2015). Determination of fluoride by using Ion Selective Electrode (ISE) method in urine of healthy volunteer and patients before-after sevoflurane anesthesia. *Latin American Journal of Pharmacy*, *34*(8), 1658–

1663.

Kaseva, M. E. (2006). Optimization of regenerated bone char for fluoride removal in drinking water: a case study in Tanzania. *Journal of Water and Health*, *4*(1), 139–147.

Kawasaki, N., Ogata, F., Tominaga, H., & Yamaguchi, I. (2009). Removal of fluoride ion by bone char produced from animal biomass. *Journal of Oleo Science*, *58*(10), 529–535.

Keshtkar, M., Dobaradarana, S., Nabipour, I., Mahvie, A. H., Ghasemi, F. F., Ahmadi, Z., & Heydari, M. (2016). Isotherm and kinetic studies on fluoride biosorption from aqueous solution by using cuttlebone obtained from the Persian Gulf. *Fluoride*, *49*(3), 343.

Khaleque, A., Alam, M. M., Hoque, M., Mondal, S., Haider, J. Bin, Xu, B., Johir, M. A. H., Karmakar, A. K., Zhou, J. L., & Ahmed, M. B. (2020). Zeolite synthesis from low-cost materials and environmental applications: A review. *Environmental Advances*, *2*, 100019.

Krstić, V. (2021). Role of zeolite adsorbent in water treatment. Handbook of Nanomaterials for Wastewater Treatment: Fundamentals and Scale up Issues, 417–481.

Kulkarni, S., & Kaware, J. (2014). Regeneration and Recovery in Adsorption- a Review. 1(8), 61–64.

Lacson, C. F. Z., Lu, M.-C., & Huang, Y.-H. (2021). Fluoride-containing water: A global perspective and a pursuit to sustainable water defluoridation management-An overview. *Journal of Cleaner Production*, *280*, 124236.

Laksmi, A. C., & Hanin, I. U. D. (2022). The Effect of Profitability, Leverage, Liquidity, and Green Accounting on Corporate Social Responsibility Disclosures: Study on Mining Companies Listed on the Indonesia Stock Exchange from 2016 to 2020. *Jurnal Aplikasi Bisnis*, *19*(2).

Lázaro, B. B. (2015). Halloysite and kaolinite: two clay minerals with geological and technological importance. *Revista de La Academia de Ciencias Exactas, Físicas, Químicas y Naturales de Zaragoza*, *70*, 7–38.

Lee, J.-I., Hong, S.-H., Lee, C.-G., & Park, S.-J. (2020). Experimental and model study for fluoride removal by thermally activated sepiolite. *Chemosphere*, *241*, 125094.

Li, P., Karunanidhi, D., Subramani, T., & Srinivasamoorthy, K. (2021). Sources and Consequences of Groundwater Contamination. *Archives of Environmental Contamination and Toxicology*, *80*(1), 1–10.

Ma, Y., Wang, S.-G., Fan, M., Gong, W.-X., & Gao, B.-Y. (2009). Characteristics and defluoridation performance of granular activated carbons coated with manganese oxides. *Journal of Hazardous Materials*, *168*(2–3), 1140–1146.

Mahfoudhi, N., & Boufi, S. (2017). Nanocellulose as a novel nanostructured adsorbent for environmental remediation: a review. *Cellulose*, *24*(3), 1171–1197.

Medellin-Castillo, N. A., Leyva-Ramos, R., Ocampo-Perez, R., Garcia de la Cruz, R. F., Aragon-Pina, A., Martinez-Rosales, J. M., Guerrero-Coronado, R. M., & Fuentes-Rubio, L. (2007). Adsorption of fluoride from water solution on bone char. *Industrial & Engineering Chemistry Research*, *46*(26), 9205–9212.

Medellin-Castillo, N. A., Leyva-Ramos, R., Padilla-Ortega, E., Perez, R. O., Flores-Cano, J.

V., & Berber-Mendoza, M. S. (2014a). Adsorption capacity of bone char for removing fluoride from water solution. Role of hydroxyapatite content, adsorption mechanism and competing anions. *Journal of Industrial and Engineering Chemistry*, *20*(6), 4014–4021.

Medellin-Castillo, N. A., Leyva-Ramos, R., Padilla-Ortega, E., Perez, R. O., Flores-Cano, J. V, & Berber-Mendoza, M. S. (2014b). Adsorption capacity of bone char for removing fluoride from water solution. Role of hydroxyapatite content, adsorption mechanism and competing anions. *Journal of Industrial and Engineering Chemistry*, *20*(6), 4014–4021.

Medellin-Castillo, N. A., Padilla-Ortega, E., Tovar-García, L. D., Leyva-Ramos, R., Ocampo-Pérez, R., Carrasco-Marín, F., & Berber-Mendoza, M. S. (2016). Removal of fluoride from aqueous solution using acid and thermally treated bone char. *Adsorption*, *22*(7), 951–961.

Mehrotra, A., Mishra, A., & Shukla, N. (2018). An Assessment of Arsenic Contamination and Mitigation Measures in District Ballia, part of Ganga and Ghagra Basins, Uttar Pradesh, India. *Earth Science India*, *11*.

Mehta, D., Mondal, P., Saharan, V. K., & George, S. (2018). In-vitro synthesis of marble apatite as a novel adsorbent for removal of fluoride ions from ground water: an ultrasonic approach. *Ultrasonics Sonochemistry*, *40*, 664–674.

Meilani, V., Lee, J.-I., Kang, J.-K., Lee, C.-G., Jeong, S., & Park, S.-J. (2021). Application of aluminum-modified food waste biochar as adsorbent of fluoride in aqueous solutions and optimization of production using response surface methodology. *Microporous and Mesoporous Materials*, *312*, 110764.

Mgbemere, H., Ekpe, I., Lawal, G., Ovri, H., & Chaudhary, A.-L. (2019). Preparation and Characterization of Zeolite type 4A using Kaolin from Ajebo, Nigeria.

Mondal, P., & George, S. (2015). A review on adsorbents used for defluoridation of drinking water. *Reviews in Environmental Science and Biotechnology*, *14*(2), 195–210.

Mondal, P., & Purkait, M. K. (2019). Preparation and characterization of novel green synthesized iron–aluminum nanocomposite and studying its efficiency in fluoride removal. *Chemosphere*, *235*, 391–402.

Moneim, M. A., & Ahmed, E. A. (2015). Synthesis of faujasite from Egyptian clays: Characterizations and removal of heavy metals. *Geomaterials*, *5*(02), 68.

Moreno-Piraján, J. C., Gómez-Cruz, R., García-Cuello, V. S., & Giraldo, L. (2010). Binary system Cu (II)/Pb (II) adsorption on activated carbon obtained by pyrolysis of cow bone study. *Journal of Analytical and Applied Pyrolysis*, *89*(1), 122–128.

Mulugeta, E., Zewge, F., Annette Johnson, C., & Chandravanshi, B. S. (2014). A high-capacity aluminum hydroxide-based adsorbent for water defluoridation. *Desalination and Water Treatment*, *52*(28–30), 5422–5429.

Mulugeta, E., Zewge, F., Johnson, C. A., & Chandravanshi, B. S. (2015). Aluminium hydro (oxide)–based (AO) adsorbent for defluoridation of drinking water: Optimisation, performance comparison, and field testing. *Water SA*, *41*(1), 121–128.

Nasr, A. Ben, Walha, K., Charcosset, C., & Amar, R. Ben. (2011). Removal of fluoride ions using cuttlefish bones. *Journal of Fluorine Chemistry*, *132*(1), 57–62.

Nigri, E. M., Bhatnagar, A., & Rocha, S. D. F. (2016). Thermal regeneration process of bone char used in the fluoride removal from aqueous solution. *Journal of Cleaner Production*, *142*, 3558–3570.

Nigri, E. M., Cechinel, M. A. P., Mayer, D. A., Mazur, L. P., Loureiro, J. M., Rocha, S. D. F., & Vilar, V. J. P. (2017a). Cow bones char as a green sorbent for fluorides removal from aqueous solutions: batch and fixed-bed studies. *Environmental Science and Pollution Research*, *24*(3), 2364–2380.

Nigri, E. M., Cechinel, M. A. P., Mayer, D. A., Mazur, L. P., Loureiro, J. M., Rocha, S. D. F., & Vilar, V. J. P. (2017b). Cow bones char as a green sorbent for fluorides removal from aqueous solutions: batch and fixed-bed studies. *Environmental Science and Pollution Research*, *24*, 2364–2380.

Nyieku, F. E., Essandoh, H. M. K., Armah, F. A., & Awuah, E. (2022). Oilfield wastewater contaminants removal efficiencies of three indigenous plants species in a free water surface flow constructed wetland. *Sustainable Environment*, *8*(1), 2076361.

Ogata, F., Imai, D., & Kawasaki, N. (2015). Adsorption of nitrate and nitrite ions onto carbonaceous material produced from soybean in a binary solution system. *Journal of Environmental Chemical Engineering*, *3*(1), 155–161.

Ooi, C. Y., Hamdi, M., & Ramesh, S. (2007). Properties of hydroxyapatite produced by annealing of bovine bone. *Ceramics International*, *33*(7), 1171–1177.

Patel, S., Han, J., Qiu, W., & Gao, W. (2015). Synthesis and characterisation of mesoporous bone char obtained by pyrolysis of animal bones, for environmental application. *Journal of Environmental Chemical Engineering*, *3*(4), 2368–2377.

Patrylak, L., Likhnyovskyi, R., Vypyraylenko, V., Leboda, R., Skubiszewska-Zięba, J., & Patrylak, K. (2001). Adsorption properties of zeolite-containing microspheres and FCC catalysts based on Ukrainian kaolin. *Adsorption Science & Technology*, *19*(7), 525–540.

Phawachalotorn, C., Wongniramaikul, W., Taweekarn, T., Kleangklao, B., Pisitaro, W., Limsakul, W., Sriprom, W., Towanlong, W., & Choodum, A. (2023). Continuous Phosphate Removal and Recovery Using a Calcium Silicate Hydrate Composite Monolithic Cryogel Column. *Polymers*, *15*(3), 539.

Pillai, P., Dharaskar, S., Pandian, S., & Panchal, H. (2021). Overview of fluoride removal from water using separation techniques. *Environmental Technology and Innovation*, *21*(xxxx), 101246.

Podgorski, J., & Berg, M. (2022). Global analysis and prediction of fluoride in groundwater. 2022, 1–9.

Rachman, R. A., Ita, T., Aulia, W., Iqbal, M., Widiastuti, N., & Kurniawan, F. (2018). Combination of Microbial Fuel Cell and Zeolite Na-Y adsorption for Chromium Removal. 020073.

Rahman, S., Nawaz, R., Khan, J. A., Ullah, H., Irfan, M., Glowacz, A., Lyp-Wronska, K., Wzorek, L., Khan, M. K. A., Jalalah, M., Alsaiari, M. A., & Almawgani, A. H. (2021). Synthesis and characterization of carbon and carbon-nitrogen doped black tio2 nanomaterials and their application in sonophotocatalytic remediation of treated agro-

industrial wastewater. *Materials*, *14*(20).

Ren, C., Yu, Z., Phillips, B. L., Wang, H., Ji, J., Pan, B., & Li, W. (2019). Molecular-scale investigation of fluoride sorption mechanism by nanosized hydroxyapatite using 19F solid-state NMR spectroscopy. *Journal of Colloid and Interface Science*, *557*, 357–366.

Rojas-Mayorga, C. K., Bonilla-Petriciolet, A., Aguayo-Villarreal, I. A., Hernandez-Montoya, V., Moreno-Virgen, M. R., Tovar-Gómez, R., & Montes-Morán, M. A. (2013). Optimization of pyrolysis conditions and adsorption properties of bone char for fluoride removal from water. *Journal of Analytical and Applied Pyrolysis*, *104*, 10–18.

Rojas-Mayorga, C. K., Bonilla-Petriciolet, A., Aguayo-Villarreal, I. A., Hernández-Montoya, V., Moreno-Virgen, M. R., Tovar-Gómez, R., & Montes-Morán, M. A. (2013). Optimization of pyrolysis conditions and adsorption properties of bone char for fluoride removal from water. *Journal of Analytical and Applied Pyrolysis*, *104*, 10–18.

Rojas-Mayorga, C. K., Bonilla-Petriciolet, A., Silvestre-Albero, J., Aguayo-Villarreal, I. A., & Mendoza-Castillo, D. I. (2015). Physico-chemical characterization of metal-doped bone chars and their adsorption behavior for water defluoridation. *Applied Surface Science*, *355*, 748–760.

Sani, T., Gómez-Hortigüela, L., Pérez-Pariente, J., Chebude, Y., & Díaz, I. (2016). Defluoridation performance of nano-hydroxyapatite/stilbite composite compared with bone char. *Separation and Purification Technology*, *157*, 241–248.

Sarkar, C., Basu, J. K., & Samanta, A. N. (2019). Experimental and kinetic study of fluoride adsorption by Ni and Zn modified LD slag based geopolymer. *Chemical Engineering Research and Design*, *142*, 165–175.

Shahid, M. K., & Choi, Y. G. (2018). The comparative study for scale inhibition on surface of RO membranes in wastewater reclamation: CO2 purging versus three different antiscalants. *Journal of Membrane Science*, *546*(October 2017), 61–69.

Shahid, M. K., Kim, J. Y., & Choi, Y.-G. (2019). Synthesis of bone char from cattle bones and its application for fluoride removal from the contaminated water. *Groundwater for Sustainable Development*, *8*, 324–331.

Shahid, M. K., Kim, J. Y., Shin, G., & Choi, Y. (2020). Effect of pyrolysis conditions on characteristics and fluoride adsorptive performance of bone char derived from bone residue. *Journal of Water Process Engineering*, *37*, 101499.

Singh, K., Lataye, D. H., Wasewar, K. L., & Yoo, C. K. (2013). Removal of fluoride from aqueous solution: status and techniques. *Desalination and Water Treatment*, *51*(16–18), 3233–3247.

Singh, P. K., Banerjee, S., Srivastava, A. L., & Sharma, Y. C. (2015). RSC Advances Kinetic and equilibrium modeling for removal of by a potential adsorbent , hydrous bismuth oxide. 35365–35376.

Smittakorn, S., Jir 1213jawongboonrod, N., Mongkolnchai-Arunya, S., & Durnford, D. (2010). Homemade bone charcoal adsorbent for defluoridation of groundwater in Thailand. *Journal of Water and Health*, *8*(4), 826–836.

Sommerville, R. P. Z. (2017). Utilisation of fly ash in the manufacture of zeolites. University

of Birmingham.

Tao, W., Zhong, H., Pan, X., Wang, P., Wang, H., & Huang, L. (2020). Removal of fluoride from wastewater solution using Ce-AlOOH with oxalic acid as modification. *Journal of Hazardous Materials*, *384*, 121373.

Taufiqurrahmi, N., Mohamed, A. R., & Bhatia, S. (2011). Nanocrystalline zeolite Y: synthesis and characterization. *IOP Conference Series: Materials Science and Engineering*, *17*(1), 12030.

Tchomgui-Kamga, E., Alonzo, V., Nanseu-Njiki, C. P., Audebrand, N., Ngameni, E., & Darchen, A. (2010). Preparation and characterization of charcoals that contain dispersed aluminum oxide as adsorbents for removal of fluoride from drinking water. *Carbon*, *48*(2), 333–343.

Thole, B. (2013). Ground water contamination with fluoride and potential fluoride removal technologies for East and Southern Africa. *Perspectives in Water Pollution*, 65–95.

Tohfegar, E., Moghaddas, J. S., Sharifzadeh, E., & Esmaeilzadeh–Dilmaghani, S. (2019). Synthesis and Characterization of Waterglass-Based Silica Aerogel Under Heat Treatment for Adsorption of Nitrate from Water : Batch and Column Studies. *Iranian Journal of Chemical Engineering*, *16*(4), 53–72.

Treacy, M. M. J., & Higgins, J. B. (2007). Collection of simulated XRD powder patterns for zeolites fifth (5th) revised edition. Elsevier.

Vithanage, M., & Bhattacharya, P. (2015). Fluoride in the environment: sources, distribution and defluoridation. *Environmental Chemistry Letters*, *13*, 131–147.

Vocciante, M., Trofa, M., Rodríguez-Estupiñán, P., Giraldo, L., D'Auria, T., Moreno-Piraján, J. C., & Erto, A. (2014). A rigorous procedure for the design of adsorption units for the removal of cadmium and nickel from process wastewaters. *Journal of Cleaner Production*, *77*, 35–46.

Waghmare, S., Arfin, T., Rayalu, S., Lataye, D., Dubey, S., & Tiwari, S. (2015). Adsorption behavior of modified zeolite as novel adsorbents for fluoride removal from drinking water: surface phenomena, kinetics and thermodynamics studies. *International Journal of Science, Engineering and Technology Research*, *4*(12), 4114–4124.

Wambu, E. W., Onindo, C. O., Ambusso, W., & Muthakia, G. K. (2013). Removal of fluoride from aqueous solutions by adsorption using a siliceous mineral of a Kenyan origin. *CLEAN–Soil, Air, Water*, *41*(4), 340–348.

Wan, K., Huang, L., Yan, J., Ma, B., Huang, X., Luo, Z., Zhang, H., & Xiao, T. (2021). Removal of fluoride from industrial wastewater by using different adsorbents: A review. *Science of the Total Environment*, *773*, 145535.

Wan, S., Lin, J., Tao, W., Yang, Y., Li, Y., & He, F. (2019). Enhanced fluoride removal from water by nanoporous biochar-supported magnesium oxide. *Industrial & Engineering Chemistry Research*, *58*(23), 9988–9996.

Wang, B., Ma, Y., Lee, X., Wu, P., Liu, F., Zhang, X., Li, L., & Chen, M. (2021). Environmental-friendly coal gangue-biochar composites reclaiming phosphate from water as a slow-release fertilizer. *Science of the Total Environment*, *758*, 143664.

Wang, J., & Guo, X. (2020a). Adsorption isotherm models: Classification, physical meaning, application and solving method. *Chemosphere*, *258*, 127279.

Wang, J., & Guo, X. (2020b). Adsorption kinetic models: Physical meanings, applications, and solving methods. *Journal of Hazardous Materials*, *390*(January), 122156.

Wang, M., Yu, X., Yang, C., Yang, X., Lin, M., Guan, L., & Ge, M. (2017). Removal of fluoride from aqueous solution by Mg-Al-Zr triple-metal composite. *Chemical Engineering Journal*, *322*, 246–253.

Wang, T., Yan, L., He, Y., Alhassan, S. I., Gang, H., Wu, B., Jin, L., & Wang, H. (2022). Application of polypyrrole-based adsorbents in the removal of fluoride: a review. *RSC Advances*, *12*(6), 3505–3517.

Wirtu, Y. D., Melak, F., Yitbarek, M., & Astatkie, H. (2021a). Aluminum coated natural zeolite for water defluoridation: a mechanistic insight. *Groundwater for Sustainable Development*, *12*, 100525.

Wirtu, Y. D., Melak, F., Yitbarek, M., & Astatkie, H. (2021b). Aluminum coated natural zeolite for water defluoridation: A mechanistic insight. *Groundwater for Sustainable Development*, *12*(June 2020), 100525.

Xu, R., Pang, W., Yu, J., Huo, Q., & Chen, J. (2009). Chemistry of zeolites and related porous materials: synthesis and structure. John Wiley & Sons.

Yagub, M. T., Sen, T. K., Afroze, S., & Ang, H. M. (2014). Dye and its removal from aqueous solution by adsorption: A review. In *Advances in Colloid and Interface Science* (Vol. 209).

Zare, K., Gupta, V. K., Moradi, O., Makhlouf, A. S. H., Sillanpää, M., Nadagouda, M. N., Sadegh, H., Shahryari-ghoshekandi, R., Pal, A., Wang, Z. jun, Tyagi, I., & Kazemi, M. (2015). A comparative study on the basis of adsorption capacity between CNTs and activated carbon as adsorbents for removal of noxious synthetic dyes: a review. In *Journal of Nanostructure in Chemistry* (Vol. 5, Issue 2).

Zewge, F. (2016). Combined aluminium sulfate/hydroxide process for fluoride removal from drinking water. *Bulletin of the Chemical Society of Ethiopia*, *30*(3), 391–401.

Zhang, H., Liu, Q., Wang, J., Liu, J., Yan, H., Jing, X., & Zhang, B. (2015). Preparation of magnetic calcium silicate hydrate for the efficient removal of uranium from aqueous systems. *RSC Advances*, *5*(8), 5904–5912.

Zúñiga-Muro, N. M., Bonilla-Petriciolet, A., Mendoza-Castillo, D. I., Reynel-Ávila, H. E., & Tapia-Picazo, J. C. (2017). Fluoride adsorption properties of cerium-containing bone char. *Journal of Fluorine Chemistry*, *197*, 63–73.

APPENDICES

Appendix A

Synthesis Bone char

a)

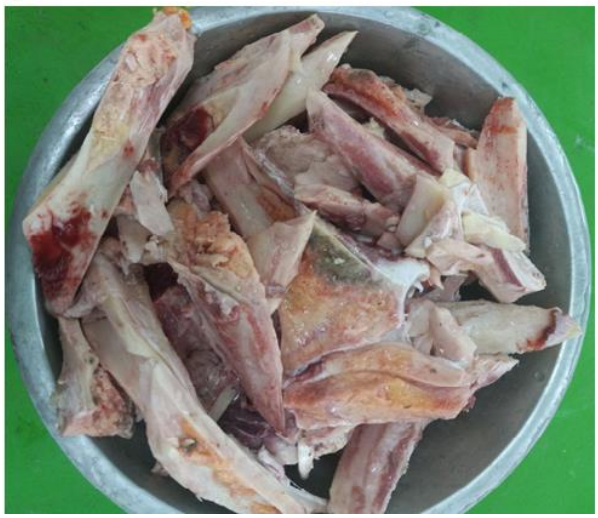

b)

c)

d)

e)

f)

g)

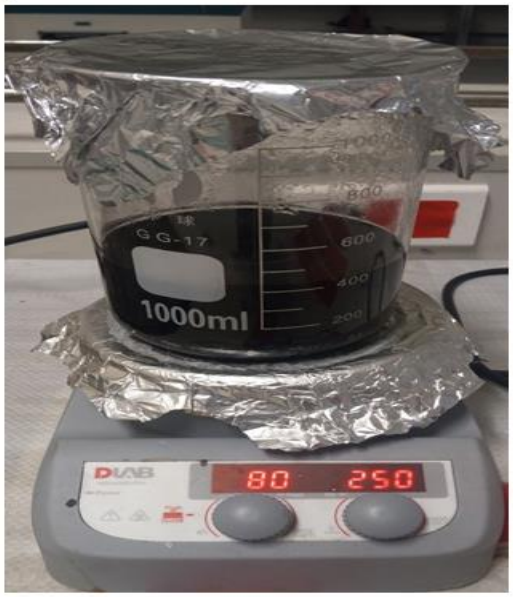

h)

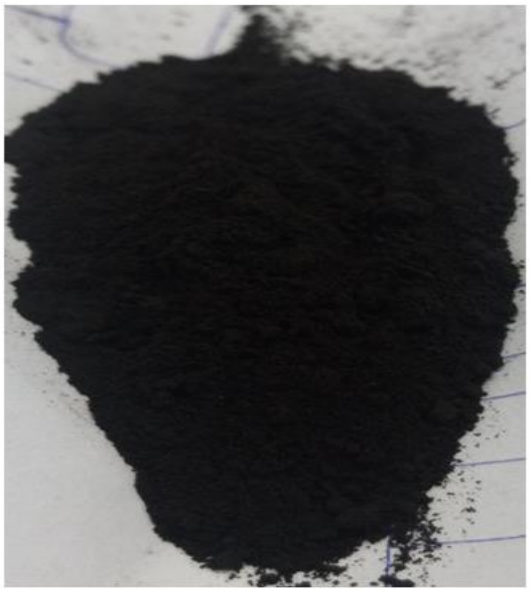

Appendix B

Synthesis Zeolite Y


Clifton

Appendix C

Synthesis Aluminum Loaded Zeolite

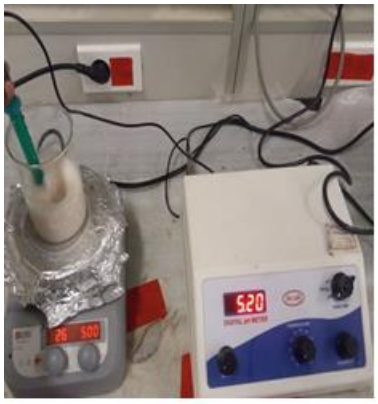

Appendix D

Synthesis of Bone char /Aluminum Loaded Zeolite Y

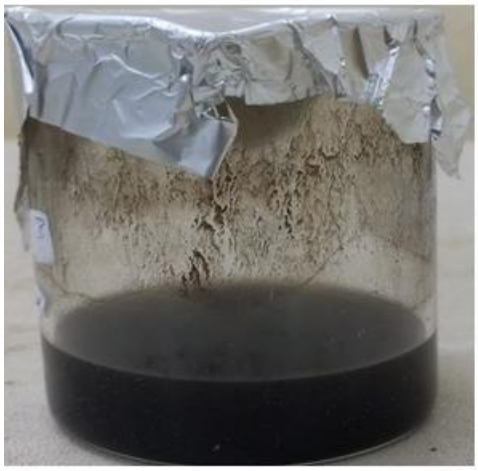

Adsorption Process